

**Trim, Control, and Performance  
Effects in Variable-Complexity  
High-Speed Civil Transport Design**

By

P.E.MacMillin, O.B.Golovidov,  
W.H.Mason, B.Grossman and R.T.Haftka\*

**MAD 96-07-01**

July 1996

Supported by the NASA Langley Research  
Center under grant NAG1-1160.

**Multidisciplinary Analysis and Design Center  
for Advanced Vehicles**

Virginia Polytechnic Institute and State University  
Blacksburg, Virginia 24061-0203

---

\*Department of Aerospace Engineering, Mechanics and Engineering Science, University of Florida, Gainesville, FL 32611-6250

# Abstract

Numerous trim, control requirements and mission generalizations have been made to our previous multidisciplinary design methodology for a high speed civil transport. We optimize the design for minimum take off gross weight, including both aerodynamics and structures to find the wing planform and thickness distribution, fuselage shape, engine placement and thrust, using 29 design variables. While adding trim and control it was found necessary to simultaneously consider landing gear integration. We include the engine-out and crosswind landing requirements, as well as engine nacelle ground strike for lateral-directional requirements. For longitudinal requirements we include nose-wheel lift-off rotation and approach trim as the critical conditions. We found that the engine-out condition and the engine nacelle ground strike avoidance were critical conditions. The addition of a horizontal tail to provide take-off rotation resulted in a significant weight penalty, and that penalty proved to be sensitive to the position of the landing gear. We include engine sizing with thrust during cruise and balanced field length conditions. Both the thrust during cruise and balanced field length constraints were critical. We include a subsonic leg in our mission analysis. The addition of a subsonic mission requirement also results in a large weight penalty.

In performing the work it became clear that several other studies were required to complete the story. Thus included in the report are also results showing the effect of increased balanced field length, sensitivity to changes in the drag coefficient, and finally, the role of the take-off rotation time constraint. This report also contains documentation for the code developed under this project.

# Acknowledgments

This work was supported by the NASA Langley Research Center under grant NAG1-1160. Peter Coen is the grant monitor. We also wish to acknowledge the support of Arnie McCullers of Vigyan and author of FLOPS for his considerable assistance.

This work is essentially Peter MacMillin's MS Thesis, and Oleg Golovidov has now taken over for Peter, and performed the sensitivity studies. The work would not have been possible without the previous work done by numerous graduate students, notably Matthew Hutchison and Eric Unger.

# Contents

<b>Abstract</b>	<b>iii</b>
<b>Acknowledgments</b>	<b>v</b>
<b>List of Symbols</b>	<b>xvii</b>
<b>1 Introduction</b>	<b>1</b>
<b>2 Design Issues</b>	<b>7</b>
2.1 Vertical Tail Sizing . . . . .	8
2.2 Engine Location Limits . . . . .	9
2.3 Nacelle and Wing Tip Strike . . . . .	9
2.4 Landing Gear Location . . . . .	11
2.5 Horizontal Tail Sizing . . . . .	13
2.6 Engine Sizing . . . . .	13
<b>3 Design Formulation</b>	<b>15</b>
3.1 Design Variables . . . . .	15
3.2 Constraints . . . . .	20
<b>4 Variable Complexity Modeling</b>	<b>23</b>
<b>5 Analysis Methods</b>	<b>27</b>
5.1 Aerodynamics . . . . .	27
5.2 Structures . . . . .	30

5.3	Center of Gravity and Inertia Estimation . . . . .	31
5.4	Stability Derivative Estimation . . . . .	32
5.4.1	Lateral-Directional Derivatives . . . . .	32
5.4.2	Accuracy of Lateral-Directional Estimates . . . . .	35
5.4.3	Longitudinal Derivatives . . . . .	36
5.5	Landing Gear . . . . .	38
5.6	Engine Out . . . . .	38
5.7	Crosswind Landing . . . . .	39
5.8	Take Off Analysis . . . . .	39
5.9	Takeoff Aerodynamics . . . . .	44
5.10	Powered Approach Trim . . . . .	46
5.11	Engine Scaling . . . . .	47
5.12	Minimum Time Climb with Dynamic Pressure Constraint . . . . .	47
5.13	Optimization Strategies . . . . .	49
<b>6</b>	<b>Results</b>	<b>51</b>
6.1	Baseline Optimization (Case 26a) . . . . .	52
6.2	Vertical Tail Considerations . . . . .	54
6.2.1	Case 27a . . . . .	54
6.2.2	Case 27b . . . . .	57
6.3	Vertical and Horizontal Tail Considerations . . . . .	65
6.3.1	Case 28a . . . . .	65
6.3.2	Case 28b . . . . .	66
6.4	Engine Sizing (Case 29a) . . . . .	69
6.5	Subsonic Leg (Case 29b) . . . . .	72
6.6	Sensitivity To Parameters and Analysis Accuracy . . . . .	75
6.6.1	Engine Sizing with Relaxed BFL Constraint (Case 29c) . . . . .	75
6.6.2	TOGW Sensitivity to Drag Change . . . . .	82
6.6.3	TOGW Sensitivity to Rotation Time (Case 29d) . . . . .	90
6.7	Minimum Time to Climb Calculation . . . . .	94

<b>7</b>	<b>Conclusions</b>	<b>97</b>
	<b>References</b>	<b>101</b>
<b>A</b>	<b>Using the HSCT code</b>	<b>109</b>
A.1	Input files . . . . .	109
A.2	Output files . . . . .	110
A.3	Other files . . . . .	111
A.4	The <code>hsct.command</code> file . . . . .	112
A.4.1	Parameter sections . . . . .	112
A.4.2	Commands . . . . .	116
A.5	Experiences optimizing with the HSCT code . . . . .	118
A.6	Sample <code>hsct.command</code> file . . . . .	119
A.7	Sample design variable file . . . . .	121
<b>B</b>	<b>HSCT Code Structure</b>	<b>123</b>
B.1	Overview of code structure . . . . .	123
B.2	<code>aero.c</code> . . . . .	125
B.3	<code>craidio.c</code> . . . . .	127
B.4	<code>dataio.c</code> . . . . .	129
B.5	<code>f77iface.c</code> . . . . .	130
B.6	<code>fminbr.c</code> . . . . .	131
B.7	<code>main.c</code> . . . . .	132
B.8	<code>modify.c</code> . . . . .	132
B.9	<code>numerics.c</code> . . . . .	134
B.10	<code>options.c</code> . . . . .	136
B.11	<code>perform.c</code> . . . . .	137
B.12	<code>servmath.c</code> . . . . .	139
B.13	<code>simpaero.c</code> . . . . .	139
B.14	<code>stability.c</code> . . . . .	143
B.15	<code>takeoff.c</code> . . . . .	145
B.16	<code>util.c</code> . . . . .	148

B.17	weight.c	151
B.18	flops_inter.f	152
B.19	harris.f	153
B.20	optimizer.f	157
B.21	rs_weight.f	157
B.22	sfeng.f	158
B.23	sfwate.f	158

# List of Tables

1	Design Variables . . . . .	17
2	Optimization Constraints . . . . .	21
3	Load cases used in structural optimization . . . . .	31
4	Comparison of stability and control derivative estimations for the XB-70A . . . . .	36
5	Comparison of stability and control derivative estimations for a F/A-18 at Mach 0.2, out of ground effect . . . . .	37
6	Overview of results . . . . .	51
7	Overview of sensitivity studies . . . . .	52
8	Comparison of Initial and Final Designs, Case 26a . . . . .	53
9	Comparison of Initial and Final Designs, Case 27a . . . . .	58
10	Comparison of Initial and Final Designs, Case 27b . . . . .	62
11	Comparison of Initial and Final Designs, Case 28a . . . . .	67
12	Comparison of Initial and Final Designs, Case 28b . . . . .	70
13	Comparison of Initial and Final Designs, Case 29a . . . . .	72
14	Comparison of Initial and Final Designs, Case 29b . . . . .	76
15	Comparison of Initial and Final Designs, Case 29c . . . . .	78
16	Comparison of Final Designs for Case 29a and 29c . . . . .	81
17	Comparison of the baseline design (Case 29c) to the changed drag designs . . . . .	88
18	Comparison of Final Designs for Case 29d and 29c . . . . .	93
19	Summary of optimizations . . . . .	98



# List of Figures

1	Wing and vertical tail weights versus spanwise nacelle location . . . . .	10
2	Wave drag versus vertical tail size . . . . .	10
3	Definition of tipback angle . . . . .	12
4	Definition of the overturn angle . . . . .	12
5	Planform Definition Parameters . . . . .	18
6	Airfoil Thickness Parameters . . . . .	19
7	Effect of increasing semi-span on wave drag prediction . . . . .	29
8	Definition of $k$ for $C_{y_{\beta_v}}$ . . . . .	33
9	Definition of $\ell_v$ and $Z_v$ . . . . .	34
10	Definition of $\left[ \frac{(\alpha_\delta)C_L}{(\alpha\delta)C_\ell} \right]$ . . . . .	35
11	Specific excess power contours for a HSCT configuration . . . . .	48
12	Convergence of Case 26a . . . . .	53
13	Initial and final planforms, Case 26a . . . . .	54
14	History of wing weight and trailing edge sweep, Case 26a . . . . .	55
15	History of drag due to lift, at $C_L = 0.1$ , Case 26a . . . . .	55
16	History of wave drag, Case 26a . . . . .	56
17	History of total drag, at $C_L = 0.1$ , Case 26a . . . . .	56
18	Convergence of Case 27a . . . . .	57
19	Initial and final planforms, Case 27a . . . . .	58
20	History of nacelle positions and vertical tail area . . . . .	59
21	History of $C_{y_\beta}$ , $C_{l_\beta}$ , and $C_{n_\beta}$ for Case 27a . . . . .	60
22	History of $C_{y_{\delta_r}}$ , $C_{l_{\delta_r}}$ , and $C_{n_{\delta_r}}$ for Case 27a . . . . .	61
23	Initial and final planforms, Case 27b . . . . .	62

24	History of $C_{y\beta}$ , $C_{l\beta}$ , and $C_{n\beta}$ for Case 27b . . . . .	63
25	History of $C_{y\delta_r}$ , $C_{l\delta_r}$ , and $C_{n\delta_r}$ for Case 27b . . . . .	64
26	Initial and final planforms, Case 28a . . . . .	66
27	Takeoff Gross Weight and Range convergence, Case 28a . . . . .	67
28	Vertical Tail Size and Nacelle Location convergence, Case 28a . . . . .	68
29	Horizontal Tail Size convergence, Case 28a . . . . .	68
30	Initial and final planforms, Case 28b . . . . .	69
31	Initial and final planforms, Case 29a . . . . .	71
32	Takeoff Gross Weight and Range convergence, Case 29a . . . . .	73
33	Balanced field length convergence, case 29a . . . . .	73
34	Initial and final planforms, Case 29b . . . . .	75
35	Takeoff Gross Weight convergence, Case 29b . . . . .	76
36	Range and BFL convergence, case 29b . . . . .	77
37	Initial and final planforms, Case 29c . . . . .	79
38	Takeoff Gross Weight and Range convergence, Case 29c . . . . .	79
39	Balanced field length convergence, Case 29c . . . . .	80
40	Comparison of planforms for Case 29a and 29c. . . . .	82
41	TOGW and range convergence for the design with a 2 count drag reduction . . . . .	83
42	TOGW and range convergence for the design with a 1 count drag reduction . . . . .	83
43	TOGW and range convergence for the design with a 1 count drag increase	84
44	TOGW and range convergence for the design with a 2 count drag increase	84
45	Baseline and negative 2 drag count planforms . . . . .	85
46	Baseline and negative 1 drag count planforms . . . . .	86
47	Baseline and positive 1 drag count planforms . . . . .	86
48	Baseline and positive 2 drag count planforms . . . . .	87
49	TOGW variation with drag change . . . . .	87
50	Fuel and wing weight variation with drag change . . . . .	88
51	Wing, horisontal and vertical tail areas variation with drag change . .	89
52	Engine thrust and wing loading variation with drag change . . . . .	89

53	Take-off Gross Weight and Range convergence, Case 29d-6 . . . . .	91
54	Balanced Field Length convergence, Case 29d-6 . . . . .	91
55	Take-off Gross Weight and Range convergence, Case 29d-20 . . . . .	91
56	Balanced Field Length convergence, Case 29d-20 . . . . .	92
57	Configurations for Cases 29c and 29d-6 . . . . .	93
58	Configurations for Cases 29c and 29d-20 . . . . .	94

# List of Symbols

$a_x$	horizontal acceleration
$a_z$	vertical acceleration
$A$	horizontal acceleration coefficient
$A_N$	engine nozzle area
$\mathcal{AR}$	aspect ratio, $b^2/S$
$\mathcal{AR}_v$	geometric aspect ratio for the isolated vertical tail
$\mathcal{AR}_{v_{eff}}$	effective vertical tail aspect ratio
$b$	wing span
$b_f$	rudder span
$B$	horizontal acceleration coefficient
$\bar{c}$	mean aerodynamic chord
$c_g$	mean geometric chord
$cg$	center of gravity
$C$	horizontal acceleration coefficient
$C_1$	constant used in calculating $C_{D_{lg}}$
$C_D$	drag coefficient, $D/qS$
$C_{D_i}$	induced drag coefficient
$C_{D_{lg}}$	landing gear drag coefficient
$C_{D_l}$	coefficient of drag due to lift
$C_{D_{wm}}$	windmilling engine drag coefficient
$C_\ell$	section lift coefficient
$C_l$	rolling moment coefficient
$C_{l_\beta}$	dihedral effect stability derivative, $\partial C_l / \partial \beta$

$C_{l_{\beta v}}$	vertical tail contribution to $C_{l_{\beta}}$
$C_{l_{\delta a}}$	rolling moment due to aileron deflection control derivative, $\partial C_l / \partial \delta_a$
$C_{l_{\delta r}}$	rolling moment due to rudder deflection control derivative, $\partial C_l / \partial \delta_r$
$C_L$	lift coefficient, $L/qS$
$C_{L_{\alpha}}$	lift curve slope, $\partial C_L / \partial \alpha$
$C_{L_{\alpha HT}}$	horizontal tail lift curve slope
$C_{L_{\alpha v}}$	vertical tail lift curve slope
$C_{L_{\delta e}}$	$\partial C_L / \partial \delta_e$
$C_{L_{\delta f}}$	$\partial C_L / \partial \delta_f$
$C_{L_g}$	lift coefficient in ground effect
$C_{L_{max}}$	$C_L$ at maximum allowable angle of attack
$C_{L_{\infty}}$	lift coefficient out of ground effect
$C_M$	pitching moment coefficient, $M/qS\bar{c}$
$C_{M_{\alpha}}$	$\partial C_M / \partial \alpha$
$C_{M_0}$	zero lift pitching moment coefficient
$C_{M_{HT}}$	horizontal tail contribution to the pitching moment
$C_{M_{\delta e}}$	$\partial C_M / \partial \delta_e$
$C_{M_{\delta f}}$	$\partial C_M / \partial \delta_f$
$C_n$	rolling moment coefficient
$C_{n_{\beta}}$	weathercock stability derivative, $\partial C_n / \partial \beta$
$C_{n_{\beta v}}$	vertical tail contribution to $C_{n_{\beta}}$
$C_{n_{\delta a}}$	yawing moment due to aileron deflection control derivative, $\partial C_n / \partial \delta_a$
$C_{n_{\delta r}}$	yawing moment due to rudder deflection control derivative, $\partial C_n / \partial \delta_r$
$C_T$	thrust coefficient
$C_{y_{\beta}}$	side force stability derivative, $\partial C_y / \partial \beta$
$C_{y_{\beta v}}$	vertical tail contribution to $C_{y_{\beta}}$
$C_{y_{\delta a}}$	side force due to aileron deflection control derivative, $\partial C_y / \partial \delta_a$
$C_{y_{\delta r}}$	side force due to rudder deflection control derivative, $\partial C_y / \partial \delta_r$
$d$	Maximum fuselage diameter at wing-body junction
$D_{nac}$	nacelle diameter
$D_{nac_{ref}}$	reference nacelle diameter

$f(\mathbf{x})$	analysis function
$f_d(\mathbf{x})$	detailed model analysis function
$f_s(\mathbf{x})$	simple model analysis function
$F_{mg}$	main landing gear reaction force
$g$	gravitational acceleration
$h$	height above ground
$h_e$	energy height
$i_t$	horizontal tail deflection
$I$	airfoil leading edge radius parameter
$I_{yy_{mg}}$	Moment of inertia about the main gear
$k$	empirical factor used to calculate $C_{y_{\beta_v}}$ , see Fig. 8
$k_r$	factor used to calculate the rotation speed
$K'$	rudder effectiveness parameter
$K_b$	parameter used to calculate $C_{y_{\delta_r}}$ , defined by Eq. 13
$\ell_{mg}$	length of the main gear
$\ell_v$	horizontal distance between aircraft $cg$ and vertical tail aerodynamic center, see Fig. 9
$l_{nac}$	nacelle length
$l_{nac_{ref}}$	reference nacelle length
$L_{ext}$	net rolling moment
$m$	chordwise location of maximum airfoil thickness
$\dot{m}$	engine mass flow
$\dot{m}_{ref}$	reference engine mass flow
$M_{cg}$	pitching moment about the center of gravity
$M_{mg}$	pitching moment about the main gear
$N_{ext}$	net yawing moment
$P_s$	specific excess power
$q$	dynamic pressure, $\frac{1}{2}\rho V^2$
$r_i$	engine inlet radius
$r_t$	leading edge radius to chord ratio
$R$	horizontal acceleration solution parameter, $B^2 - 4AC$

$s_{eng}$	constant used to calculate engine weight
$S$	wing area
$S_{HT}$	horizontal tail wing area
$S_v$	vertical tail area
$t$	time
$t/c$	airfoil thickness to chord ratio
$T$	thrust
$T_0, T_1, T_2$	thrust coefficients
$T_{ref}$	reference thrust
$V$	Aircraft velocity
$V_{crit}$	critical engine failure speed
$V_{crit_g}$	guess for $V_{crit}$
$V_H$	horizontal tail volume coefficient
$V_{MC}$	minimum control speed
$V_N$	engine nozzle velocity
$V_r$	rotation speed
$V_s$	stall speed
$V_x$	horizontal component of the aircraft velocity
$V_z$	vertical component of the aircraft velocity
$W$	aircraft weight
$W_{eng}$	engine weight
$W_{eng_{ref}}$	reference engine weight
$\mathbf{x}$	vector of design variables
$\mathbf{x}_0$	vector of initial design variables
$x_{BFL}$	balanced field length distance
$x_{cg}$	horizontal distance from nose of aircraft to $cg$
$x_{cg_{mg}}$	horizontal distance between the $cg$ and the main gear contact point
$x_{L_{cg}}$	horizontal distance between the aerodynamic center and the $cg$
$x_{L_{mg}}$	horizontal distance between the aerodynamic center and the main gear contact point
$x_{main}$	horizontal distance from nose of aircraft to main landing gear

$x_{nose}$	horizontal distance from nose of aircraft to nose gear
$x_{Tmg}$	horizontal distance between the thrust vector and the main gear contact point
$X$	horizontal distance
$Y_{ext}$	net side force
$z_{cgmg}$	vertical distance between the $cg$ and the main gear contact point
$z_{Dcg}$	vertical distance between the aerodynamic center and the $cg$
$z_{Dmg}$	vertical distance between the aerodynamic center and the main gear contact point
$z_{Tcg}$	vertical distance between the thrust vector and the $cg$
$z_{Tmg}$	vertical distance between the thrust vector and the main gear contact point
$Z_v$	vertical distance between aircraft $cg$ and vertical tail aerodynamic center, see Fig. 9
$Z_w$	vertical distance from the wing root quarter chord point to the fuselage centerline, positive downward

### Greek Symbols

$\alpha$	angle of attack
$\left[ \frac{(\alpha_\delta)_{C_L}}{(\alpha_\delta)_{C_\ell}} \right]$	Defined in Figure 10
$(\alpha_\delta)_{C_\ell}$	Defined in Figure 10
$\beta$	sideslip angle
$\beta_g$	parameter for calculating $C_{L_g}$
$\beta_M$	$\sqrt{1 - M^2}$
$\delta_a$	aileron deflection, positive down
$\delta_e$	elevator deflection, positive down
$\delta_f$	flap deflection, positive down
$\delta_r$	rudder deflection, positive to the left (results in positive side force)
$\eta_v$	dynamic pressure ratio for vertical tail
$\gamma$	flight path angle



$\Lambda_{c/2}$	half chord sweep angle
$\Lambda_{c/4}$	quarter chord sweep angle
$\Lambda_T$	thrust vectoring angle
$\mu_{grd}$	coefficient of friction of the runway
$\phi$	bank angle
$\rho$	atmospheric density
$\rho_0$	atmospheric density at sea level
$\sigma$	atmospheric density ratio, $\rho/\rho_0$
$\sigma_g$	parameter for calculating ground effects
$\sigma(\mathbf{x})$	scaling function
$\frac{d\sigma}{d\beta}$	sidewash factor
$\tau_{TE}$	airfoil trailing edge half angle
$\ddot{\theta}_{mg}$	pitch rate about the main gear
$\varepsilon$	downwash angle

### Subscripts

$a$	initial point
$b$	final point

### Superscripts

$\cdot$	first derivative with respect to time
$\ddot{\phantom{x}}$	second derivative with respect to time

### Acronyms

BFL	<b>B</b> alanced <b>F</b> ield <b>L</b> ength
FLOPS	<b>F</b> light <b>O</b> ptimization <b>S</b> ystem
HSCT	<b>H</b> igh- <b>S</b> peed <b>C</b> ivil <b>T</b> ransport
MDO	<b>M</b> ultidisciplinary <b>D</b> esign <b>O</b> ptimization

TOGW	<b>T</b> ake <b>O</b> ff <b>G</b> ross <b>W</b> eight
VCM	<b>V</b> ariable- <b>C</b> omplexity <b>M</b> odeling
VLM	<b>V</b> ortex <b>L</b> attice <b>M</b> ethod

# Chapter 1

## Introduction

Designing a supersonic transport is an extremely demanding task. Many of the mission requirements conflict with one another. To satisfy all of the requirements, the designer must completely integrate the various technologies in the design, such as trading supersonic cruising efficiency for takeoff and landing performance. The efficiency and economic feasibility of the final design is determined by the quality of the technology integration. To make intelligent compromises the designer requires data from many disciplines and must be aware of the disciplinary interactions. If any of the major disciplinary interactions are neglected in the conceptual/preliminary design phase, it is likely there will be a significant weight penalty in the final design because of the need to account for the neglected interactions after the configuration has been *frozen*.

Multidisciplinary design optimization (MDO) is a methodology for the design of systems where interactions between disciplines are explicitly addressed. For vehicles designed for extremely demanding missions, MDO is an enabling technology, without which the design goals will not be achieved. Sobieski has provided much of the impetus for this approach and has written the key reviews describing MDO<sup>1, 2, 3</sup>. The coupling inherent in MDO produces increased complexity, due in part to the increased size of the MDO problem compared to single disciplinary optimization. The number of design variables increases with each additional discipline. Since solution times for most analysis and optimization algorithms increase at a superlinear rate, the

computational cost of MDO is usually much higher than the sum of the costs of the single-discipline optimizations for the disciplines represented in the MDO. In this work we focus on one area where this computational problem is acute: combined aerodynamic-structural-controls-propulsion design of the high-speed civil transport (HSCT).

Aircraft design at the conceptual level has always been multidisciplinary, because the tradeoffs between the requirements of the different disciplines are easily addressed due to the simplicity of the modeling of the system. Often these are statistically-derived, experience-based algebraic models. At the preliminary design level, however, more detailed numerical models of both structures and aerodynamics are employed.

Early studies of combined aerodynamic and structural optimization relied on simple aerodynamic and structural models and a small number of design variables<sup>4</sup>, so that computational cost was not an issue. Rather, the goal was to demonstrate the advantages of the optimized design. For example, Grossman *et al.*<sup>5</sup> used lifting line aerodynamics and beam structural models to demonstrate that simultaneous aerodynamic and structural optimization can produce superior designs compared to the use of a sequential approach. Similar models were used by Wakayama and Kroo<sup>6</sup> who showed that optimal designs are strongly affected by compressibility drag, aeroelasticity and multiple structural-design conditions. Gallman *et al.*<sup>7</sup> used beam structural models together with vortex-lattice aerodynamics to explore the advantages of joined-wing aircraft.

However, as soon as more detailed numerical simulations are considered it becomes difficult to preserve interdisciplinary communications, and until recently, MDO has not been used at the detailed design level. Modern single-disciplinary designs in both aerodynamics and structures go well beyond simple models. Aerodynamic optimization for transports is often performed with three-dimensional nonlinear models e.g., Euler equations<sup>8</sup>. Structural optimization is performed with large finite-element models. For example, Tzong<sup>9</sup> performed a structural optimization with static aeroelastic effects of a high-speed civil transport using a finite element model with 13,700 degrees of freedom and 122 design variables.

There is a corresponding pressure to use more detailed models in MDO. For example, Borland<sup>10</sup> performed a combined aerodynamic-structural optimization of a subsonic transport wing with a fixed planform using a large finite-element model and thin-layer Navier-Stokes aerodynamics. However, due to computational cost, they only used three aerodynamic design variables along with 20 structural design variables.

The aerodynamic design and structural design of a wing are closely related, and the tradeoff between structural weight and aerodynamic performance determines the shape parameters of the wing, including thickness and aspect ratio. However, there is a fundamental asymmetry in the level of detail that each discipline needs to supply the other. The structural designer needs detailed load distributions from the aerodynamicist. Therefore, it is not possible to perform accurate structural optimization with conceptual-level aerodynamics. In contrast, the aerodynamic designer can perform aerodynamic optimization using only the structural weight. Of course, accurate estimation of the sensitivities of the weight is also required for aerodynamic optimization.

The structural weight, being an integral measure of the structure, is amenable to accurate estimation by conceptual-level weight equations. Weight equations have traditionally been developed semi-analytically using actual wing weights. McCullers<sup>11</sup> developed a transport weight function based on both historical data and structural optimization solutions for numerous planform and thickness combinations. These equations are used in the Flight Optimization System (FLOPS)<sup>11</sup>. Scott<sup>12</sup>, Udin and Anderson<sup>13</sup>, and Torenbeek<sup>14</sup> have discussed the considerations used in developing modern wing weight equations. Huang *et al.*<sup>15</sup> compared the FLOPS equation with both structural optimization and another wing weight equation for HSCT-class planforms.

The high cost of using detailed analysis methods in an MDO procedure prevents their use in conceptual design. To reduce the computational cost of MDO, we have been developing the variable-complexity modeling concept. Variable-complexity modeling uses multiple levels of analysis methods. The detailed numerical analysis methods are only used sparingly to improve the accuracy of the approximate analysis

methods. An in-depth discussion of the various types of variable-complexity approximations and the aerodynamic and structural analysis methods we are using can be found in the papers by Hutchison *et al.*<sup>16, 17, 18</sup> and Dudley *et al.*<sup>19</sup>.

In this work we extend the previous work of Hutchison *et al.*<sup>16, 17, 18</sup> to handle additional mission details and to include trim, control and propulsion considerations directly in the variable-complexity design procedure.

Explicit consideration of trim and control in conceptual aircraft sizing methodology is unusual. For subsonic configuration optimizations there have been related studies by Sliwa<sup>20, 21</sup> and by Gallman *et al.*<sup>7</sup>. Both considered longitudinal trim and control, and both found that including trim and control considerations affected the design. In the study by Gallman *et al.*<sup>7</sup> the take-off rotation control requirement was found to be a critical issue in the comparison of equivalent conventional and joined-wing configurations.

We include vertical and horizontal tail sizing by examining critical stability and control requirements, such as takeoff rotation and the engine out condition. As part of the integration of aircraft trim and control requirements, the engine and landing gear locations emerge as significant considerations. Both of these considerations are included in the methodology described in this paper.

Stability derivatives must be available to include trim and control in the optimization. We use our variable-complexity modeling concept to estimate them. Specifically, we use the so-called interlacing technique described by Dudley *et al.*<sup>19</sup>. They used the approach to incorporate detailed finite element structural analysis in the optimization.

We extend our mission requirements with the addition of a subsonic leg and a minimum time climb with a dynamic pressure constraint. Most routes that this aircraft might fly will require an initial subsonic leg to avoid sonic booms near populated areas. We examine the effect of this on our design by requiring an initial portion of our specified range be flown at Mach 0.9. The subsonic leg is flown at a much lower altitude than the supersonic portion. We investigate using a minimum time to climb profile to transition from the subsonic to the supersonic legs.

We include engine sizing using thrust scaling. Thrust required is determined by examining mission thrust requirements and balanced field length (BFL). An HSCT

must be able to use existing runways, which limits the allowable BFL. One of the most important factors in determining the BFL is the thrust to weight ratio of the aircraft.

In the next chapter we discuss the design issues addressed in this work. Chapter 3 describes how we formulate our design problem. Variable-complexity modeling is explained in detail in Chapter 4. Our analysis methods are described in Chapter 5. In Chapter 6 we present our results and finally we discuss our conclusions in Chapter 7.

# Chapter 2

## Design Issues

The size, shape, and location of almost every component on an aircraft is determined by various critical requirements. Often there are multiple issues affecting the design of a component. Our work uses the conceptual/preliminary design control authority assessment methods developed by Kay *et al.*<sup>22</sup>. In particular, Kay established a set of stability and control requirements which must be addressed in the initial stages of vehicle design. A study of control requirements specific to HSCT configurations has recently been conducted by McCarty *et al.*<sup>23</sup>. Their work is consistent with the approach of Kay, and has been used to focus the work presented here. The ratio of dynamic pressure at cruise (M2.4 at 65K ft) to that at the low speed critical field performance conditions (150kt, sea level) is more than 6. Thus, References [22] and [23] find that the large control power requirements during take-off and landing combined with the low dynamic pressure results in the low speed field performance conditions being the critical design conditions.

Assuming the low speed conditions define the control surface sizes, we incorporate trim and control requirements for both lateral-directional and longitudinal control conditions. In the lateral-directional case, the conditions are engine-out trim performance and crosswind landing. For engine-out trim performance we require the aircraft be capable of trimmed flight after two engines on the same side fail. Thus the vertical tail must be capable of handling the yawing moment generated by the thrust imbalance. This is especially important since the wing weight decreases when



the engines are placed well outboard. This effect is exploited during the optimization, sending the engines as far outboard as practical. In the longitudinal axis, take-off rotation has been found to be the critical condition for this class of aircraft, and we consider take-off rotation and approach trim. The engine location becomes important because of both asymmetric thrust considerations and the requirement that the engine nacelles not strike the runway during take-off and landing. The landing gear location and length play a key role in defining the control power required to rotate the aircraft at take-off. In the following sections we discuss what we consider to be the critical issues for the vertical and horizontal tails, engines, and landing gear.

## 2.1 Vertical Tail Sizing

For civilian aircraft with four engines, where maneuverability is not a primary consideration, the vertical tail size is based either on the requirement that the aircraft be capable of trimmed flight with two engines inoperative as specified in FAR 25.147, or to handle the crosswind landing requirement. The pilot must have sufficient control authority to trim the aircraft in these situations, as well as to be able to perform necessary maneuvers. Therefore, we require the aircraft be trimmed directionally using no more than 75% of the maximum available control authority.

The engine out condition generates a yawing moment what must be balanced. The magnitude of the yawing moment depends on the thrust of the engines, and their positions. The crosswind landing condition requires the aircraft balance the yawing moment caused by a 20 *knot* crosswind, as specified in FAR 25.237. Deflecting the rudder creates the balancing yawing moment, but also causes a sideforce which must be counteracted. This is done with a combination of sideslip and bank. Both sideslip and bank can make landing difficult if the angle is too great. Large sideslip causes rough landings as the aircraft must suddenly straighten out upon touchdown. Excessive bank introduces the possibility of the wing tip scraping the ground before the landing gear touches down. These considerations require us to limit the allowable amount of sideslip and bank to  $10^\circ$  and  $5^\circ$ , respectively. The rudder deflection also creates a rolling moment that is usually controlled using the ailerons.

## 2.2 Engine Location Limits

Moving the engine outboard provides wing bending moment relief, thereby reducing the wing weight. As the engine moves outboard, the vertical tail must increase in size to satisfy the engine out condition. But, the increase in vertical tail weight is small compared to the reduction in wing weight, as shown in Fig. 1. There is a practical limit to the amount of wing bending moment relief moving the engine outboard can produce. After this limit is reached, moving the engine further outboard does not result in any further reduction in wing weight. But vertical tail size and weight continue to increase. This produces a minimum in the sum of the wing and vertical tail weights at the point where the limit is reached.

Also, the increase in drag due to increasing the vertical tail size and including the associated movement of the nacelle is small, as shown in Fig. 2. The increase in volumetric wave drag is less than two counts, and the increase in friction drag is about three counts. Thus the minimum TOGW is achieved using a very large vertical tail and placing the engine at the point where the limit in wing bending moment is achieved. Placing the engine extremely far outboard could cause problems with flutter, engine-out trim, nacelle strike during landing, and airframe stresses during ground operations, such as full fuel taxi. A constraint is needed to prevent the optimizer from placing the engines too far outboard on the wing.

## 2.3 Nacelle and Wing Tip Strike

HSCT configurations generally have low lift curve slopes. This results in high landing angles of attack, approximately  $12^\circ$ . When landing at such a high angle of attack, it is possible for the engine nacelles to strike the runway. This is dependent on the positioning of the nacelles, with 25% overhang, and the sweep of the wing trailing edge, as well as the length and position of the landing gear. An allowance must also be made for up to  $5^\circ$  of bank.

A similar problem exists with the wing tips. A large amount of trailing edge sweep can place the trailing edge of the wing tip well behind the main gear. When this is

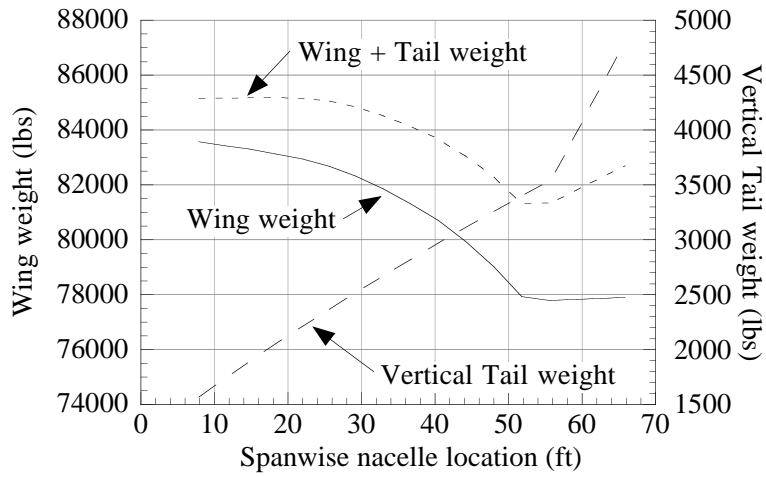


Figure 1: The sum of the wing and vertical tail weights decreases as the engine is moved outboard.

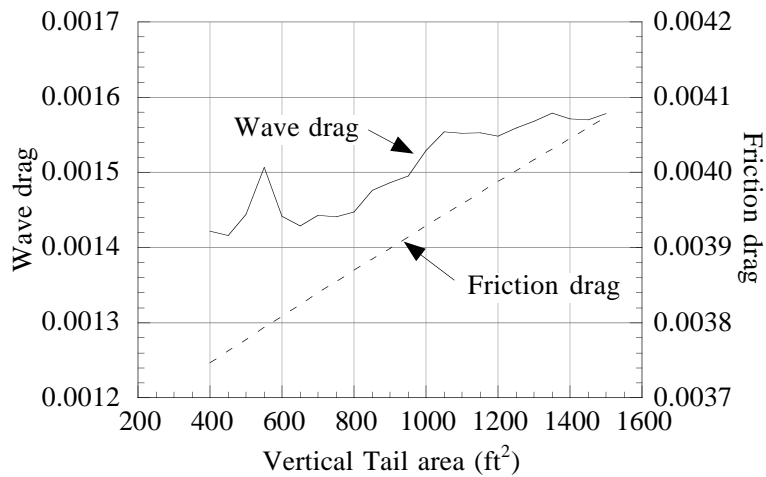


Figure 2: The wave drag increases very little with nacelles moving outboard and increasing vertical tail area.

coupled with the relatively high landing angle of attack and even a small amount of bank, it can cause the wing tips to strike the runway.

## 2.4 Landing Gear Location

Landing gear position relative to the center of gravity is important for take-off rotation, as well as the effect on the engine nacelle strike constraint. Both the nose and main gear positions must be known for the center of gravity calculation. On landing, the main gear touches down first, so the position and length of the main gear is critical to the nacelle and wing tip strike constraints. Increasing the length of the main gear results in more ground clearance, which is the distance between the nacelles and the runway. Moving the main landing gear closer to the engines on the wing reduces the effect of pitch and bank on the ground clearance. In general, pitch will reduce nacelle ground clearance and banking will further reduce ground clearance on the wing which is banked toward the ground.

The weight distribution on the landing gear is important during take-off rotation. If the nose gear is too heavily loaded, it will be difficult to rotate to the take-off attitude. If the nose gear is too lightly loaded, the aircraft will be hard to steer and could rotate before there is enough control authority to control the aircraft's attitude. Torenbeek<sup>24</sup> recommends the nose gear support between 8% and 15% of the total weight. We elected to place the nose gear so that it would be supporting 11.5% of the total weight.

Other important considerations include the tipback and overturn angles. Both angles relate the main gear's position to the location of the center of gravity. The tipback angle is the angle between the main gear and the *cg* as seen in the side view, as seen in Fig. 3, and it should be 15° or less. If the main gear is not far enough behind the center of gravity, the aircraft could tip back on its tail. As the tipback angle is increased, the pitching moment required to rotate the aircraft for takeoff also increases. The horizontal tail size is very sensitive to this parameter. The overturn angle is a measure of the likelihood of the aircraft tipping over sideways while taxiing in a turn. It should be less than 63°, as shown in Figure 4.

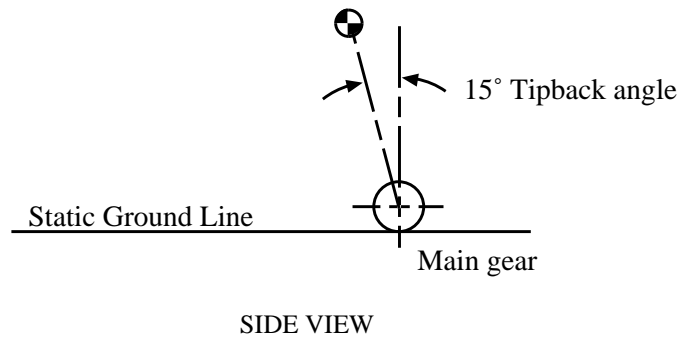


Figure 3: Definition of tipback angle

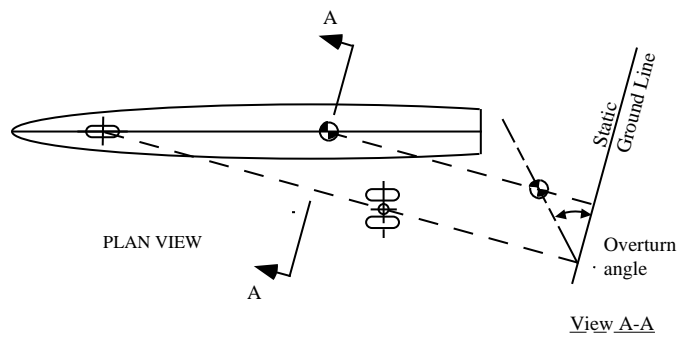


Figure 4: Definition of the overturn angle

## 2.5 Horizontal Tail Sizing

Several longitudinal control and trim issues are important. The field performance requirements are among the most critical. For most airplanes, take-off involves rotating on the main landing gear to a pitch attitude at which the wings can generate enough lift to become airborne. This rotation is caused by the pitching moment generated by a longitudinal control effector, such as the horizontal tail or the wing trailing edge flap for a tailless configuration. The civilian FAR<sup>25</sup> regulations require the aircraft be able to take off safely. If the takeoff rotation requires too much time, it will greatly increase the takeoff distance. This limits the number of airports that the aircraft can use. In most of this report we require the aircraft be able to rotate to lift-off in under 5 *sec*\*. Section 6.6 presents the results of assessing the impact of this constraint.

Approach trim is also important. The aircraft must be able to be trimmed at an angle of attack well above normal operating conditions. There should also be enough additional control power beyond trim to maneuver. This allows the pilot to deal with gusts and emergencies. For unstable aircraft, the actual amount of nose down pitching moment at high angle of attack required for safe flight is a current research topic<sup>26</sup>.

## 2.6 Engine Sizing

Engine size is determined primarily by bypass ratio and the maximum massflow the engine is required to handle. The maximum massflow is proportional to the maximum thrust the engine can produce. So, for a given bypass ratio, the size of the engine is based on the maximum thrust required.

Lower thrust requirements mean a lighter, smaller engine, which creates less drag, can be used. But less thrust also means longer takeoff lengths. The second segment climb requirements are sometimes the critical conditions for sizing the engine. Also,

---

\*This requirement was determined by investigating typical rotation times for large aircraft. Since there are very few aircraft of this type there is not a large body of data to base our requirement on. Requiring the aircraft to rotate in under 5 *sec* is a somewhat arbitrary but reasonable assumption. This constraint was incorporated into the code before take-off distance calculation was developed and included.

the thrust available during flight must be sufficient to overcome drag. It is desirable to use the smallest engine possible, while satisfying all of the mission requirements.

# Chapter 3

## Design Formulation

Our design problem is to optimize an HSCT configuration to minimize takeoff gross weight (TOGW) for a range of 5500 n.mi., and 251 passengers. Our main mission is a supersonic cruise-climb at Mach 2.4 with a maximum altitude of 70,000 *ft*. In this work, we expand our mission to include take off, a subsonic cruise at Mach 0.9, and a minimum time climb with a dynamic pressure limit.

The choice of gross weight as the figure of merit (objective function) directly incorporates both aerodynamic and structural considerations, in that the structural design directly affects aircraft empty weight and drag, while aerodynamic performance dictates the required fuel weight. Trim, control, and propulsion requirements are explicitly treated also. The current work incorporates the influence of structural considerations in the aerodynamic design by a variable-complexity modeling approach. We employ the weight equations of McCullers<sup>11</sup>. A procedure called *interlacing* is used to estimate stability and control derivatives. Variable-complexity modeling and interlacing will be described in Chapter 4.

### 3.1 Design Variables

A key problem in MDO is to characterize the complete configuration with relatively few design variables. For the level of analysis considered here, costs limit this number



to be small, typically below 100. We have achieved this goal for a complex wing-body configuration by selecting a few parameters which contain the primary effects required to provide flexible, realistic parametric geometry. We then utilize physical or geometric bases for representing the entire configuration using these parameters. We develop this geometry model for a specific baseline configuration. Although the geometries developed are not completely general, they have sufficient generality to identify the key design trends. More design variables would improve the generality of the configurations at a significant increase of computational cost.

The model we have developed to characterize the geometry completely defines the configuration using 29 design variables. While the configuration is defined using this set of parameters, the aircraft geometry is actually stored as a discrete numerical description in the Craidon format<sup>27</sup>.

The variables fall into seven categories: wing planform, airfoil, nacelle placement, engine thrust, fuselage shape, mission variables, and tail areas. Table 1 presents the set of design variables.

The eight design parameters used to define the planform are shown in Fig. 5. The leading and trailing edges of the wing are defined using a blending of linear segments, as described in Ref. [28]. The airfoil sections have round leading edges. We define the thickness distribution using an analytic description<sup>29</sup>. It is defined by four parameters: the thickness-to-chord ratio,  $t/c$ , the leading-edge radius parameter,  $I$ , the chordwise location of maximum thickness,  $m$ , and the trailing-edge half angle,  $\tau_{TE}$ ; see Fig. 6. The thickness distribution at any spanwise station is then defined using the following rules:

1. The wing thickness-to-chord ratio is specified at the wing root, the leading-edge break and the wing tip. The wing thickness varies linearly between these control points.
2. The chordwise location of maximum airfoil thickness is constant across the span.
3. The airfoil leading-edge radius parameter is constant across the span. The leading edge radius-to-chord ratio,  $r_t$ , is defined by  $r_t = 1.1019 [(t/c) (I/6)]^2$ .

Table 1: Design Variables

Baseline		
Number	Value	Description
1	142.01	Wing root chord ( <i>ft.</i> )
2	99.65	L.E. break, x ( <i>ft.</i> )
3	28.57	L.E. break, y ( <i>ft.</i> )
4	142.01	T.E. break, x ( <i>ft.</i> )
5	28.57	T.E. break, y ( <i>ft.</i> )
6	138.40	L.E. wing tip, x( <i>ft.</i> )
7	9.30	Wing tip chord, ( <i>ft.</i> )
8	67.32	Wing semi-span, ( <i>ft.</i> )
9	0.50	Chordwise max <i>t/c</i> location
10	4.00	L.E. radius parameter
11	2.96	Airfoil <i>t/c</i> at root, %
12	2.36	Airfoil <i>t/c</i> at L.E. break, %
13	2.15	Airfoil <i>t/c</i> at tip, %
14	70.00	Fuselage restraint 1, x ( <i>ft.</i> )
15	6.00	Fuselage restraint 1, r ( <i>ft.</i> )
16	135.00	Fuselage restraint 2, x( <i>ft.</i> )
17	5.80	Fuselage restraint 2, r( <i>ft.</i> )
18	170.00	Fuselage restraint 3, x( <i>ft.</i> )
19	5.80	Fuselage restraint 3, r( <i>ft.</i> )
20	215.00	Fuselage restraint 4, x( <i>ft.</i> )
21	6.00	Fuselage restraint 4, r( <i>ft.</i> )
22	17.79	Nacelle 1, y ( <i>ft.</i> )
23	32.07	Nacelle 2, y ( <i>ft.</i> )
24	290,905	Mission fuel, ( <i>lbs.</i> )
25	50,000	Starting cruise altitude, ( <i>ft.</i> )
26	100.00	Cruise climb rate, ( <i>ft/min</i> )
27	450.02	Vertical tail area, ( <i>ft</i> <sup>2</sup> )
28	750.00	Horizontal tail area, ( <i>ft</i> <sup>2</sup> )
29	46,000	Maximum sea level thrust per engine, ( <i>lbs</i> )

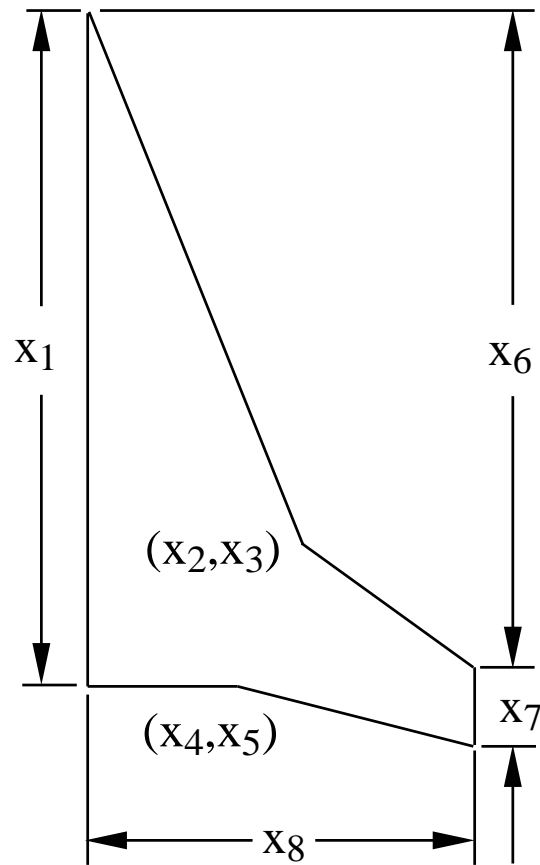


Figure 5: Planform Definition Parameters

- The trailing-edge half-angle of the airfoil section varies with the thickness-to-chord ratio according to  $\tau_{TE} = 3.03125(t/c) - 0.044188$ . This relationship is fixed throughout the design.

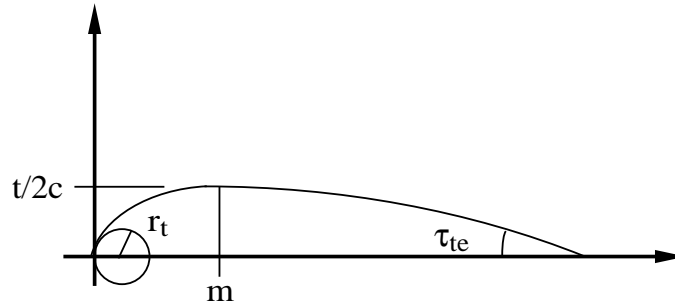


Figure 6: Airfoil Thickness Parameters

The nacelle locations are allowed to vary during the optimization process. However, we do not consider thermal and exhaust scrubbing effects, and hence fix the axial location of the nacelles in relation to the wing's trailing edge. We used a value of 25% overhang. Another design variable specifies the maximum engine thrust. The nacelle diameter and length are scaled by the square root of the ratio of current thrust to baseline thrust. The weight of the engine is also a function of this ratio.

The fuselage is assumed to be axisymmetric with area ruling. The axial location and radius of each of four *restraint* locations are the design variables<sup>18</sup>. We define the shape of the fuselage between these restraints by requiring that it be a minimum wave-drag body for the specified length and volume<sup>30</sup>. The vertical tail and horizontal tail are trapezoidal planforms. For each of these control surfaces, the aspect ratio, taper ratio, and quarter-chord sweep are specified, and the area varies<sup>31</sup>. The geometric model can be extended. However, this model provides a wide range of designs and is a simplification of our original model.

Three variables define the idealized cruise mission. One variable is the mission fuel and the other two specify the Mach 2.4 cruise in terms of the initial supersonic cruise altitude and the constant climb rate used in the range calculation. The resulting aircraft range is calculated using the fuel weight design variable, assuming that 85% of the mission fuel is used in cruise and the remaining 15% is the reserve fuel.

## 3.2 Constraints

The constraints used in the problem fall into three categories: constraints implicit in the analysis, performance/aerodynamic constraints, and geometric constraints. The implicit constraints are not handled by the optimization program, but rather are part of the analysis or geometry:

1. The maximum altitude, 70,000 *ft*, is enforced in the range calculation.
2. The fuselage volume is fixed at 23,270 *ft*<sup>3</sup> and the fuselage length is fixed at 300 *ft*.
3. The axial location of the wing's MAC quarter chord is adjusted to match the value found on the baseline configuration (147.3 *ft* aft of the aircraft nose).
4. The nacelles are fixed axially as noted in Section 3.1 above. In the studies done with engine thrust fixed at 39,000 *lbs*, the nacelles are approximately 27 *ft* long and 5 *ft* in diameter. When the thrust is allowed to vary, the baseline thrust is 46,000 *lbs*, the baseline length and diameter are 35 *ft* and 6.5 *ft*, respectively.

Aside from these implicit constraints we also use up to 70 explicit constraints, summarized in Table 2. The range is constrained to be 5500 *n.mi.* or more. The  $C_L$  at landing speed must be less than 1, the  $C_\ell$  for each of the 18 wing sections must be less than 2 \* (an elliptic load distribution is assumed), and the landing angle of attack is constrained to be less than or equal to 12°. The mission fuel must not require more space than the available fuel volume, which we assume to be 50% of the total wing volume.

Another group of constraints is designed to keep the optimizer from developing geometrically impossible or implausible designs. For example, a constraint is used to prevent the design of a wing which is highly swept back into a spiked shape. In this category are the thickness-to-chord constraints, without which the optimizer could attempt to create a wing with negative thickness. The constraint numbered 51

---

\*Although high, this constraint prevents excessively small chords during intermediate iterations. This constraint is rarely active for a final design, except possibly at the tip.

forces the wing’s trailing edge to end before the horizontal tail’s leading edge begins. Constraints 64 and 65 require nacelle 1 to be outboard of the fuselage and inboard of nacelle 2. Constraint 66 requires the aircraft trim with two engines out if the vertical tail is included in the optimization; otherwise the outer nacelle limit is fixed at 50% semi-span.

Table 2: Optimization Constraints

Number	Description
1	Range $\geq 5,500$ <i>n.mi.</i>
2	Required $C_L$ at landing speed $\leq 1$
3-20	Section $C_\ell \leq 2$
21	Landing angle of attack $\leq 12^\circ$
22	Fuel volume $\leq$ half of wing volume
23	Spike prevention
24-41	Wing chord $\geq 7.0$ <i>ft.</i>
42-45	Engine scrape at landing
46	Wing tip scrape at landing
47	Rudder deflection for crosswind landing $\leq 22.5^\circ$
48	Bank angle for crosswind landing $\leq 5^\circ$
49	Takeoff rotation to occur $\leq 5$ <i>sec</i> <sup>a</sup>
50	Tail deflection for approach trim $\leq 22.5^\circ$
51	Wing root T.E. $\leq$ horiz. tail L.E.
52	Balanced field length $\leq 10,000$ <i>ft</i> <sup>a</sup>
53	T.E. break scrape at landing with $5^\circ$ roll
54	L.E. break $\leq$ semispan
55	T.E. break $\leq$ semispan
56-58	Root, break, tip $t/c \geq 1.5\%$
59-63	Fuselage restraints in order
64-65	Nacelles in order
66	Engine-out limit with vertical tail design; otherwise 50%
67-70	Maximum thrust required $\leq$ available thrust

<sup>a</sup>Sensitivity to these constraints is examined in Section 6.6

Trim and control considerations require 11 constraints: numbers 42–50, 53 and 66 in Table 2, most of which are related to landing. The landing constraints are enforced for assumed emergency conditions, i.e. a landing altitude of 5,000 *ft* with an

outside temperature of 90° F, and with the aircraft carrying 50% fuel. The vertical tail is sized based on either the requirement that the aircraft be capable of trimmed flight with two engines on the same side inoperative or to meet the 20 *kt* crosswind landing requirement. The pilot must have sufficient control authority to trim the aircraft in these situations, as well as to be able to perform necessary maneuvers safely. Therefore, we require the aircraft be trimmed directionally using no more than 75% of the available control authority and limit bank to 5°. For the engine-out condition these constraints are implicit in the analysis. For the crosswind landing requirements these are explicit in constraints 47 and 48.

The engine nacelle strike constraint requires that the nacelles do not strike the runway during landing, which limits the allowable spanwise engine location. This is checked at main gear touch down, with the aircraft at the landing angle of attack and 5° bank, the typical certification requirement. This constraint not only limits the spanwise engine location, but effectively limits the allowable trailing edge sweep, because the nacelles are mounted at the trailing edge, with 25% overhang. Another constraint checks wing tip strike under the same conditions. During the crosswind landing, the aileron and rudder deflections are limited to 75% of maximum, or 22.5°, and the bank must be less than 5°.

Constraints on take-off rotation time (no. 49) and approach trim (no. 50) determine the size of the horizontal tail. We require the aircraft rotate to lift-off attitude in less than 5 *seconds*<sup>†</sup>. For the approach trim, the aircraft must trim at the approach attitude with a horizontal tail deflection of less than 22.5°.

The constraint on the balanced field length insures the aircraft can operate from existing airports. Requiring the BFL be less than 10,000 *ft*<sup>†</sup> allows the aircraft to use most major airports in the world. This constraint limits the maximum wing loading and the minimum thrust to weight ratio. The final four constraints require the maximum thrust required in each segment of the mission be less than the thrust that is actually available at the given flight condition.

---

<sup>†</sup>The impact of these constraints is investigated in Section 6.6.

# Chapter 4

## Variable Complexity Modeling

A growing practice in MDO is the use of approximation associated with what we term variable-complexity modeling (VCM). For example, the structural design of an aircraft is often performed with a complex structural model, but with loads obtained from simple aerodynamic models. Similarly, the aerodynamic designer may use advanced aerodynamic models with a simple structural model to account for wing flexibility effects.

We employ a VCM approach using both the simple and complex models during the optimization procedure. Our aim is to take advantage of the low computational cost of the simpler models while improving their accuracy with periodic use of the more sophisticated models. The sophisticated models provide scale factors for correcting the simpler models. These scale factors are updated periodically during the design process. For example, in Ref. [16] we combined the use of simple and complex aerodynamic models to predict the drag of an HSCT during the optimization process. Similarly, in Ref. [19] we employed structural optimization together with a simple weight equation to predict wing structural weight in combined aerodynamic and structural optimization of the HSCT. We have also used this approach to handle the estimation of stability and control derivatives<sup>31</sup>.

The variable-complexity modeling approach is used within a sequential approximate optimization technique whereby the overall design process is composed of a



series of optimization cycles. Each optimization cycle is performed using approximate analysis. At the beginning of each cycle, approximations are constructed using either scaled, global-local or interlacing approximations. The optimization converges using only the approximate analysis, but move limits are imposed on the design variables to limit the discrepancies between the approximate and the complex analysis. These discrepancies result in constraint violations. The approximations must be updated and the design must be refined by continuing the optimization. This process continues until the design converges and the constraints are satisfied.

The scaled approximation employs a constant scaling function  $\sigma(\mathbf{x})$ , where  $\mathbf{x}$  represents a vector of design variables, given as

$$\sigma(\mathbf{x}_0) = \frac{f_d(\mathbf{x}_0)}{f_s(\mathbf{x}_0)}, \quad (1)$$

where  $f_d$  represents a detailed model analysis result, and  $f_s$  represents a simple model analysis result, both evaluated at a specified design point,  $\mathbf{x}_0$ , at the beginning of an optimization cycle. During an optimization cycle the scaled approximate analysis results,  $f(\mathbf{x})$ , are calculated as

$$f(\mathbf{x}) \approx \sigma(\mathbf{x}_0)f_s(\mathbf{x}). \quad (2)$$

Thus, the scaled simple analysis is used throughout the cycle until convergence. Then a new value of the scale factor is computed and the optimization is repeated. Move limits are imposed during the optimization cycles.

A procedure which varies the scale factor during the optimization cycles is called the global-local approximation technique. The approximation is again constructed from the simple model

$$f(\mathbf{x}) \approx \sigma(\mathbf{x})f_s(\mathbf{x}) \quad (3)$$

with the scaling parameter approximated using

$$\sigma(\mathbf{x}) \approx \sigma(\mathbf{x}_0) + \nabla\sigma \cdot (\mathbf{x} - \mathbf{x}_0) \quad (4)$$

The gradient of  $\sigma$  at  $\mathbf{x}_0$  is performed by forward finite differences involving both  $f_d$  and  $f_s$ . In our aerodynamic analysis we have used the scaled approximation for the drag due to lift and the global-local for the wave drag<sup>16, 18</sup>.

For more expensive analyses the scaled approximation is used, but with the scale factor updated only every fifth cycle. This procedure, called interlacing, is used for estimating the stability and control derivatives. The complex model is used after every five optimization cycles. (The choice of five is somewhat arbitrary). The stability derivatives calculated by the complex model are used to provide scale factors for the next five optimization cycles. The simple and complex models used to estimate the stability derivatives are described in Section 5.4. Interlacing has also been used by Dudley *et al.*<sup>19</sup> for estimating wing weight.

# Chapter 5

## Analysis Methods

To analyze trim and control conditions it is necessary to obtain information not normally used in initial sizing programs. This includes the location of the center of gravity ( $cg$ ), the inertias, and the stability and control derivatives. These are found for a given geometry and flight condition. We continue to use the aerodynamic drag analysis and representation of the wing structure using weight equations used previously, these are briefly described in the following sections. Detailed descriptions of these can be found in References [16, 17, 18].

### 5.1 Aerodynamics

The primary aerodynamic analysis is the calculation of drag at cruise, consisting of the contributions from volumetric wave drag, drag due to lift, and friction drag. We have used detailed and approximate models for both the wave drag and the drag due to lift calculations.

The detailed wave drag estimates are calculated using the Harris<sup>32</sup> wave drag program. This program computes the value of the far-field integral arising from slender-body theory, and has been found to adequately predict the wave drag of supersonic transport class aircraft. However, we found that the drag estimates do not vary smoothly with geometry, presenting difficulties in derivative estimation. Our

approximate wave drag model continues to use the classical far-field slender body formulation, and is due to Hutchison<sup>33</sup>. To reduce the computational time, the oblique cross-sectional area calculations are replaced by the use of the normal areas of an assemblage of axisymmetric bodies distributed spatially to represent the wing volume. This model, although not as accurate as the classical Harris wave drag model, was shown to predict trends for differing designs accurately. Computationally, the approximate model is roughly 50 times faster than the Harris code analysis.

The drag due to lift is calculated using linear theory, which has been shown by Hollenback and Bloom<sup>34</sup> to provide results comparable to the parabolized Navier-Stokes predictions for an HSCVT configuration. Using linear supersonic aerodynamics, the computations reduce to the calculation of the drag polar shape parameter  $1/C_{L\alpha} - C_T/C_L^2$ , where  $C_{L\alpha}$  is the wing lift-curve slope, and  $C_T$  is the thrust coefficient. The component of drag due to lift is then given by

$$C_{D_t} = (1/C_{L\alpha} - C_T/C_L^2)C_L^2 \quad (5)$$

For this analysis, we use the methods developed by Carlson *et al.*<sup>35, 36</sup> which solve the linearized supersonic potential equation for wings of arbitrary planform. The panel method implementation provides the detailed prediction of drag due to lift. The value of  $C_T$  obtained by linear theory is then reduced to levels expected using Carlson’s *attainable thrust* concept<sup>36</sup> to simulate the levels that could be achieved by detailed design for camber and twist.

As a simpler approximation to the drag due to lift, the wing is replaced by an equivalent cranked delta wing<sup>18</sup>. Assuming that the flow can be described by linearized supersonic thin-wing theory, analytical solutions are available for cranked delta wings<sup>37</sup>. First we define a correspondence between a general wing and the cranked delta wing. Details of this process are given in References [18] and [33].

Both the panel code and the Harris wave drag code produce “wiggly” results when examined on a fine-scale level. Figure 7 provides an example. The noisy analysis results present difficulties in the numerical evaluation of derivatives. The authors of the codes never anticipated the need for such smoothness in the predictions. In contrast, the algebraic model yields smooth results. Computationally, the time required

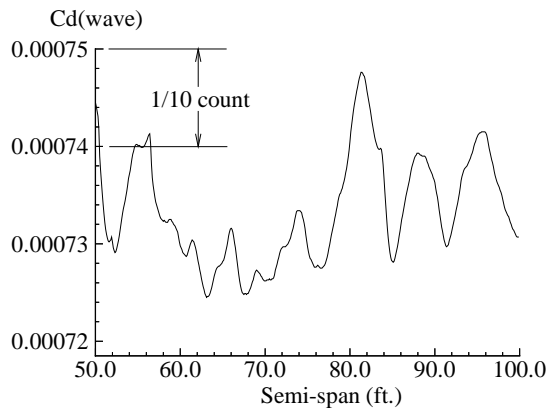


Figure 7: Effect of increasing semi-span on wave drag prediction

to calculate the drag due to lift using the linearized theory model is more than two orders of magnitude smaller than that required for the panel method code.

Skin friction is computed using standard algebraic estimates. The boundary layer is assumed to be turbulent. The Van Driest II method, as recommended by Hopkins and Inouye<sup>38</sup> has been utilized and form-factor corrections have been applied to account for the effect of surface curvature.

The low aspect ratio configurations required for efficient supersonic flight have low values of subsonic lift-curve slope,  $C_{L_\alpha}$ . This requires the aircraft fly at high angles of attack during low speed flight, especially landing. As with the supersonic aerodynamics, we employ two levels of modeling to estimate the subsonic aerodynamics. A vortex-lattice code serves as the detailed model for estimating the subsonic lift-curve slope, while the simple model uses a  $C_{L_\alpha}$  model due to Diederich<sup>39</sup>. Leading-edge vortex effects are incorporated through the Polhamus suction analogy<sup>40</sup> and the influence of ground effect during landing is included using the slender-wing correlation of experimental data found in Küchemann<sup>41</sup>. The details of this computation are discussed in Ref. [17].

## 5.2 Structures

We use the weight equations taken from FLOPS<sup>11</sup> to determine the takeoff gross weight, and to estimate the effect of wing geometry change on structural weight. For the wing bending-material weight, which is the major part of the structural weight affected by the geometry, we use structural optimization as a more sophisticated estimation method. We incorporate the structural optimization using our interlacing technique, which is described in Chapter 4.

The structural optimization procedure, described in Ref. [15], minimizes the wing weight for a fixed given arrangement of the spars and ribs with the thicknesses of skin panels, spar and rib cap areas as design variables. There are a total of 40 design variables, 26 are for the skin panel thicknesses, 12 are for the spar cap areas, and 2 are for the rib cap areas. The structural optimization is performed by sequential linear programming with a typical starting move limit of 20%.

Our finite-element model consists of 963 elements, 193 nodes, and has 1032 degrees of freedom. To deal with many different aerodynamic optimization designs, we developed a program to automatically generate the finite-element models. The geometry of the aircraft is input to the program as a Craidon geometry description file. We also specify the number of frames in the fuselage, the number of spars and ribs in the wing, and the chord fractions taken by the leading and trailing-edge control surfaces. The outputs of the program are the finite-element nodal coordinates, element topology data, the locations of all non-structural weights, and the geometric definition of all the fuel tanks.

The EAL<sup>42</sup> program is used for the finite-element analysis. The loads applied to the structural model are composed of the aerodynamic forces and the inertia forces due to the distributed weight of the structure, non-structural items, and fuel. The static aeroelastic effects of load redistribution are discussed in Ref. [15] where it is shown that they can be ignored without introducing a large error. It is important to note that structural and non-structural weights except for the wing bending-material weight were estimated by the FLOPS weight equations.

Aerodynamic loads are generated on the wing using the same codes that were

developed for the aerodynamic optimization. That is, the loads in supersonic flight are determined from the supersonic panel method, and loads in subsonic flight from the vortex-lattice method. In the aerodynamic design we did not specify a wing camber distribution. For structural loads, however, the wing camber and twist affect the aerodynamic load directly. We used Carlson’s WINGDES<sup>35</sup> program to define the cruise twist and camber. The wing structure is assumed to be rigid for the aerodynamic forces. The loads at the aerodynamic nodes are mapped to the structural node points using a two-dimensional interpolation scheme.

We selected the critical loads from Barthelemy *et al.*<sup>43</sup>. We consider five load cases. Load case 1 is a supersonic cruise. Case 2 is a transonic case. Cases 3 and 4 are subsonic and supersonic pull-ups. Finally, case 5 examines taxiing loads. The cases are summarized in Table 3.

Table 3: Load cases used in structural optimization

Load case	Mach number	Load factor	Altitude (ft.)	% of fuel
1	2.4	1.0	63175	50
2	1.2	1.0	29670	90
3	0.6	2.5	10000	95
4	2.4	2.5	56949	80
5	0.0	1.5	0	100

### 5.3 Center of Gravity and Inertia Estimation

In stability and control calculations the location of the center of gravity is important, but estimation of the center of gravity in the preliminary design phase is not trivial. During cruise and landing approach, we attempt to place the *cg* at the center of pressure by transferring fuel between tanks. This minimizes the use of control surfaces to trim the aircraft, reducing drag during the cruise. We calculate the center of pressure for the wing at subsonic speed using a vortex lattice method (VLM) and, for this preliminary design, use this as the *cg*.

During take-off, it is not possible to place the  $cg$  at the center of pressure, and a more detailed estimation of the location of the  $cg$  must be used. We use expressions given by Roskam<sup>44</sup> to estimate the center of gravity of the various components, and place miscellaneous equipment, such as avionics and cargo, using an initial estimate of the aircraft layout. The fuselage  $cg$  is placed at 45% of the length. The wing  $cg$  is placed at 55% of the wing chord at 35% of the semispan. The horizontal tail  $cg$  is placed at 42% of the chord from the leading edge, at 38% of the semispan. The vertical tail  $cg$  is placed using the same formula as the horizontal tail. Finally, the engine  $cg$  is placed at 40% of the nacelle length. Once the  $cg$  for each of the components is calculated, it is straightforward to calculate the  $cg$  for the aircraft. The inertias for the aircraft are estimated using a routine from FLOPS<sup>11</sup> which is based on a modified DATCOM<sup>45</sup> method.

## 5.4 Stability Derivative Estimation

The analysis of the take-off rotation and engine out condition requires stability and control derivatives. We use two methods to calculate these derivatives; empirical algebraic relations from the U.S.A.F. Stability and Control DATCOM<sup>45</sup>, as interpreted by J. Roskam<sup>46</sup>, and a VLM code developed by Kay<sup>22</sup>. The DATCOM methods rely on simple theories and some experimental data, and do not handle unusual configurations well. The VLM code is better able to handle different configurations, but is more expensive computationally.

The primary use of the simple method is to predict the trends of the derivatives, as the design of our aircraft changes. Then, these trends are used with a more accurate prediction to update the stability derivatives. To predict the trends, we use the estimation methods from DATCOM.

### 5.4.1 Lateral-Directional Derivatives

We assume the vertical tail affects six of the nine primary lateral-directional stability and control derivatives:  $C_{y\beta}$ ,  $C_{l\beta}$ ,  $C_{n\beta}$ ,  $C_{y\delta_r}$ ,  $C_{l\delta_r}$ , and  $C_{n\delta_r}$ . The other three



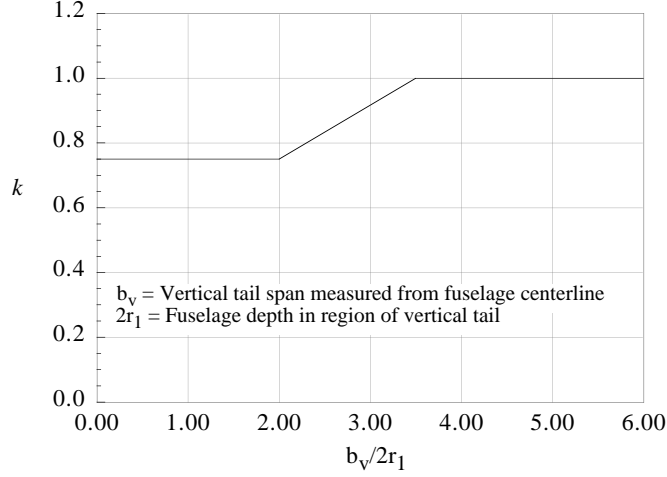


Figure 8: Definition of  $k$  for  $C_{y_{\beta_v}}$

derivatives,  $C_{y_{\delta_a}}$ ,  $C_{l_{\delta_a}}$ , and  $C_{n_{\delta_a}}$ , are assumed to be independent of changes in the vertical tail size. In the case of  $C_{y_{\beta}}$ ,  $C_{l_{\beta}}$ , and  $C_{n_{\beta}}$ , only the vertical tail contribution to the stability derivative is calculated, since that is the only contribution that should change with a change in vertical tail size and these values are used to scale the more accurate VLM predictions. All of the equations in this section are from Ref. [46].

The vertical tail contribution for  $C_{y_{\beta}}$ , is calculated using:

$$C_{y_{\beta_v}} = -k C_{L_{\alpha_v}} \left( 1 + \frac{d\sigma}{d\beta} \right) \eta_v \frac{S_v}{S} \quad (6)$$

where  $k$  is an empirical factor defined in Figure 8.

The term  $\left( 1 + \frac{d\sigma}{d\beta} \right) \eta_v$  is calculated from:

$$\left( 1 + \frac{d\sigma}{d\beta} \right) \eta_v = 0.724 + 3.06 \left( \frac{S_v S}{1 + \cos \Lambda_{c/4}} \right) + 0.4 \frac{Z_w}{d} + 0.009 AR \quad (7)$$

where  $Z_w$  is the vertical distance from the wing root quarter chord point to the fuselage centerline, positive downward and  $d$  is the maximum fuselage diameter at the wing-body junction.

The vertical tail lift-curve slope is calculated using:

$$C_{L_{\alpha_v}} = \frac{2\pi AR_{v_{eff}}}{2 + \sqrt{\frac{AR_{v_{eff}}^2}{k^2} (\beta^2 + \tan^2 \Lambda_{c/2})} + 4} \quad (8)$$

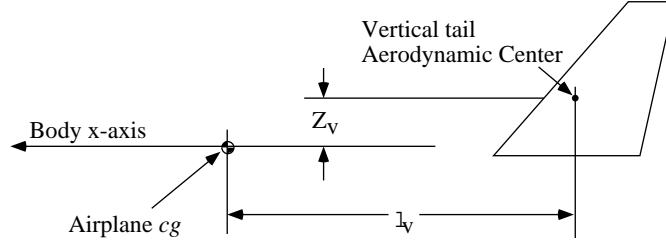


Figure 9: Definition of  $\ell_v$  and  $Z_v$

with  $\beta_M = \sqrt{1 - M^2}$ , and where  $\mathcal{AR}_{v_{eff}}$  comes from:

$$\mathcal{AR}_{v_{eff}} = \left( \frac{\mathcal{AR}_{v(B)}}{\mathcal{AR}_v} \right) \mathcal{AR}_v \quad (9)$$

with  $\mathcal{AR}_v$  being the geometric aspect ratio for the isolated vertical tail,  $\mathcal{AR}_{v(B)}/\mathcal{AR}_v$  is the ratio of the aspect ratio of the vertical panel in the presence of the body to that of the isolated panel, assumed to be 1. This method is only applicable to a single vertical tail on the plane of symmetry.

The vertical tail contribution to  $C_{l_{\beta_v}}$  is given as

$$C_{l_{\beta_v}} = C_{y_{\beta_v}} \left( \frac{Z_v \cos \alpha - \ell_v \sin \alpha}{b} \right) \quad (10)$$

where  $b$  is the wing span, and  $\ell_v$  and  $Z_v$  are the x and z distances, respectively, between the airplane center of gravity and the vertical tail aerodynamic center, see Figure 9.

Similarly, the vertical tail contribution to  $C_{n_{\beta}}$  is given as

$$C_{n_{\beta_v}} = -C_{y_{\beta_v}} \left( \frac{\ell_v \cos \alpha + Z_v \sin \alpha}{b} \right) \quad (11)$$

The derivative  $C_{y_{\delta r}}$  is calculated by:

$$C_{y_{\delta r}} = C_{L_{\alpha_v}} \left[ \frac{(\alpha_{\delta})_{C_L}}{(\alpha_{\delta})_{C_\ell}} \right] (\alpha_{\delta})_{C_\ell} K' K_b \frac{S_v}{S} \quad (12)$$

where  $\left[ \frac{(\alpha_{\delta})_{C_L}}{(\alpha_{\delta})_{C_\ell}} \right]$  and  $(\alpha_{\delta})_{C_\ell}$  are calculated from Figure 10, and  $K_b$  is found using:

$$K_b = \frac{2}{\pi} \left[ b_f \sqrt{1 - b_f^2} + \sin^{-1} b_f \right] \quad (13)$$

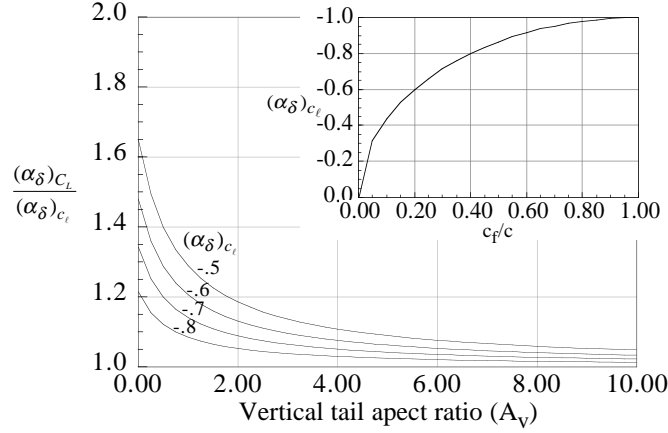


Figure 10: Definition of  $\left[ \frac{(\alpha_\delta)_{C_L}}{(\alpha_\delta)_{C_L}} \right]$

where  $b_f$  is the rudder span. As a first approximation,  $K'$  was assumed to be 1.

The derivative  $C_{l_{\delta_r}}$  is found from:

$$C_{l_{\delta_r}} = C_{y_{\delta_r}} \left( \frac{Z_v \cos \alpha - \ell_v \sin \alpha}{b} \right) \quad (14)$$

Similarly,  $C_{n_{\delta_r}}$  is found from:

$$C_{n_{\delta_r}} = C_{y_{\delta_r}} \left( \frac{\ell_v \cos \alpha + Z_v \sin \alpha}{b} \right) \quad (15)$$

#### 5.4.2 Accuracy of Lateral-Directional Estimates

To test the accuracy of the DATCOM and VLM based predictions, we compared the results from both methods with experimentally determined stability and control derivatives. We modeled an XB-70A, in the powered approach configuration, using data from Heffley<sup>47</sup>. Since the vertical tail is the primary factor in this calculation, only the vertical tail contribution is calculated for the  $\beta$  derivatives. Similarly, the effect of the aileron derivatives is considered small, so these are not calculated with the DATCOM methods, but are updated with the VLM estimates.

Table 4 compares the experimental results with the VLM and DATCOM approximations. Generally, the VLM results are good, although there are sign discrepancies

Table 4: Comparison of stability and control derivative estimations for the XB-70A

Derivative	Experimental	VLM	DATCOM
$C_{y\beta}$	-0.183	-0.177	-0.088
$C_{l\beta}$	-0.072	-0.011	0.0016
$C_{n\beta}$	0.132	0.042	0.036
$C_{y\delta r}$	0.120	0.152	0.072
$C_{l\delta r}$	-0.0018	0.0035	-0.0013
$C_{n\delta r}$	-0.103	-0.077	-0.029
$C_{y\delta a}$	-0.063	0.0	0.0
$C_{l\delta a}$	0.042	-0.095	—
$C_{n\delta a}$	-0.0052	0.0086	—

on  $C_{l\delta r}$ ,  $C_{l\delta a}$  and  $C_{n\delta a}$ . The error in the aileron derivatives is due to different sign conventions. Heffley defines a positive aileron deflection as resulting in a positive rolling moment. Kay defines a positive aileron deflection as resulting in a positive lift increment. The error in  $C_{l\delta r}$  is possibly due to poor modeling of the XB-70A in Kay's VLM code, which defines the planform and the side view with 5 trapezoids for each. A code which allows for a more detailed model could improve these results. The DATCOM results also have a sign discrepancy, on  $C_{l\beta}$ , but this term is only the tail contribution, not the derivative for the entire aircraft.

Comparison of experimental, VLM, and DATCOM results for a F/A-18 from Kay shows good agreement between the experimental and the VLM data, notably the  $C_{n\beta}$  and  $C_{n\delta r}$  derivatives. Some of his results<sup>22</sup> are shown in Table 5. Razgonyaev and Mason<sup>48</sup> also compared these techniques. They found the DATCOM techniques were good for conventional aircraft, but the VLM based techniques were better for designs like the HSCT.

### 5.4.3 Longitudinal Derivatives

We are interested in two longitudinal control derivatives,  $C_{L\delta_e}$  and  $C_{M\delta_e}$ .  $C_{L\delta_e}$  is estimated using a VLM routine. The aircraft is analyzed at zero angle of attack with the horizontal tail undeflected and then again with the horizontal tail deflected. The difference in lift for these two cases is used to calculate  $C_{L\alpha_{HT}}$ , the horizontal tail lift

Table 5: Comparison of stability and control derivative estimations for a F/A-18 at Mach 0.2, out of ground effect

Derivative	Experimental	VLM	DATCOM
$C_{y\beta}$	-0.917	-0.526	-0.561
$C_{l\beta}$	-0.050	-0.080	-0.055
$C_{n\beta}$	0.096	0.086	0.066
$C_{y\delta r}$	0.134	0.108	0.103
$C_{l\delta r}$	0.012	0.017	0.015
$C_{n\delta r}$	-0.046	-0.045	-0.030
$C_{l\delta a}$	0.150	0.167	0.136

curve slope. The horizontal tail lift curve slope is assumed to be constant throughout the optimization cycle, since the shape of the horizontal tail is fixed. The change in lift coefficient due to horizontal tail deflection is calculated from

$$C_{L\delta e} = C_{L\alpha_{HT}} \frac{S}{S_{HT}}. \quad (16)$$

The approximate pitching moment stability derivative is calculated by applying the moment arm between the pitching moment reference location, and the horizontal tail aerodynamic center. The pitching moment reference location is the aerodynamic center of the aircraft, which is also calculated by the VLM code and assumed to be at a constant percentage of the wing root chord throughout an optimization cycle. The horizontal tail aerodynamic center is assumed to be at the quarter chord of the mean aerodynamic chord.

The detailed calculation for  $C_{M\alpha}$  is also performed using the VLM routine. The routine calculates the pitching moment at zero angle of attack and at one degree angle of attack. The difference in these pitching moments divided by the change in angle of attack in radians is  $C_{M\alpha}$ . Because there is no camber or twist in our wing, the zero lift pitching moment,  $C_{M_0}$ , is zero.

## 5.5 Landing Gear

The position of the main gear is calculated using the calculated  $cg$  location and specifying the tipback angle. We found that a tipback angle of  $15^\circ$  resulted in a reasonable position for the main gear. This is slightly higher than the angle found on many large aircraft. The nose gear location is found using

$$x_{nose} = \frac{1}{0.115} (x_{cg} - 0.885x_{main}) \quad (17)$$

where the distances are measured from the nose of the aircraft to the nose gear for  $x_{nose}$ , to the  $cg$  for  $x_{cg}$ , and to the main gear for  $x_{main}$ . This equation positions the nose gear so it supports 11.5% of the TOGW. After the landing gear positions are known, the overturn angle can be calculated.

## 5.6 Engine Out

After finding the stability derivatives for a given tail size, we calculate the control surface deflections and engine location required for trimmed flight. In trimmed flight the sum of the forces and moments must be zero. This can be expressed with the following equations:

$$\text{Sideforce:} \quad C_{y\delta_a} \delta_a + C_{y\delta_r} \delta_r + C_{y\beta} \beta + C_L \sin \phi = -\frac{Y_{ext}}{qSb} \quad (18)$$

$$\text{Rolling Moment:} \quad C_{l\delta_a} \delta_a + C_{l\delta_r} \delta_r + C_{l\beta} \beta = -\frac{L_{ext}}{qSb} \quad (19)$$

$$\text{Yawing Moment:} \quad C_{n\delta_a} \delta_a + C_{n\delta_r} \delta_r + C_{n\beta} \beta = -\frac{N_{ext}}{qSb} \quad (20)$$

By assuming that the net rolling moment,  $L_{ext}$ , and the net side force,  $Y_{ext}$ , are zero, equations (18) - (20) can be solved for bank angle,  $\phi$ , aileron deflection,  $\delta_a$ , and net yawing moment,  $N_{ext}$ .

$$\phi = \sin^{-1} \left( \frac{\delta_r \left( \frac{C_{y\delta_a} C_{l\delta_r}}{C_{l\delta_a}} - C_{y\delta_r} \right) - \beta \left( C_{y\beta} - \frac{C_{y\delta_a} C_{l\beta}}{C_{l\delta_a}} \right)}{C_L} \right) \quad (21)$$

$$\delta_a = -\frac{C_{l_{\delta_r}} \delta_r + C_{l_{\beta}} \beta}{C_{l_{\delta_a}}} \quad (22)$$

$$N_{ext} = -qSb \left( C_{n_{\delta_a}} \delta_a + C_{n_{\delta_r}} \delta_r + C_{n_{\beta}} \beta \right) \quad (23)$$

The bank angle is determined by minimizing  $\beta$ , without violating the  $5^\circ$  limit imposed on  $\phi$ . Equation (22) can be solved by setting the rudder deflection to 75% of the maximum allowable. Then Eq. (23) is solved for the yawing moment.

## 5.7 Crosswind Landing

We required the aircraft be able to land with a 20 knot crosswind. Assuming an approach speed of 145 knots, this results in a sideslip angle of  $7.85^\circ$ . The aircraft must be able to trim directionally at a sideslip of  $7.85^\circ$ . Using equations (18) through (20), where  $\beta$  is known, and all right hand side terms are zero, it is possible to solve for bank angle,  $\phi$ , aileron deflection,  $\delta_a$ , and the rudder deflection,  $\delta_r$ . This results in

$$\delta_r = \frac{(C_{n_{\delta_a}} C_{l_{\beta}} - C_{l_{\delta_a}} C_{n_{\beta}})}{(C_{n_{\delta_r}} C_{l_{\delta_a}} - C_{n_{\delta_a}} C_{l_{\delta_r}})} \beta \quad (24)$$

$$\delta_a = -\frac{C_{l_{\delta_r}} \delta_r + C_{l_{\beta}} \beta}{C_{l_{\delta_a}}} \quad (25)$$

$$\phi = \sin^{-1} \left[ -\frac{1}{C_L} (C_{y_{\delta_a}} \delta_a + C_{y_{\delta_r}} \delta_r + C_{y_{\beta}} \beta) \right] \quad (26)$$

## 5.8 Take Off Analysis

Takeoff can be broken into three segments: a ground run, rotation, and climb out. The takeoff can be simulated by integrating the equations of motion for each segment. The equations are integrated using a fifth order, self adapting Runge-Kutta method.

The longest segment is the ground run. Our analysis of this segment is based on the work of Powers<sup>49</sup>. The aircraft is initially stopped and accelerates to the rotation speed,  $V_r$ . The rotation speed is calculated from  $V_r = k_r V_s$ , where  $V_s$  is the aircraft stall speed and  $k_r$  is a user specified, non-dimensional factor, generally between 1.10

and 1.26. FAR 25.107 states  $V_r$  may not be less than 105% of  $V_{MC}$ , where  $V_{MC}$  is “the calibrated airspeed at which, when the critical engine is suddenly made inoperative, it is possible to maintain control of the airplane with that engine still inoperative and maintain straight flight with an angle of bank of not more than 5 degrees.”<sup>25</sup> Assuming  $V_{MC}$  is not less than  $1.05V_s$  leads to a lower bound on  $V_r$  of  $1.10V_s$ . FAR 25.149 specifies that  $V_{MC}$  may not exceed  $1.2V_s$ . In this situation,  $V_r$  must be greater than or equal to  $1.26V_s$ .

Wings of the type used for supersonic aircraft are often capable of flying at very high angles of attack without stalling. So, it is not useful to calculate stall speed using the maximum obtainable  $C_L$  which would occur at an angle of attack much higher than would be acceptable for takeoff or landing. Instead, we limit the maximum angle of attack and use the  $C_L$  obtained at this attitude. For our work, we limit the angle of attack to be no greater than  $12^\circ$ . This gives

$$V_s = \sqrt{\frac{2W}{\rho S C_L(\alpha = \alpha_{max})}} \quad (27)$$

therefore

$$V_r = k_r V_s = k_r \sqrt{\frac{2W}{\rho S C_L(\alpha = \alpha_{max})}} \quad (28)$$

Assuming there is no vertical or lateral motion, or any changes in the attitude of the aircraft during the ground run, eliminates all but one equation of motion, the equation for the horizontal acceleration. This is given by

$$a_x = \frac{g}{W} \{T [\cos(\Lambda_T + \alpha) + \mu_{grd} \sin(\Lambda_T + \alpha)] + qS (\mu_{grd} C_L - C_D) - \mu_{grd} W\} \quad (29)$$

where  $g$  is the acceleration of gravity,  $W$  is the TOGW,  $T$  is the thrust at the current speed and altitude,  $\Lambda_T$  is the thrust vectoring angle,  $\alpha$  is the angle of attack,  $\mu_{grd}$  is the coefficient of friction of the runway, generally between 0.02 and 0.03. The coefficients of lift and drag,  $C_L$  and  $C_D$ , are calculated in ground effect. The ground effect calculations are discussed in section 5.9. Finally,  $q$  is the dynamic pressure, and  $S$  is the wing area.

Assuming the thrust varies quadratically with airspeed in the takeoff speed range. This is given by:

$$T = T_0 + T_1 V + T_2 V^2 \quad (30)$$



where  $T_0$ ,  $T_1$ , and  $T_2$  are thrust coefficients and are determined by curve fitting engine data. This allows Equation (29) to be rewritten in the form:

$$a_x = \frac{dV}{dt} = AV^2 + BV + C \quad (31)$$

where

$$A = \left[ (\mu \sin \Lambda_T + \cos \Lambda_T) T_2 + \frac{1}{2} \rho S (\mu C_L - C_D) \right] \frac{g}{W} \quad (32)$$

$$B = (\mu \sin \Lambda_T + \cos \Lambda_T) T_1 \frac{g}{W} \quad (33)$$

$$C = (\mu \sin \Lambda_T + \cos \Lambda_T) T_0 \frac{g}{W} - \mu g \quad (34)$$

The assumption of no attitude changes during the ground run means the aerodynamic coefficients are constant. If we also assume the weight, friction coefficient, and the thrust vectoring angle are constant, then the coefficients  $A$ ,  $B$ , and  $C$  are constant and Eq. (31) can be integrated analytically. Rearranging to separate the variables, we have:

$$\int_{t_a}^{t_b} dt = \int_{V_a}^{V_b} \frac{dV}{AV^2 + BV + C}$$

There are two solutions to this integral, depending on the sign of  $R$ , which is defined as

$$R \equiv B^2 - 4AC$$

These solutions are

$$t_b - t_a = \frac{1}{\sqrt{R}} \ln \left| \frac{\ddot{V}_b - \sqrt{R} \ddot{V}_a + \sqrt{R}}{\ddot{V}_b + \sqrt{R} \ddot{V}_a - \sqrt{R}} \right| \quad R > 0 \quad (35)$$

$$= \frac{2}{\sqrt{-R}} \left[ \arctan \left( \frac{\ddot{V}_b}{\sqrt{-R}} \right) - \arctan \left( \frac{\ddot{V}_a}{\sqrt{-R}} \right) \right] \quad R < 0 \quad (36)$$

where  $\ddot{V} = 2AV + B$ . Given the initial and final velocities,  $V_a$  and  $V_b$ , these equations give the time required to accelerate or decelerate the aircraft.

Since we are interested in the takeoff distance, it is also necessary to relate distance and velocity. This is done by multiplying the left hand side of Eq. (31) by  $dX/dX$  and noting that  $dX/dt = V$ . After rearranging this results in

$$dX = \frac{V dV}{AV^2 + BV + C} \quad (37)$$

Using the same assumptions as above, this can be integrated directly, giving

$$X_b - X_a = \frac{1}{2A} \ln \left| \frac{\dot{V}_b}{\dot{V}_a} \right| - \frac{B}{2A} (t_b - t_a) \quad (38)$$

where  $\dot{V} = dV/dt$  is given in Eq. (31) and  $t_b - t_a$  is evaluated using the above equations.

The rotation segment is the most complicated and the shortest segment. It requires detailed geometric and weight data, and usually only lasts a few seconds. For these reasons, it is often approximated by continuing the ground run for 2-3 seconds. To determine if the aircraft can rotate to the lift-off attitude, it is necessary to integrate the horizontal vertical, and pitch rotation equations. We assume that this is one of the critical horizontal tail requirements, so it is necessary to perform the integration to determine horizontal tail size. The horizontal, vertical and pitch accelerations are calculated using:

$$a_x = \frac{g}{W} [T \cos(\Lambda_T + \alpha) - qSC_D - \mu_{grd} F_{mg}] \quad (39)$$

$$a_z = \frac{g}{W} [qSC_L + T \sin(\Lambda_T + \alpha) - W + F_{mg}] \quad (40)$$

$$\ddot{\theta}_{mg} = \frac{M_{mg}}{I_{yy_{mg}}} \quad (41)$$

The reaction force at the main gear,  $F_{mg}$ , must be non-negative. It is calculated from

$$F_{mg} = W - qSC_L - T \sin(\Lambda_T + \alpha) \quad (42)$$

if this is negative then  $F_{mg} = 0$ . When this term is positive, the vertical acceleration will always evaluate to zero. Obviously, the instant  $F_{mg}$  becomes non-positive is the moment of lift-off, and the aircraft will start to accelerate upwards.

The pitching moment about the main gear,  $M_{mg}$ , is calculated using

$$\begin{aligned} M_{mg} = & qS \left[ \bar{c}C_M + (C_D \cos \alpha - C_L \sin \alpha) z_{D_{mg}} + (C_L \cos \alpha + C_D \sin \alpha) x_{L_{mg}} \right] \\ & - W \left[ \left( \cos \alpha - \frac{a_x}{g} \sin \alpha \right) x_{cg_{mg}} - \left( \frac{a_x}{g} \cos \alpha + \sin \alpha \right) z_{cg_{mg}} \right] \\ & - T \left( z_{T_{mg}} \cos \Lambda_T - x_{T_{mg}} \sin \Lambda_T \right) \end{aligned} \quad (43)$$

where  $x_{T_{mg}}$  and  $z_{T_{mg}}$  are the horizontal and vertical distance between the thrust vector and the main gear contact point,  $x_{L_{mg}}$  and  $z_{D_{mg}}$  are the horizontal and vertical

distance between the aerodynamic center and the main gear contact point, and  $x_{cg_{mg}}$  and  $z_{cg_{mg}}$  are the horizontal and vertical distances between the center of gravity and the main gear contact point. The term  $I_{yy_{mg}}$  in Eq. (41) is simply the moment of inertia transferred from the center of gravity to the main gear.

At the beginning of the rotation integration, the horizontal tail is instantly deflected. The integration continues until the aircraft has a positive vertical velocity. At this point, the attitude of the aircraft is fixed, and the horizontal tail is returned to its undeflected position.

The final phase of the takeoff is the climb out. In the climb out segment, the attitude of the aircraft is held constant and the horizontal and vertical acceleration equations are integrated until the aircraft reaches an FAR<sup>25</sup> specified height of 35 ft. The equations for this segment are

$$a_x = \frac{g}{W} [T \cos (\Lambda_T + \gamma + \alpha) - qS (C_D \cos \gamma + C_L \sin \gamma)] \quad (44)$$

$$a_z = \frac{g}{W} [T \sin (\Lambda_T + \gamma + \alpha) - W + qS (C_L \cos \gamma - C_D \sin \gamma)] \quad (45)$$

where the flight path angle is  $\gamma = \arctan \left( \frac{V_z}{V_x} \right)$ .

The sum of the horizontal distance travelled in these three segments is the takeoff field length. The balanced field length (BFL) or FAR takeoff distance is the distance required to take off with one engine failing at a speed  $V_{crit}$ , the critical speed. When an engine fails during the takeoff, the pilot must decide whether it would be shorter to continue the takeoff or to stop. If the engine fails at speed lower than  $V_{crit}$  then the stopping distance is shorter. Otherwise, it is best to continue the takeoff. If the engine fails at  $V_{crit}$ , then the stopping distance equals the takeoff distance. This is the longest required field length and determines what airfields the aircraft can operate from.

The BFL is calculated iteratively. A guess is made for the critical speed,  $V_{crit_g}$ . Then both the takeoff and stopping distances are calculated with and engine failing at  $V_{crit_g}$ . A secant method is used to converge to the speed where the two distances are equal.

The approximate BFL is calculated using an equation from Loftin<sup>50</sup>. This is a

simple algebraic equation that captures most of the physics of the takeoff

$$x_{BFL} = 37.7 \frac{(W/S)}{\sigma C_{L_{max}} (T/W)} \quad ft \quad (46)$$

and gives the BFL in *feet*, where  $\sigma$  is the density ratio. This equation does not model any rotation or horizontal tail effects. Note that this equation can be rewritten as

$$x_{BFL} = 37.7 \frac{V_s^2 \rho_o}{2(T/W)} \quad ft. \quad (47)$$

## 5.9 Takeoff Aerodynamics

There are a number of special aerodynamic considerations for the takeoff integration. All of the aerodynamic coefficients must include ground effects and there is added drag due to things such as landing gear, and a windmilling engine. Also, it is necessary to include the effect of high lift devices such as leading and trailing edge flaps.

Generally, lift increases with proximity to the ground. Our approximation for ground effect on lift is due to Torenbeek<sup>24</sup>, although we have also used Küchemann's<sup>41</sup> approximation previously. Torenbeek's approximation is calculated using the equations

$$\sigma_g = \exp \left\{ -2.48 (2h/b)^{0.768} \right\} \quad (48)$$

$$\beta_g = \sqrt{1 + (2h/b)^2} - 2h/b \quad (49)$$

$$\frac{C_{L_g}}{C_{L_\infty}} = 1 + \sigma_g - \frac{\sigma_g \mathcal{AR} \cos \Lambda_{c/2}}{2 \cos \Lambda_{c/2} + \sqrt{\mathcal{AR}^2 + (2 \cos \Lambda_{c/2})^2}} - \frac{\beta_g}{4\pi h/c_g} \left( C_{L_\infty} - \frac{C_{L_\alpha}}{16h/c_g} \right) \quad (50)$$

where  $C_{L_g}$  is the lift coefficient in ground effect,  $C_{L_\infty}$  is the lift coefficient out of ground effect,  $\Lambda_{c/2}$  is the wing sweep at the half chord,  $\mathcal{AR}$  is the wing aspect ratio,  $h$  is the height above the ground,  $b$  is the wing span, and  $c_g$  is the mean geometric chord.

Induced drag is reduced when the aircraft is near or on the ground. Nicolai<sup>51</sup> gives the change in drag as

$$\Delta C_{D_i} = -\frac{\sigma_g C_L^2}{\pi \mathcal{AR}} \quad (51)$$

where  $\sigma_g$  is calculated using Eq. (48).

The landing gear remains extended for the entire takeoff. It is necessary to include this contribution to the total drag when analyzing takeoff. For preliminary design, Torenbeek<sup>24</sup> suggests using

$$C_{D_{lg}} = C_1 \frac{W^{0.785}}{S} \left[ 1 - 0.04 \frac{C_L S}{\ell_{mg} b} \right]^2 \quad (52)$$

where  $\ell_{mg}$  is the length of the main gear, and  $C_1$  is  $4.05 \times 10^{-3}$  for English units, and  $7.0 \times 10^{-4}$  for metric measurements.

When an engine fails, not only is the thrust of that engine lost, but there is an increase in drag due to the windmilling engine. This increment in drag is calculated using

$$C_{D_{wm}} = \frac{1}{S} \left[ 0.1\pi r_i^2 + \frac{2}{1 + 0.16M^2} A_N \frac{V_N}{V} \left( 1 - \frac{V_N}{V} \right) \right] \quad (53)$$

from Ref. [24]. In this equation,  $r_i$  is the engine inlet radius,  $A_N$  is the nozzle area, and  $\frac{V_N}{V}$  is the ratio of the nozzle velocity to the airspeed velocity. Torenbeek suggests using  $\frac{V_N}{V} = 0.42$  for low bypass ratio engines with mixed flow.

High lift devices are critically important for efficient low speed operation of an HSCT. Antani<sup>52</sup> discusses the requirements and issues for high lift systems for an HSCT. Neglecting the effects of the high lift systems would lead to unrealistic designs with low wing loading and poor overall performance, as the supersonic efficiency would have to be drastically compromised to satisfy the field performance requirements. Benoiel<sup>53</sup> provides a survey of data for many different HSCT type planforms, and Baber<sup>54</sup> provides very detailed data on the AST-105-1 configuration. Data from these sources was used to add lift and moment flap effects for our configuration. Specifically, for the longitudinal derivatives with respect to flap deflection, we assume

$$C_{L_{\delta_f}} = 0.2508 \quad (54)$$

$$C_{M_{\delta_f}} = -0.0550 \quad (55)$$

and these values are fixed throughout the optimization. This results in

$$\begin{aligned} \Delta C_L = C_{L_{\delta_f}} \delta_f &= 0.2508 \delta_f \\ \Delta C_M = C_{M_{\delta_f}} \delta_f &= -0.0550 \delta_f. \end{aligned}$$

We are currently assuming a takeoff flap deflection of 30° \*. We neglect changes in drag due to flap deflection.

## 5.10 Powered Approach Trim

The powered approach trim requirement involves calculating the pitching moment about the  $cg$ , in the approach configuration. In this case the net pitching moment should be zero. This is given by

$$M_{cg} = Tz_{Tcg} + qSC_Dz_{Dcg} - qSC_Lx_{Lcg} + qS\bar{c}C_M = 0 \quad (56)$$

which can be rewritten as

$$C_M = \frac{1}{\bar{c}} \left( C_Lx_{Lcg} - C_D(z_{Tcg} + z_{Dcg}) - \frac{W \sin \alpha}{qS} z_{Tcg} \right) \quad (57)$$

where  $\alpha$  is the landing angle of attack, which is calculated assuming that  $L = W$ . Equation (57) is the pitching moment generated by the lift, drag, thrust, and weight. The pitching moment to balance this, as given by Etkin<sup>56</sup> is

$$C_M = C_{M_\alpha}\alpha + C_{M_{HT}} \quad (58)$$

or

$$C_M = C_{M_\alpha}\alpha + C_{L_{\alpha HT}}V_H i_t \left[ 1 - \frac{C_{L_{\alpha HT}}S_{HT}}{C_{L_\alpha}S} \left( 1 - \frac{d\varepsilon}{d\alpha} \right) \right] \quad (59)$$

where  $V_H$  is the horizontal tail volume coefficient, and  $\varepsilon$  is the downwash angle. This can be solved for the horizontal tail deflection,  $i_t$ ,

$$i_t = \frac{C_M - C_{M_\alpha}\alpha}{C_{L_{\alpha HT}}V_H \left[ 1 - \frac{C_{L_{\alpha HT}}S_{HT}}{C_{L_\alpha}S} \left( 1 - \frac{d\varepsilon}{d\alpha} \right) \right]} \quad (60)$$

Substituting the pitching moment calculated in Eq. (57) into Eq. (60) gives the required tail deflection. This analysis neglects the effects of flaps.

---

\*This analysis has been extended to be more realistic by Crisafulli <sup>55</sup>.

## 5.11 Engine Scaling

Modern high thrust, high bypass ratio engines have fan diameters of over 10 *ft*. Although the HSCT will not use engines with fans this large, thrust requirements can rapidly increase the size of the engine. As engine size increases, so does the weight and the drag on the nacelle. Engine size is largely determined by the mass flow of air required for a given bypass ratio. The thrust is highly dependent on the mass flow through the engine. We assume that the thrust is directly proportional to the mass flow.

$$\frac{T}{T_{ref}} = \frac{\dot{m}}{\dot{m}_{ref}} \quad (61)$$

With this, we can scale the engine nacelle size directly from thrust using equations from Nicolai<sup>51</sup>:

$$\frac{D_{nac}}{D_{nac_{ref}}} = \sqrt{\frac{T}{T_{ref}}} \quad (62)$$

$$\frac{l_{nac}}{l_{nac_{ref}}} = \sqrt{\frac{T}{T_{ref}}} \quad (63)$$

where  $D_{nac}$  and  $l_{nac}$  are the diameter and length of the nacelle.

Thrust is also used to calculate the weight of the engine in the FLOPS<sup>11</sup> weight routine

$$\frac{W_{eng}}{W_{eng_{ref}}} = \left( \frac{T}{T_{ref}} \right)^{s_{eng}} \quad (64)$$

We use  $s_{eng} = 1.081$  in the equation.

## 5.12 Minimum Time Climb with Dynamic Pressure Constraint

To investigate the effect of climb requirements, we added a minimum time climb to transition from the subsonic leg to the supersonic leg. The minimum time climb is calculated using the energy approach as described by Rutowski<sup>57</sup> and Bryson *et al.*<sup>58</sup>. In this approach, the specific excess power,

$$P_s = \frac{(T - D)V}{W} \quad (65)$$

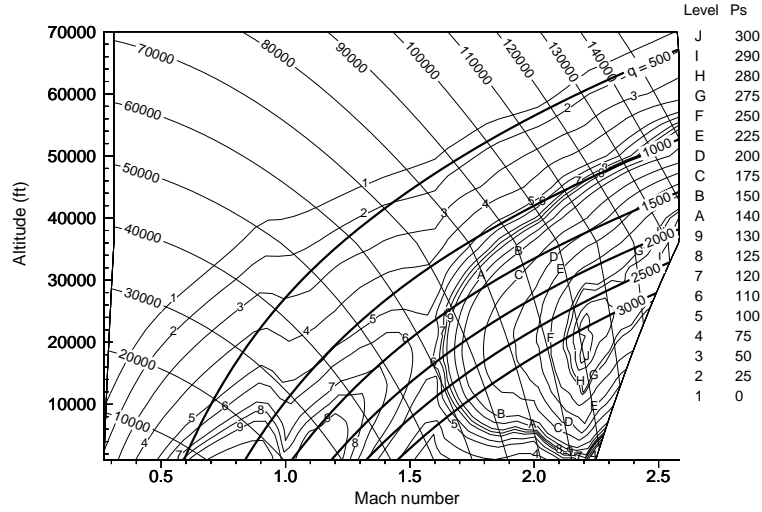


Figure 11: Specific excess power contours for a HSCT configuration

is maximized for a constant energy height,

$$h_e = h + \frac{V^2}{2g}. \quad (66)$$

This is done by varying the speed,  $V$ , and at each speed and altitude calculating thrust ( $T$ ) and drag ( $D$ ). To efficiently find the maximum, we use a routine which combines a golden section search with parabolic interpolation. This can be done for a range of energy heights and will calculate the minimum time climb flight path for the aircraft. Often, the optimum flight path would require the aircraft to fly at unrealistically high dynamic pressures. We must place a limit on the maximum allowable dynamic pressure, which limits the flight path.

Figure 11 shows a plot of specific excess power curves with lines of constant energy height ranging from 10,000 *ft* to 150,000 *ft* and constant dynamic pressure ranging from 500 *psf* to 3,000 *psf*. Due to structural considerations, we limit the maximum dynamic pressure to be 1,000 *psf*. This eliminates much of the region shown in Fig. 11, and for this aircraft the minimum time climb would be along the  $q = 1000$  *psf* curve.



## 5.13 Optimization Strategies

Most optimizations of complex engineering systems replace the objective function and/or constraints with easy-to-calculate approximations. The optimum of the approximate problem is found and then the approximation is updated in the neighborhood of this optimum and the process repeated. The sequential linear programming used for the structural optimization is the simplest form of such sequential approximate optimization—it employs linear approximations. For the overall design we employ sequential approximate optimization using the VCM approximation described earlier. The numerical optimization is performed using the NEWSUMT-A program<sup>59</sup> which employs an extended interior penalty function. Newton’s method with approximate second derivatives is used for unconstrained minimization.

During the typical optimization process the move limits on the variables were selected to avoid excessive errors in the approximations. Typical initial move limits were approximately fifteen percent, and they were decreased throughout the optimization process to approximately two percent as the optimization neared completion.

# Chapter 6

## Results

In this chapter, we describe the results of a number of optimization runs. First, we will discuss a case with no vertical or horizontal tail sizing. Then, two cases with vertical tail sizing using slightly different starting conditions are presented, followed by two cases with vertical and horizontal tail sizing. The second case shows the effect of engine technology. Then we discuss a case with engine sizing and a case with all of the above and a subsonic leg added to our mission. Table 6 lists the cases and charts the progression of the cases. These cases show the difficulties in optimizing, as well as the successes.

Table 6: Overview of results

Case	Basic	+ VT	+ HT	+ New engine	+ Engine sizing (new engine)	+ Subsonic leg
26a	X					
27a		X				
27b		X				
28a			X			
28b						
29a			Shows effect of engine technology		X	
29b						X

The sensitivity studies follow the main results sections. In this section we describe the effects of relaxing BFL on the HSCT (Case 29a is taken as the basis for this case with changed BFL limit), sensitivity of TOGW to the drag coefficient value and the role of the rotation time constraint on the HSCT configuration and weight. Table 7 shows the cases that were investigated during the sensitivity studies.

Table 7: Overview of sensitivity studies

Case	Relaxed BFL (new baseline)	Changed drag designs	Relaxed rotation time designs
29c	X		
Weight to Drag sensitivity		X	
29d			X

## 6.1 Baseline Optimization (Case 26a)

This optimization, case 26a, is used as a control case. It allows us to determine the effects of the changes we make. It has 26 design variables, and 62 constraints. Constraints numbered 47-52, 69 and 70 in Table 2 were not used in this case. The mission is entirely supersonic, the vertical tail is fixed in both size and shape, and there is no horizontal tail.

The initial design violated three constraints, the range constraint and the two thrust constraints. After 30 optimization cycles, the TOGW has been reduced by 34,200 *lbs* with all of the constraints satisfied. A convergence history of the TOGW is shown in Fig. 12. The initial and final planforms are shown in Figure 13 and Table 8 compares the two designs.

The final design has an unusual planform, with the inboard trailing edge swept forward. The optimizer moved immediately to this design, and as can be seen in Figure 14 the wing weight is reduced by about 14,000 *lbs*. Due to the lower aspect

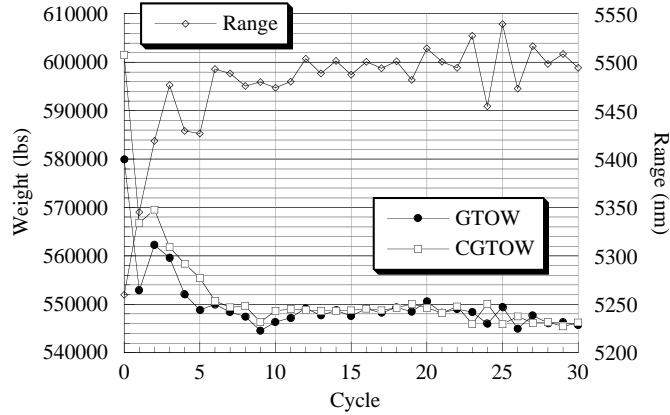


Figure 12: Convergence of Case 26a

ratio, the drag due to lift does increase, Fig. 15, but this is offset by a reduction in volumetric wave drag, shown in Figure 16. Overall, the total drag decreases slightly by the end of the optimization, Fig. 17.

The initial design has a wing loading of  $63.68 \text{ psf}$ . In the final design the wing loading has been reduced to  $56.30 \text{ psf}$ . Lowering the aspect ratio improves the supersonic efficiency, but it also lowers the lift curve slope. This means that for a given wing area, the aircraft would have to fly at a higher angle of attack to generate the same lift. To keep from violating the  $12^\circ$  angle of attack constraint the optimizer increased the wing area, which decreased the wing loading.

Table 8: Comparison of Initial and Final Designs, Case 26a

	Initial	Final
Gross Weight ( <i>lbs</i> )	580,000	545,800
Fuel Weight ( <i>lbs</i> )	290,900	273,600
Fuel Wt / Gross Wt	50.2%	50.1%
Wing Area ( $\text{ft}^2$ )	9,108	9,693
Wing Weight ( <i>lbs</i> )	81,900	68,070
Aspect Ratio	2.36	1.59
Range ( <i>n.mi.</i> )	5,260.0	5,494.6
Landing angle of attack	$11.35^\circ$	$11.99^\circ$
$(L/D)_{max}$	9.473	9.588

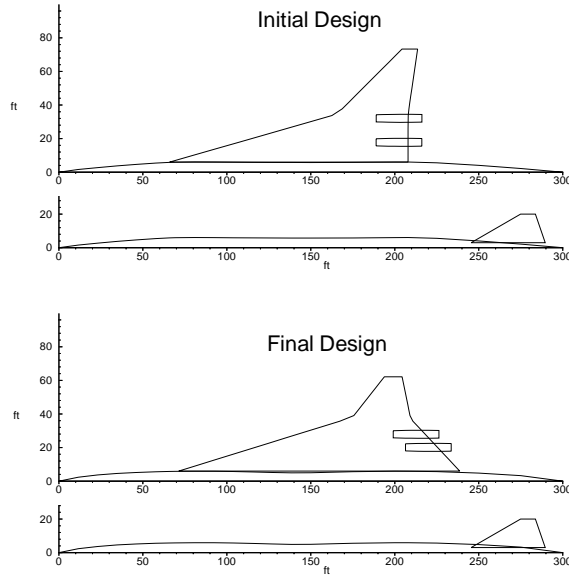


Figure 13: Initial and final planforms, Case 26a

## 6.2 Vertical Tail Considerations

These optimizations include the vertical tail sizing, and require 27 design variables with 64 constraints. Constraint number 66 is changed to the engine out limit from the arbitrary limit of 50% of the semispan, and constraints 47 and 48 are added for the crosswind landing. Again, the mission is entirely supersonic, and there is no horizontal tail, but the vertical tail is allowed to vary in size.

### 6.2.1 Case 27a

The same initial design is used as in Case 26a, with the exception that the initial value of the starting altitude was changed from 50,000 *ft* to 60,000 *ft*, and the climb rate was changed from 100 *ft/sec* to 50 *ft/sec*. These changes increased the range by over 80 *n.mi*. In addition to the three constraint violations mentioned previously, the engine out limit is violated. The engines are too far out for the vertical tail to trim in an emergency. After 30 optimization cycles, the TOGW has been reduced by 32,700 *lbs* with all of the constraints satisfied. A convergence history of the TOGW

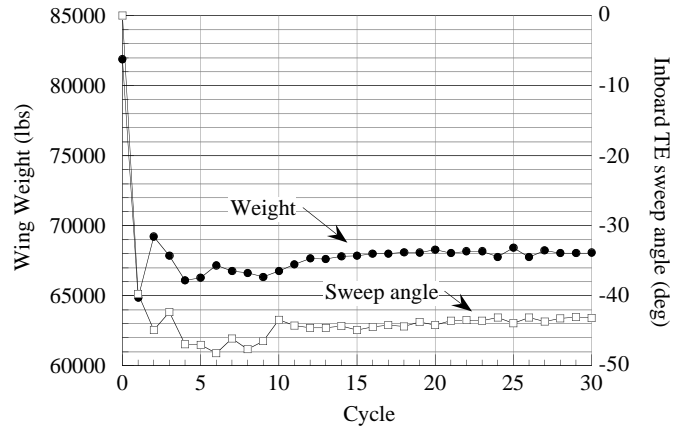


Figure 14: History of wing weight and trailing edge sweep, Case 26a

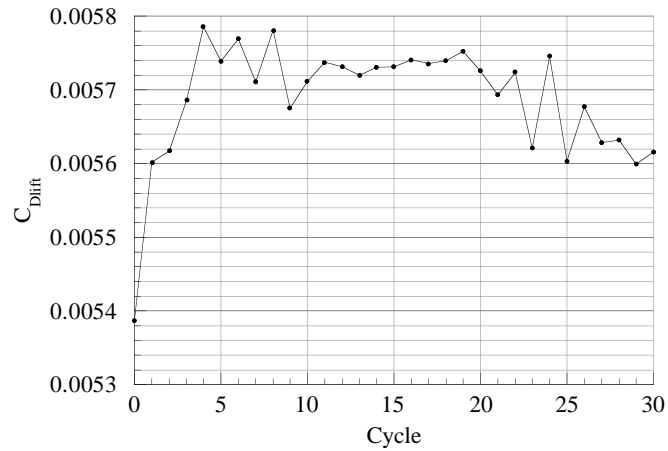


Figure 15: History of drag due to lift, at  $C_L = 0.1$ , Case 26a

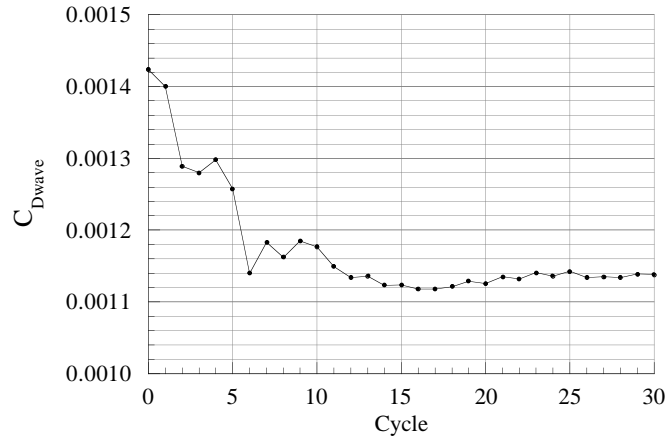


Figure 16: History of wave drag, Case 26a

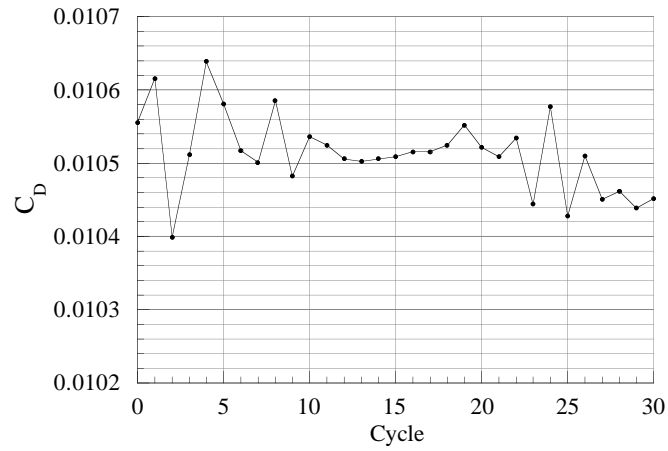


Figure 17: History of total drag, at  $C_L = 0.1$ , Case 26a

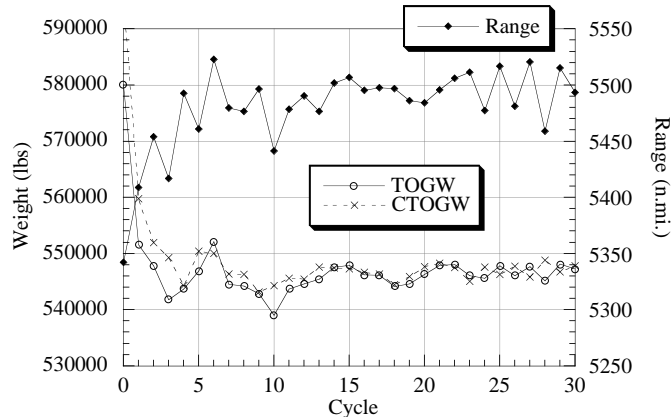


Figure 18: Convergence of Case 27a

is shown in Fig. 18. The initial and final planforms are shown in Figure 19 and Table 9 compares the two designs.

The vertical tail initially increased in size to satisfy the engine out constraint, but was reduced as the engines continued to move inboard, see Fig. 20. In this case, more weight is saved by moving the engines in and reducing the vertical tail size than by taking advantage of wing bending moment relief to reduce the wing weight. In the final design, the engines are moved in as far as the constraints allow. This results in a slightly heavier wing compared to Case 26a. But this also allows a small vertical tail to be used to satisfy the engine out constraint. The weight penalty for going to this design is very small, about 0.27% of the TOGW.

The stability and control derivatives were estimated using the interlacing technique. This technique worked well, as shown in Figures 21 and 22. The jumps that occur every five cycles are the updated derivatives from Kay's code. The estimations for  $C_{l_\beta}$  show the greatest differences, although the magnitude of the jumps is not larger than the jumps in the other derivatives.

### 6.2.2 Case 27b

It seemed odd that the optimizer moved the engines inboard, which reduces the wing bending moment relief, resulting in a heavier wing. So we performed a second optimization, Case 27b, using the same initial design as Case 27a, but we started with



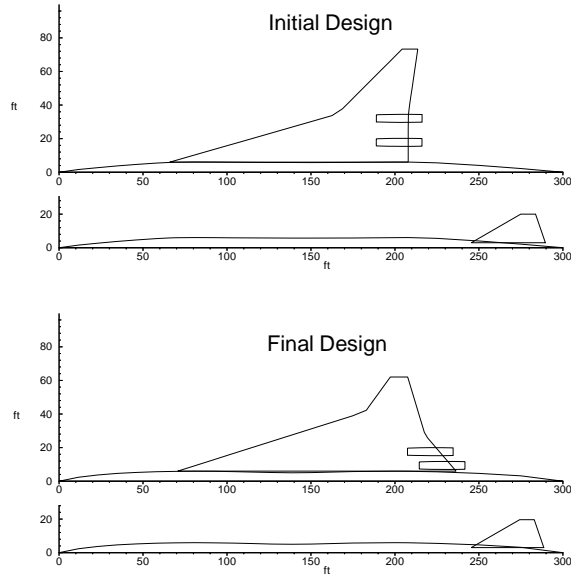


Figure 19: Initial and final planforms, Case 27a

Table 9: Comparison of Initial and Final Designs, Case 27a

	Initial	Final
Gross Weight ( <i>lbs</i> )	580,000	547,300
Fuel Weight ( <i>lbs</i> )	290,900	272,800
Fuel Wt / Gross Wt	50.2%	49.8%
Wing Area ( <i>ft</i> <sup>2</sup> )	9,108	9,808
Wing Weight ( <i>lbs</i> )	81,900	70,060
Aspect Ratio	2.36	1.57
Vertical Tail Area ( <i>ft</i> <sup>2</sup> )	450.0	431.0
Vertical Tail Weight ( <i>lbs</i> )	1,730	1,640
Nacelle 1 position, <i>y</i> ( <i>ft</i> )	17.8	9.4
Nacelle 2 position, <i>y</i> ( <i>ft</i> )	32.1	17.6
Range ( <i>n.mi.</i> )	5,342.4	5,493.4
Landing angle of attack	11.35°	11.99°
$(L/D)_{max}$	9.239	9.577

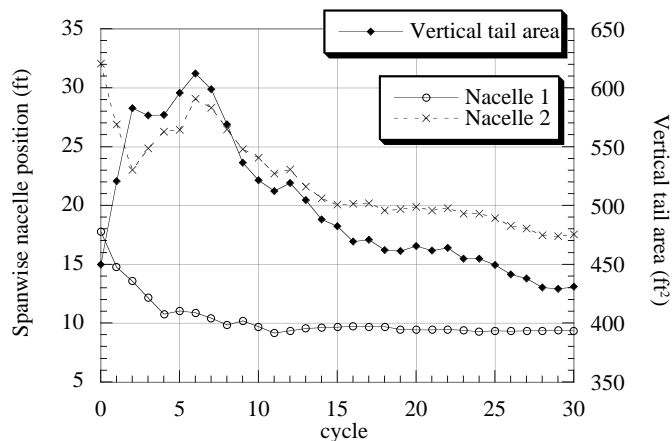


Figure 20: History of nacelle positions and vertical tail area

a larger vertical tail. There was initially no violation of the engine out constraint. This allowed the engines to remain well outboard where there is a larger wing bending moment relief effect.

The optimal design occurred after only 11 optimization cycles, but due to noisy derivatives, the optimizer slowly wandered away from this design. The optimal design has a TOGW of 543,700 *lbs*, a reduction of 37,700 *lbs* from the initial design. The initial and final planforms are shown in Figure 23 and Table 10 compares the two designs.

The range decreased by 100 *n.mi.* when the vertical tail size was increased by 400 *ft²*. This is due to the increased drag from the larger tail. Although this seems like a large penalty, the final design is slightly better than the Case 27a final design. The nacelles are split because the vertical tail must balance the net yawing moment. Thus, the net yawing moment will remain the same by moving nacelle 1 in and nacelle 2 out by equal distances. These cases show our derivative based optimization is very susceptible to local minima. Also, these two cases indicate that nacelle position is not a design driver and nacelles can be placed using other considerations, such as landing gear interference with inlet flow or rotor burst.

The stability and control derivatives are well estimated for this case. Although there is a large jump after the initial five cycles, the approximate analysis agrees well

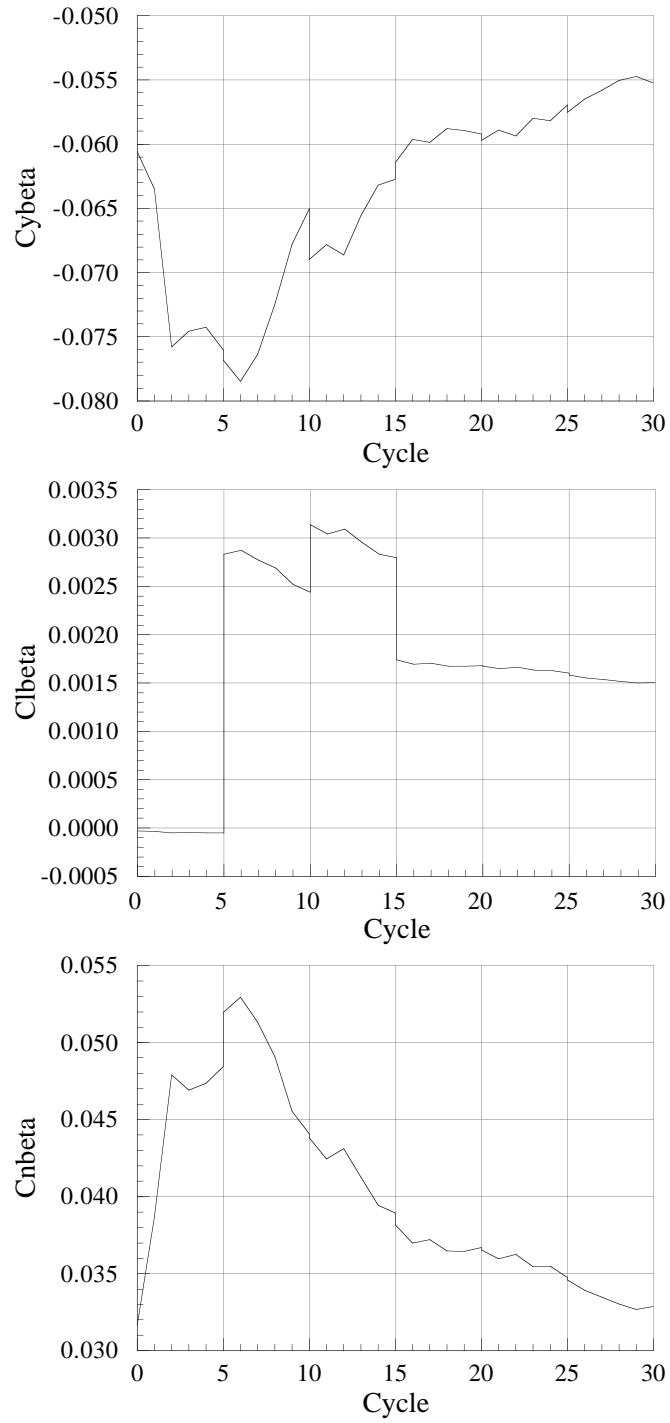


Figure 21: History of  $C_{y\beta}$ ,  $C_{l\beta}$ , and  $C_{n\beta}$  for Case 27a

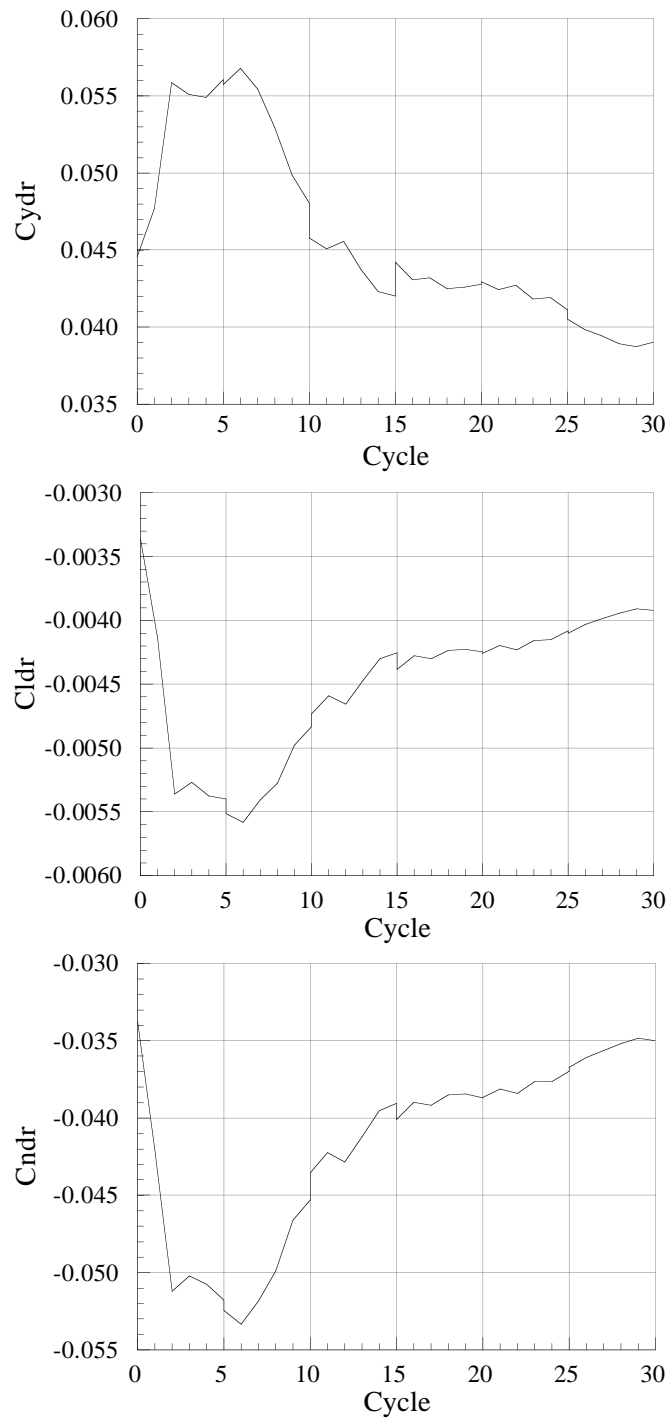


Figure 22: History of  $C_{y_{\delta r}}$ ,  $C_{l_{\delta r}}$ , and  $C_{n_{\delta r}}$  for Case 27a

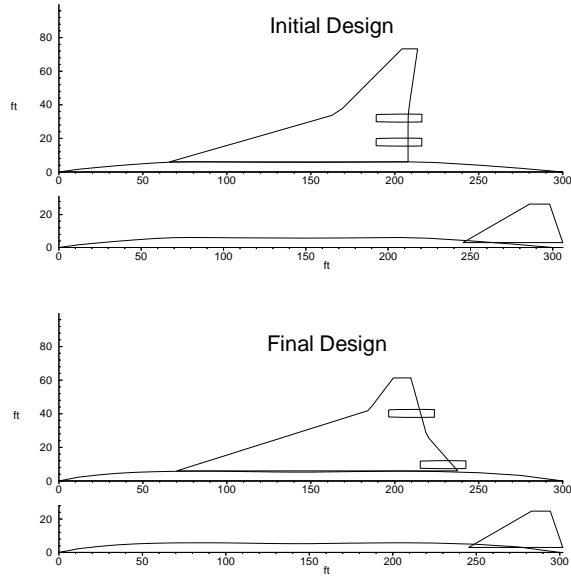


Figure 23: Initial and final planforms, Case 27b

Table 10: Comparison of Initial and Final Designs, Case 27b

	Initial	Final
Gross Weight ( <i>lbs</i> )	581,400	543,700
Fuel Weight ( <i>lbs</i> )	290,900	272,100
Fuel Wt / Gross Wt	50.0%	50.0%
Wing Area ( $ft^2$ )	9,108	9,870
Wing Weight ( <i>lbs</i> )	82,010	67,940
Aspect Ratio	2.36	1.53
Vertical Tail Area ( $ft^2$ )	850.0	734.8
Vertical Tail Weight ( <i>lbs</i> )	2,970	2,570
Nacelle 1 position, <i>y</i> ( <i>ft</i> )	17.8	9.7
Nacelle 2 position, <i>y</i> ( <i>ft</i> )	32.1	40.2
Range ( <i>n.mi.</i> )	5,242.7	5,499.0
Landing angle of attack	11.39°	11.99°
$(L/D)_{max}$	9.092	9.574

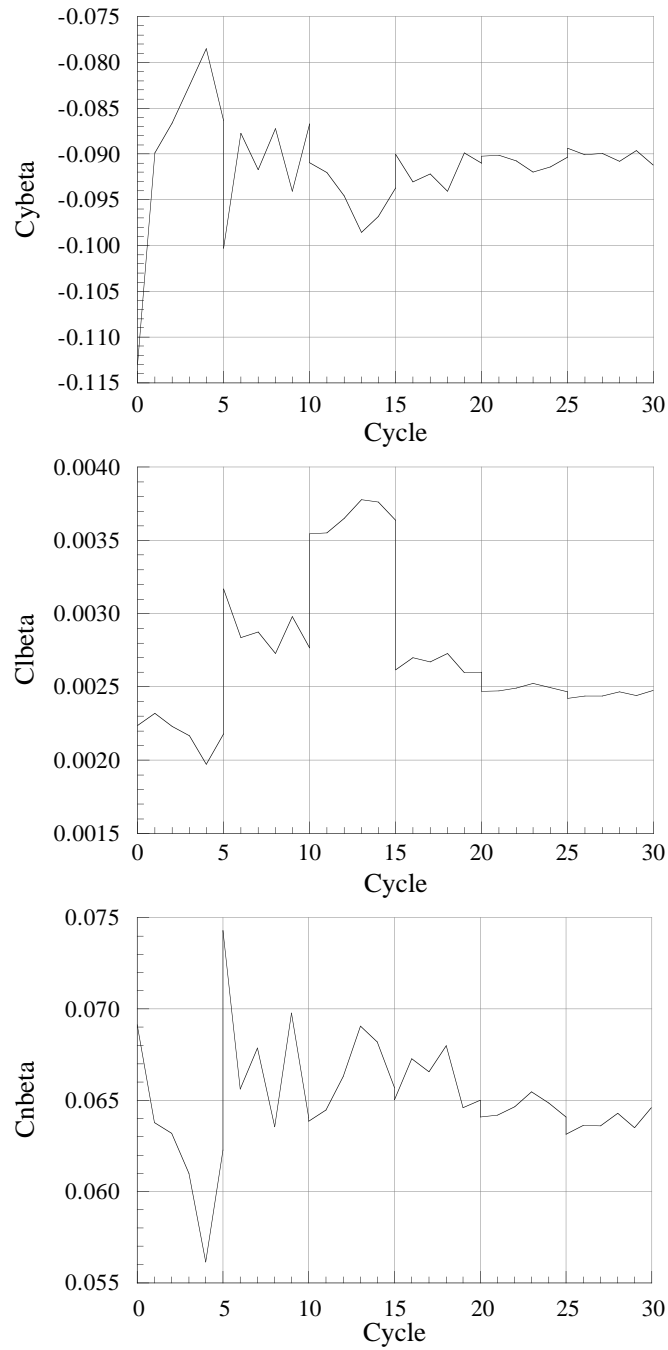


Figure 24: History of  $C_{y\beta}$ ,  $C_{l\beta}$ , and  $C_{n\beta}$  for Case 27b

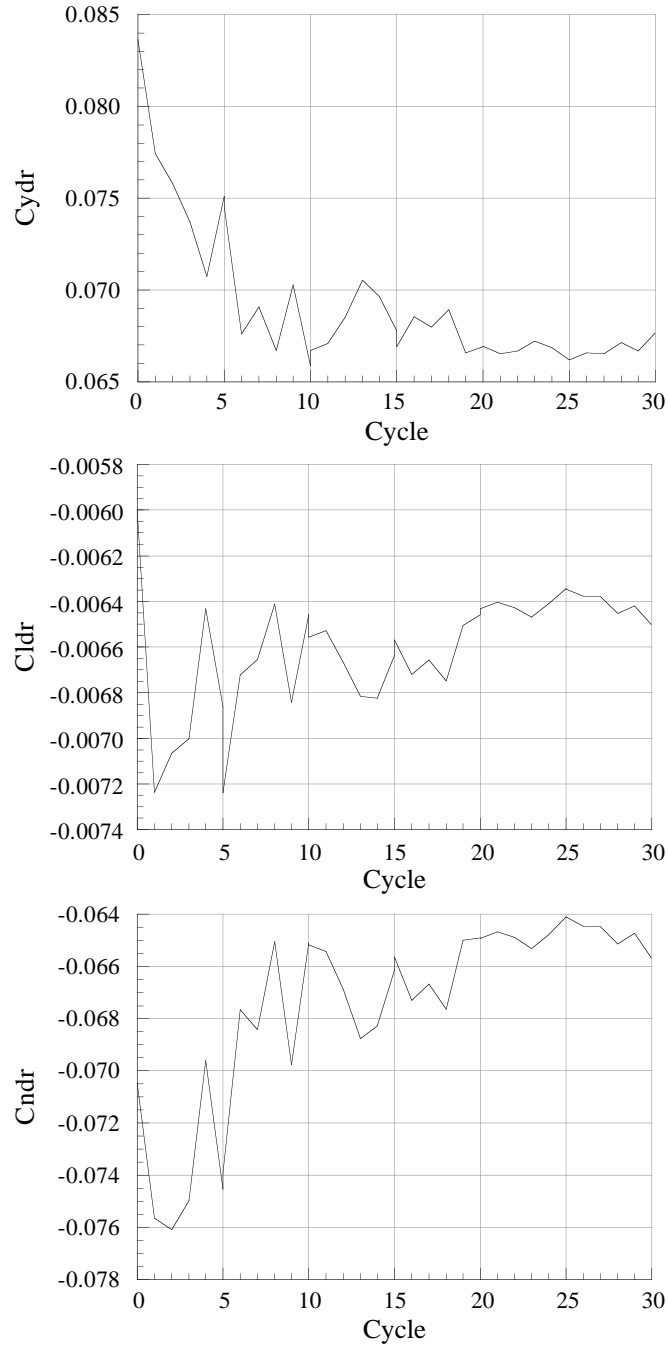


Figure 25: History of  $C_{y\delta r}$ ,  $C_{l\delta r}$ , and  $C_{n\delta r}$  for Case 27b

with the detailed estimations after this. The history of the derivatives is shown in Figures 24 and 25.

The most critical constraints for the final design are range and the engine out constraint. Some of the section  $C_\ell$  constraints and the landing angle of attack constraint are also critical. Also important in this design is fuel volume, nacelle strike on the inboard nacelle, and minimum wing  $t/c$ .

## 6.3 Vertical and Horizontal Tail Considerations

Next, we added horizontal tail sizing to our optimization. This increased the number of design variables to 28 and the number of constraints to 67. The constraints added are the takeoff rotation constraint, the approach trim constraint and a constraint to prevent the wing and horizontal tail from overlapping.

### 6.3.1 Case 28a

The starting design from Case 27a is used, with the addition of a horizontal tail. Adding the horizontal tail only increased the weight by 9,000 *lbs*, but the additional drag caused a 400 *n.mi.* reduction in the range. This design satisfies the three additional constraints for the horizontal tail.

The weight of the final design is 630,000 *lbs*, an increase of over 40,000 *lbs* from the starting weight, and more than 80,000 *lbs* heavier than the previous optimized designs. Most of this weight increase is fuel weight. Almost 70,000 *lbs* more fuel is required for this design than for Case 27a. The planforms are all very similar, although the trailing edge is somewhat less swept in this case.

The initial and final planforms are shown in Figure 26 and Table 11 compares the two designs. The convergence histories of the TOGW, vertical tail size and nacelle locations, and horizontal tail size are shown in Figures 27, 28, 29. The noisy convergence is a product of our variable complexity modeling and the noisy analysis.

For the final design, range and landing angle of attack are again the critical constraints. There are a number of constraints which were important, but not critical,



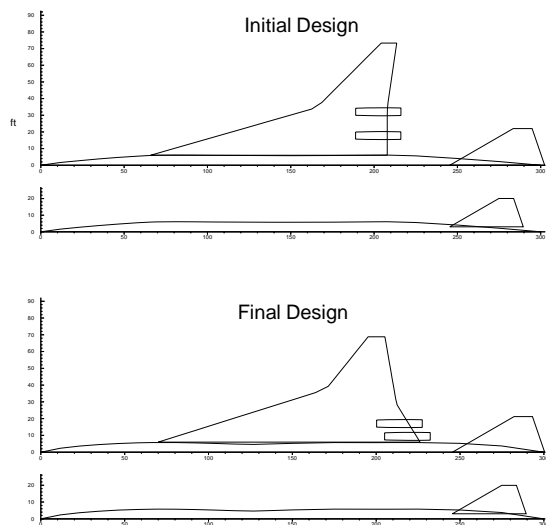


Figure 26: Initial and final planforms, Case 28a

to this design. These include fuel volume, section  $C_\ell$ , time required to rotate, minimum nacelle spacing, the engine out limit, and maximum thrust required during the cruise-climb.

### 6.3.2 Case 28b

We performed another optimization using the same initial design variables, but increasing the size and thrust of the engines to see the effects of engine technology. Engine thrust increased from 39,000 *lbs* to 46,000 *lbs* per engine, nacelle diameter and length increased from 5 *ft* and 27 *ft* to 6.5 *ft* and 35 *ft*, respectively. The engine thrust to weight ratio was reduced by 1, which increased the propulsion system weight by over 28,000 *lbs* and the TOGW by about 35,600 *lbs*. Also, the range decreased by 436 *n.mi.*, although the drag on the aircraft only increased by about two counts. The initial weight of this design is only about 5,000 *lbs* less than the optimized design in the previous case. The range is 1,000 *n.mi.* less than our required range.

After 40 optimization cycles, our TOGW is 755,400 *lbs*. Although this could be a poor local minimum, this large increase in weight can be explained. With no other changes, the large range deficiency would require approximately 100,000 *lbs* of fuel to satisfy the range constraint. Adding this much fuel weight would cause numerous other constraint violations, such as the thrust constraints, the fuel volume constraint, the landing angle of attack, and the takeoff rotation constraint. Satisfying these

Table 11: Comparison of Initial and Final Designs, Case 28a

	Initial	Final
Gross Weight ( <i>lbs</i> )	589,200	630,000
Fuel Weight ( <i>lbs</i> )	290,900	340,200
Fuel Wt / Gross Wt	50.0%	54.0%
Wing Area ( <i>ft</i> <sup>2</sup> )	9,108	9,713
Wing Weight ( <i>lbs</i> )	82,630	77,720
Aspect Ratio	2.36	1.95
Vertical Tail Area ( <i>ft</i> <sup>2</sup> )	450.0	447.1
Vertical Tail Weight ( <i>lbs</i> )	1,740	1,760
Nacelle 1 position, <i>y</i> ( <i>ft</i> )	17.8	9.4
Nacelle 2 position, <i>y</i> ( <i>ft</i> )	32.1	17.1
Horz. Tail Area ( <i>ft</i> <sup>2</sup> )	1,500.0	1,400.1
Horz. Tail Weight ( <i>lbs</i> )	7,930	7,510
Time to rotate ( <i>sec</i> )	4.56	4.67
Range ( <i>n.mi.</i> )	4,935.9	5,465.2
Landing angle of attack	11.27°	11.97°
$(L/D)_{max}$	8.709	8.711

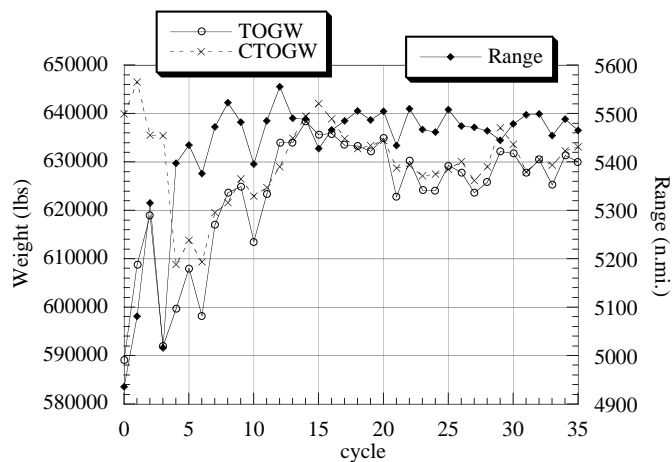


Figure 27: Takeoff Gross Weight and Range convergence, Case 28a

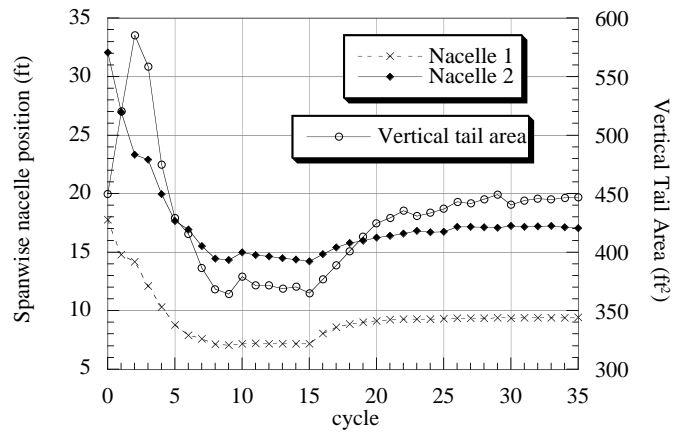


Figure 28: Vertical Tail Size and Nacelle Location convergence, Case 28a

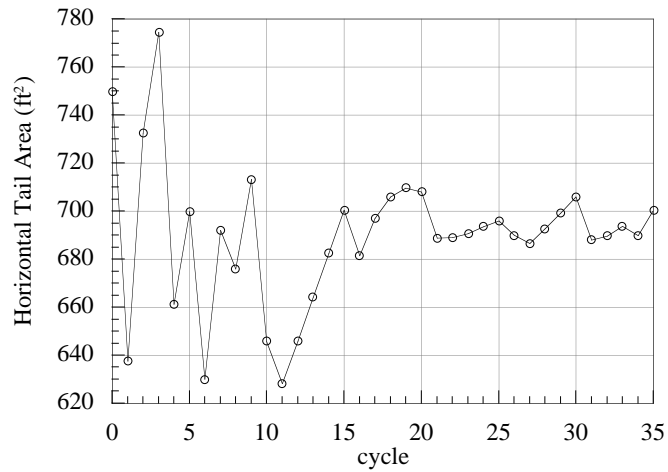


Figure 29: Horizontal Tail Size convergence, Case 28a

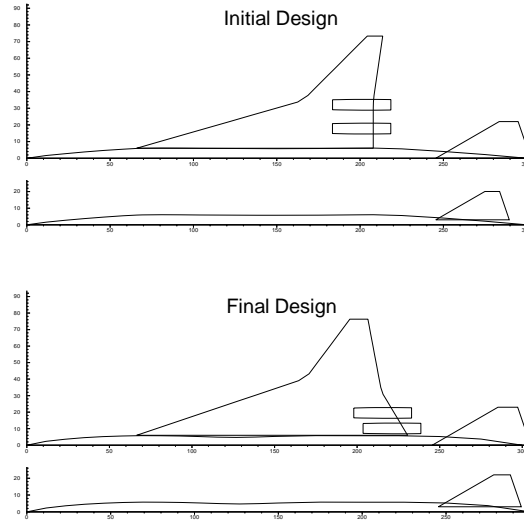


Figure 30: Initial and final planforms, Case 28b

constraints would further increase the weight. The actual increase in fuel weight is about 118,000 *lbs*.

The final planform is very similar to our previous designs, but the wing is much bigger. The initial and final planforms are shown in Figure 30. These designs are also compared in Table 12. In this design, range, landing angle of attack, section  $C_\ell$ , and the engine out limit are the critical constraints. Once again, fuel volume, inboard nacelle strike, time to rotate, and maximum thrust required for cruise-climb are the other important constraints.

## 6.4 Engine Sizing (Case 29a)

Our next optimization included engine sizing, as well as the vertical and horizontal tail sizing. This added one design variable, up to 29, and one constraint, up to 68. The balanced field length constraint of 10,000 *ft* is the additional constraint. Cases 28a and 28b both violate this constraint considerably with balanced field lengths of 11,650.9 *ft* and 12794.3 *ft*, respectively. The initial design for this case is the final design from case 28b.

Table 12: Comparison of Initial and Final Designs, Case 28b

	Initial	Final
Gross Weight ( <i>lbs</i> )	624,800	755,400
Fuel Weight ( <i>lbs</i> )	290,900	408,600
Fuel Wt / Gross Wt	50.0%	54.0%
Wing Area ( <i>ft</i> <sup>2</sup> )	9,108	11,193
Wing Weight ( <i>lbs</i> )	84,300	95,800
Aspect Ratio	2.36	2.08
Vertical Tail Area ( <i>ft</i> <sup>2</sup> )	450.0	564.6
Vertical Tail Weight ( <i>lbs</i> )	1,770	2,270
Nacelle 1 position, <i>y</i> ( <i>ft</i> )	17.8	10.1
Nacelle 2 position, <i>y</i> ( <i>ft</i> )	32.1	19.5
Horz. Tail Area ( <i>ft</i> <sup>2</sup> )	1,500.0	1,647.1
Horz. Tail Weight ( <i>lbs</i> )	8,030	9,150
Time to rotate ( <i>sec</i> )	4.47	4.68
Range ( <i>n.mi.</i> )	4,500.6	5,471.9
Landing angle of attack	12.26°	12.00°
$(L/D)_{max}$	8.573	8.684

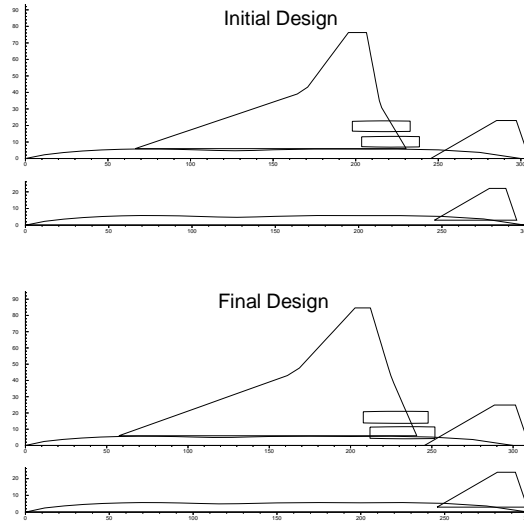


Figure 31: Initial and final planforms, Case 29a

The final design is much heavier than the initial design. The weight increases by 110,000 *lbs*. The final design has a much larger wing. Wing area increases by 1,569 *ft*<sup>2</sup> and wing weight increases by over 33,000 *lbs*. Increasing the wing area often reduces the wing loading, which decreases the balanced field length, but in this case, the wing loading increases from 59.04 *lbs/ft*<sup>2</sup> to 60.22 *lbs/ft*<sup>2</sup>. This is a relatively small increase in wing loading and it allows a smaller, lighter wing to be used.

To satisfy the balanced field length constraint the thrust to weight ratio is increased by 13.5%, from 0.244 to 0.277. This is accomplished by increasing the thrust per engine by almost 14,000 *lbs*. Increasing the thrust causes the propulsion system weight to increase by almost 25,000 *lbs*. Clearly, the balanced field length constraint was a critical requirement.

For the final design, the constraints on range, nacelle strike, BFL, and the engine out condition were all critical. The nacelle strike constraint is limiting the landing angle of attack in this case. The BFL constraint sizes the engine, and the engine out condition sizes the vertical tail. The constraints on maximum thrust required, section  $C_\ell$ , time to rotate, and horizontal tail/wing overlap were nearly critical. The horizontal tail is sized by the time to rotate constraint.

Table 13: Comparison of Initial and Final Designs, Case 29a

	Initial	Final
Gross Weight ( <i>lbs</i> )	755,400	865,000
Fuel Weight ( <i>lbs</i> )	408,600	453,800
Fuel Wt / Gross Wt	54.1%	52.5%
Wing Area ( <i>ft</i> <sup>2</sup> )	12,794	14,363
Wing Weight ( <i>lbs</i> )	95,780	129,200
Aspect Ratio	2.08	2.00
Vertical Tail Area ( <i>ft</i> <sup>2</sup> )	564.6	670.5
Vertical Tail Weight ( <i>lbs</i> )	2,270	2,740
Nacelle 1 position, <i>y</i> ( <i>ft</i> )	10.1	7.9
Nacelle 2 position, <i>y</i> ( <i>ft</i> )	19.5	17.3
Horz. Tail Area ( <i>ft</i> <sup>2</sup> )	1,646.6	1,924.3
Horz. Tail Weight ( <i>lbs</i> )	9,150	10,990
Time to rotate ( <i>sec</i> )	4.68	4.95
Engine thrust ( <i>lbs</i> )	46,000	59,798
Nacelle length ( <i>ft</i> )	35.00	39.91
Nacelle diameter ( <i>ft</i> )	6.50	7.41
Propulsion system weight ( <i>lbs</i> )	77,290	101,200
Range ( <i>n.mi.</i> )	5,472.1	5,500.1
Landing angle of attack	12.00°	10.62°
Balanced Field Length ( <i>ft</i> )	12,794	10,044
$(L/D)_{max}$	8.684	9.000

The initial and final planforms are shown in Figure 31 and the designs are compared in Table 13. The convergence is very noisy between cycles 10 and 30, but is good for cycles 30 to 45 as can be seen in Figure 32. Figure 33 shows the history of the balanced field length.

## 6.5 Subsonic Leg (Case 29b)

For this optimization, we added a subsonic leg to our mission requirement. We required the initial 500 *n.mi.* be flown at Mach 0.9 and then continue on with the supersonic cruise-climb. This did not add any design variables, but did require two

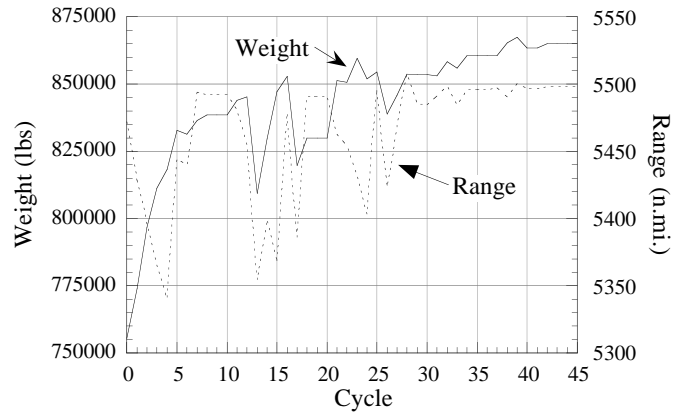


Figure 32: Takeoff Gross Weight and Range convergence, Case 29a

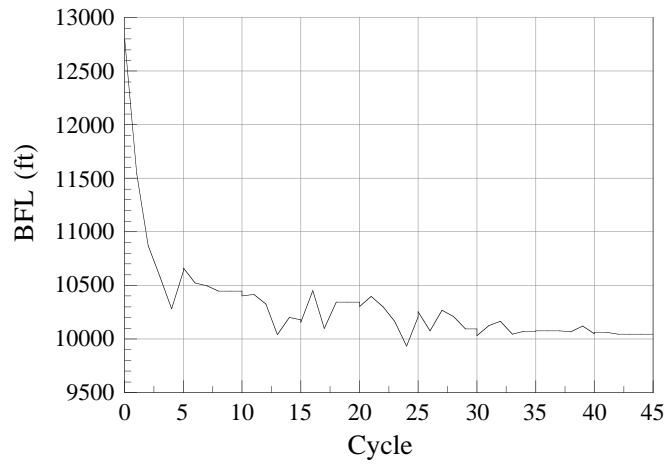


Figure 33: Balanced field length convergence, case 29a



more constraints. The additional constraints require that the available thrust be greater than the required thrust for the subsonic leg and the transition from the subsonic to supersonic leg. In this optimization, the transition is an instantaneous jump. The addition of these constraints results in 29 design variables and 70 constraints.

The initial design for this case is the final design from Case 29a. After adding the subsonic leg to the mission, the range for this design dropped to 5,221.5 *n.mi.*, a 280 *n.mi.* decrease. The range constraint is the only constraint which is initially violated.

The optimizer had trouble improving the range without violating the BFL constraint. Many attempts were made using different move limits to find a design which would satisfy both constraints. The final design satisfies both constraints, but weighs 100,000 *lbs* more than the initial design.

Seventy percent of the increase in weight is due to added fuel. Another 20% of the increase comes from increased wing weight. The rest of the weight increase comes from various sources, including the vertical tail, horizontal tail, and the propulsion system.

The final design does not appear too different from the initial design. There is an increase in aspect ratio which improves the subsonic aerodynamic performance. Figure 34 shows both the starting and ending designs and Table 14 compares them. Convergence of TOGW, range, and BFL is shown in Figures 35 and 36.

The increase in weight agrees with trends predicted in other studies. A study by the Douglas Aircraft Company<sup>60</sup> showed large increases in weight with increasing subsonic mission segments. Martin *et al.*<sup>61</sup> also predicted increases in weight corresponding to increasing subsonic leg.

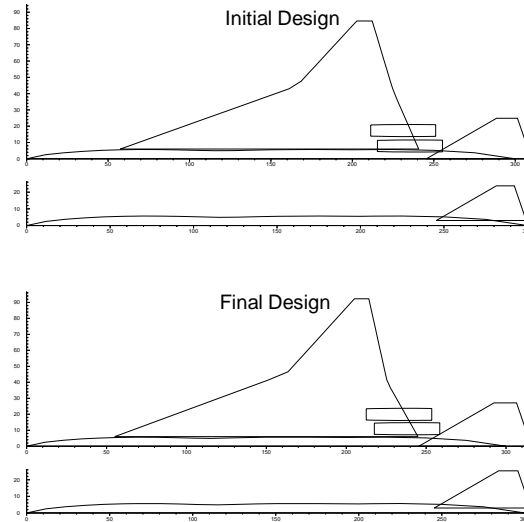


Figure 34: Initial and final planforms, Case 29b

The actual subsonic leg requirements for an HSCT could be less than the 500 *n.mi.* that we have used. Reducing this requirement would make it easier for the optimizer to find a feasible design. An increase in the allowable BFL could also help the optimizer.

## 6.6 Sensitivity To Parameters and Analysis Accuracy

### 6.6.1 Engine Sizing with Relaxed BFL Constraint (Case 29c)

This optimization run was conducted in order to investigate the effect of relaxing the BFL constraint on the engine size and overall aircraft parameters, including the TOGW and horizontal and vertical tail sizes. Since this requirement was one of the most critical for optimizing the configuration of HSCT in case 29a, it is reasonable to relax this constraint to determine the size of the expected weight reduction.

The number of design variables (29) and the values and number of constraints (68) was unchanged compared to case 29a, and the only requirement that changed was

Table 14: Comparison of Initial and Final Designs, Case 29b

	Initial	Final
Gross Weight ( <i>lbs</i> )	865,000	966,400
Fuel Weight ( <i>lbs</i> )	453,800	523,900
Fuel Wt / Gross Wt	52.5%	54.2%
Wing Area ( <i>ft</i> <sup>2</sup> )	14,363	15,610
Wing Weight ( <i>lbs</i> )	129,200	148,900
Aspect Ratio	1.99	2.18
Vertical Tail Area ( <i>ft</i> <sup>2</sup> )	670.5	778.2
Vertical Tail Weight ( <i>lbs</i> )	2,740	3,210
Nacelle 1 position, <i>y</i> ( <i>ft</i> )	7.9	11.0
Nacelle 2 position, <i>y</i> ( <i>ft</i> )	17.3	19.9
Horz. Tail Area ( <i>ft</i> <sup>2</sup> )	1,924.3	2,293.4
Horz. Tail Weight ( <i>lbs</i> )	10,990	13,400
Time to rotate ( <i>sec</i> )	4.95	4.86
Engine thrust ( <i>lbs</i> )	59,798	62,972
Nacelle length ( <i>ft</i> )	39.91	40.95
Nacelle diameter ( <i>ft</i> )	7.41	7.61
Propulsion system weight ( <i>lbs</i> )	101,200	107,200
Range ( <i>n.mi.</i> )	5,221.5	5,519.2
Landing angle of attack	10.62°	10.25°
Balanced Field Length ( <i>ft</i> )	10,047	9,984
$(L/D)_{max}$	8.998	8.953

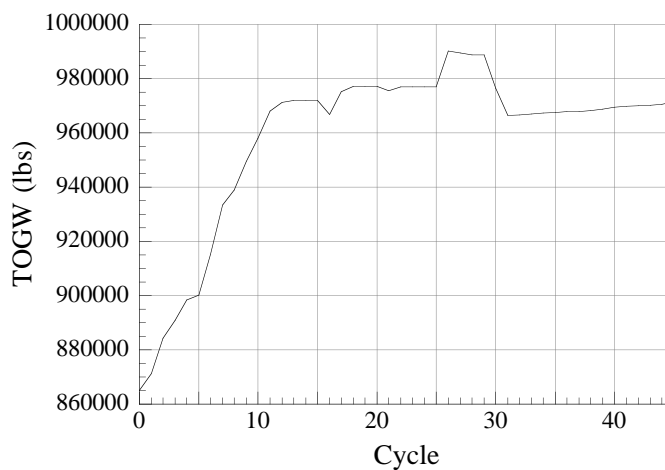


Figure 35: Takeoff Gross Weight convergence, Case 29b

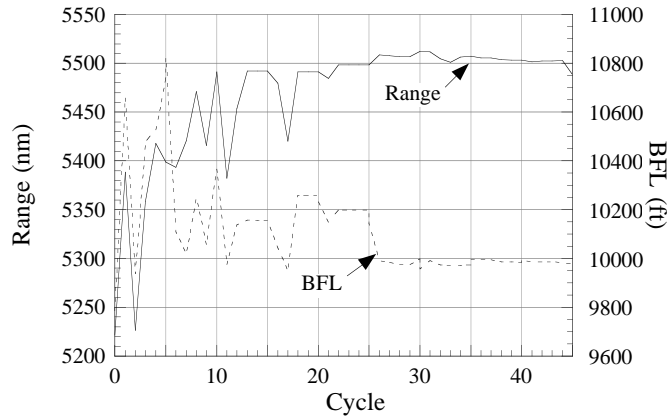


Figure 36: Range and BFL convergence, case 29b

the BFL constraint, which was set to 11,000 *ft* instead of 10,000 *ft* for case 29a. The initial design for this case was one of the intermediate designs from the optimization run 29a.

The final design is considerably heavier than the initial design for the optimization but still much less than the TOGW for case 29a (10,000 *ft* BFL). Take-off weight of the HSCT increased during the optimization from 732,741 *lbs* up to 772,981 *lbs* (40,240 *lbs* increase). The wing area increased by 578 *ft*<sup>2</sup> and the wing weight increased by 9,839 *lbs*.

For the final design, the constraints of range, nacelle strike, wing and horizontal tail overlap, bank angle and the engine out condition were all critical. Interestingly, the BFL constraint is not critical any more, and engine sizing is done by the requirements on the thrust at cruise. The rotation time constraint determines the horizontal tail size, and vertical tail size is determined by the engine out condition.

The initial and final configurations are shown in Figure 37 and the designs are compared in Table 15. The convergence is noisy throughout the optimization, which partly is due to using large values for the move limits. The optimization history is shown in Figures 38 and 39.

Table 15: Comparison of Initial and Final Designs, Case 29c

	Initial	Final
Gross Weight ( <i>lbs</i> )	732,741	772,981
Fuel Weight ( <i>lbs</i> )	376,454	403,346
Fuel Wt / Gross Wt	51.4%	52.1%
Wing Area ( <i>ft</i> <sup>2</sup> )	12,612	13,191
Wing Weight ( <i>lbs</i> )	103,247	113,086
Aspect Ratio	1.88	1.99
Vertical Tail Area ( <i>ft</i> <sup>2</sup> )	514.3	454.1
Vertical Tail Weight ( <i>lbs</i> )	2,077	1,898
Nacelle 1 position, y ( <i>ft</i> )	8.26	7.08
Nacelle 2 position, y ( <i>ft</i> )	21.37	14.41
Horz. Tail Area ( <i>ft</i> <sup>2</sup> )	778.9	747.2
Horz. Tail Weight ( <i>lbs</i> )	8,608	8,346
Time to rotate ( <i>sec</i> )	5.07	5.27
Engine thrust ( <i>lbs</i> )	46,480	49,258
Nacelle length ( <i>ft</i> )	35.18	37.40
Nacelle diameter ( <i>ft</i> )	6.53	6.95
Propulsion system weight ( <i>lbs</i> )	77,884	82,791
Range ( <i>n.mi.</i> )	5,373.5	5,502.9
Landing angle of attack	10.85°	10.58°
Balanced Field Length ( <i>ft</i> )	11,094	10,922
$(L/D)_{max}$	9.132	9.155

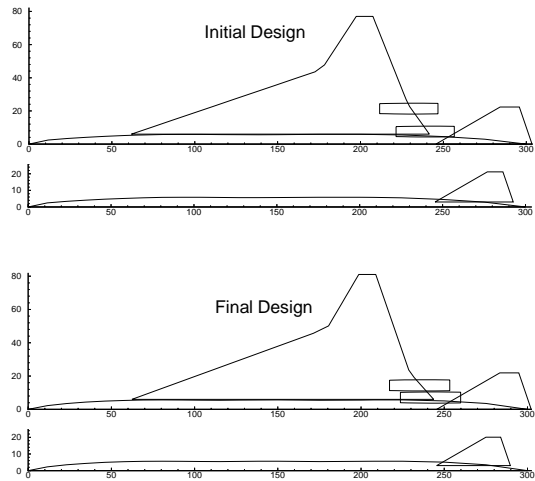


Figure 37: Initial and final planforms, Case 29c

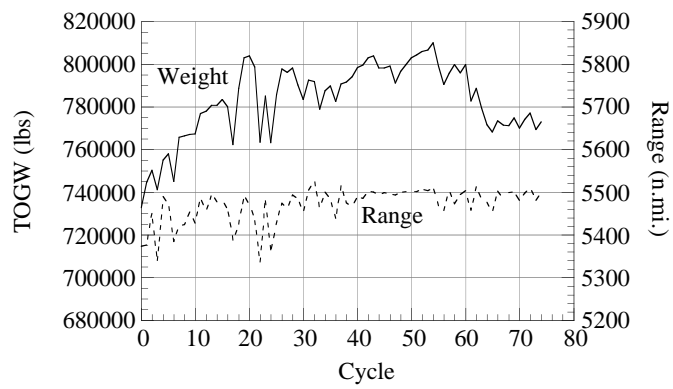


Figure 38: Takeoff Gross Weight and Range convergence, Case 29c

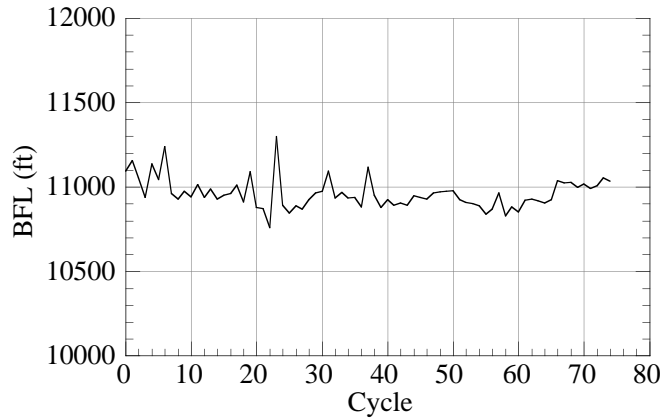


Figure 39: Balanced field length convergence, Case 29c

### Comparison of Cases 29a and 29c

Cases 29a and 29c are identical except for the BFL constraint which was set to 10000 *ft* for 29a and to 11000 *ft* for 29c. The purpose of optimizing the HSCT for relaxed BFL constraint (Case 29c) was to investigate the sensitivity of TOGW and other parameters to the field length requirement. As pointed out earlier, the BFL requirement was critical in Case 29a and basically it was the driving factor for engine sizing, and consequently, for HSCT weight. Thus, relaxing this requirement can lead to significant weight and size savings for HSCT.

The final designs for Cases 29a and 29c are compared in the Table 16. Apparent are significant weight and size reductions of the HSCT from Case 29a to 29c. TOGW is reduced by over 92,000 *lbs*, fuel weight is reduced by over 50,000 *lbs*. Noticable area reductions are observed for wing (1,172 *ft*<sup>2</sup> change), vertical tail (216.4 *ft*<sup>2</sup> change) and horizontal tail (1,177.1 *ft*<sup>2</sup> change). Relaxing the BFL constraint made it non-critical for the thrust requirements, which led to engine sizing based on the cruise thrust requirement, thus decreasing the size and weight of the engines. Propulsion weight was reduced by 18,409 *lbs* and engine thrust reduced by 10,540 *lbs*. Reduced engine thrust also led to reduced vertical tail size, which is driven by the engine out condition. The overall reduction of weight and inertia moments resulted in considerably reduced horizontal tail area, which is driven by the rotation time constraint.

Table 16: Comparison of Final Designs for Case 29a and 29c

	Case 29a	Case 29c
Gross Weight ( <i>lbs</i> )	865,000	772,981
Fuel Weight ( <i>lbs</i> )	453,800	403,346
Fuel Wt / Gross Wt	52.5%	52.1%
Wing Area ( <i>ft</i> <sup>2</sup> )	14,363	13,191
Wing Weight ( <i>lbs</i> )	129,200	113,086
Aspect Ratio	2.00	1.99
Vertical Tail Area ( <i>ft</i> <sup>2</sup> )	670.5	454.1
Vertical Tail Weight ( <i>lbs</i> )	2,740	1,898
Nacelle 1 position, <i>y</i> ( <i>ft</i> )	7.9	7.08
Nacelle 2 position, <i>y</i> ( <i>ft</i> )	17.3	14.41
Horz. Tail Area ( <i>ft</i> <sup>2</sup> )	1,924.3	747.2
Horz. Tail Weight ( <i>lbs</i> )	10,990	8,346
Time to rotate ( <i>sec</i> )	4.95	5.27
Engine thrust ( <i>lbs</i> )	59,798	49,258
Nacelle length ( <i>ft</i> )	39.91	37.40
Nacelle diameter ( <i>ft</i> )	7.41	6.95
Propulsion system weight ( <i>lbs</i> )	101,200	82,791
Range ( <i>n.mi.</i> )	5,500.1	5,502.9
Landing angle of attack	10.62°	10.58°
Balanced Field Length ( <i>ft</i> )	10,044	10,922
$(L/D)_{max}$	9.000	9.155



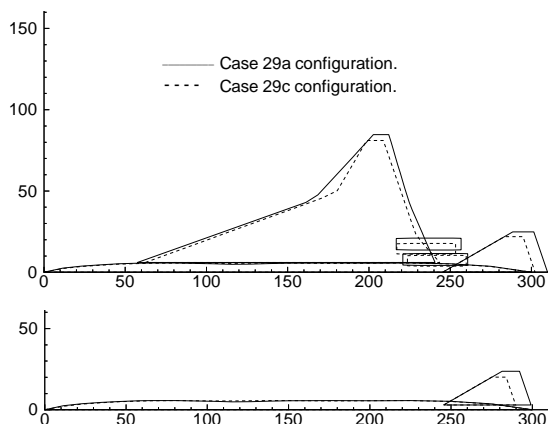


Figure 40: Comparison of planforms for Case 29a and 29c.

The configurations for cases 29a and 29c are compared on the Figure 40. Apparent are reductions of the wing and tail areas, giving smaller overall aircraft size.

### 6.6.2 TOGW Sensitivity to Drag Change

A series of optimization runs was made to investigate the sensitivity of take-off weight of the HSCT to changes in drag. Several reasons led to this investigation, among which were the uncertainty of the drag coefficient values when using simplified aerodynamics equations, and the need to assess the penalty in TOGW with changes in trim drag for possible inclusion of control system design into MDO of HSCT.

As well known, small changes in the drag coefficient of a high speed aircraft can cause drastic changes in its performance, thus considerably changing the appearance of the optimized HSCT. Usually, a 1-2 drag count change can lead to a noticeable difference in performance. For this investigation it was decided to use the 29c case configuration as the baseline and then run the optimizer with changed friction drag values to compare the new optimized configurations with the baseline configuration. Four different runs were conducted during the investigation, with drag changes of -2, -1, +1 and +2 counts. The starting point for all four designs was the final configuration of case 29c (the baseline configuration for sensitivity studies). Changes were made in

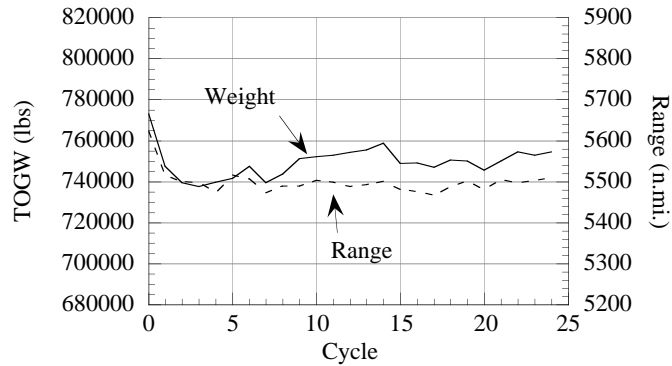


Figure 41: TOGW and range convergence for the design with a 2 count drag reduction

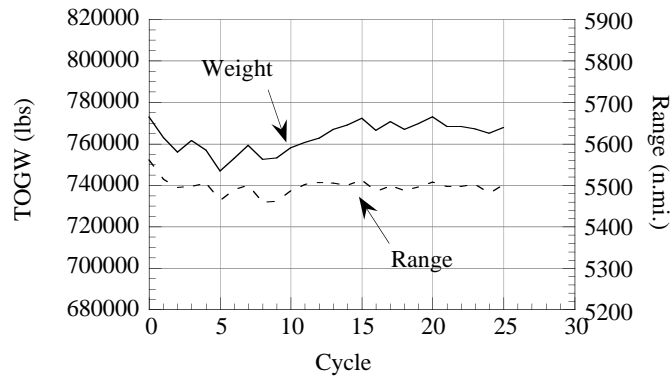


Figure 42: TOGW and range convergence for the design with a 1 count drag reduction

the friction drag subroutine so that the drag coefficient over the entire flight profile is changed. The optimization history of TOGW and range for the changed drag designs is shown on figures 41 to 44.

In all four cases the optimizer converged to different configurations, which can be seen in Figures 45 to 48. The new planforms are plotted along with the baseline configuration for comparison. Configurations for -1 and +1 drag count change are very close to the baseline planform, which makes it difficult to make specific conclusions. The weight nevertheless decreases with a decrease in drag and vice versa. On the other hand, the configurations for -2 and +2 drag counts show a clear tendency to change the wing sweep with a change in drag. Increased drag causes the optimizer to reduce the drag using a wing planform with more sweep to get better supersonic performance to compensate for the drag penalties. In the opposite case, when drag

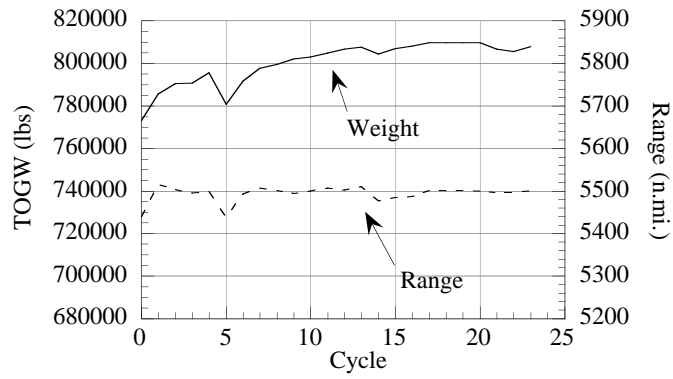


Figure 43: TOGW and range convergence for the design with a 1 count drag increase

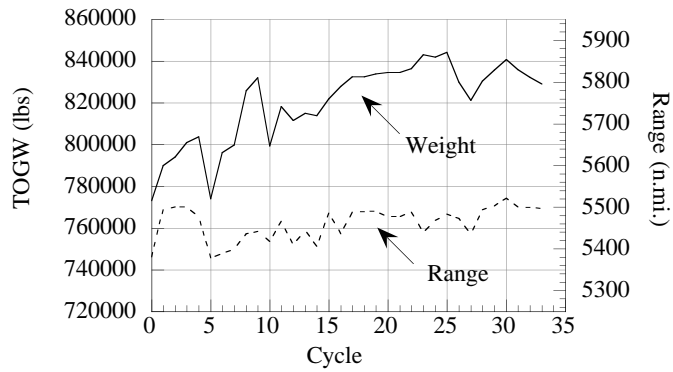


Figure 44: TOGW and range convergence for the design with a 2 count drag increase

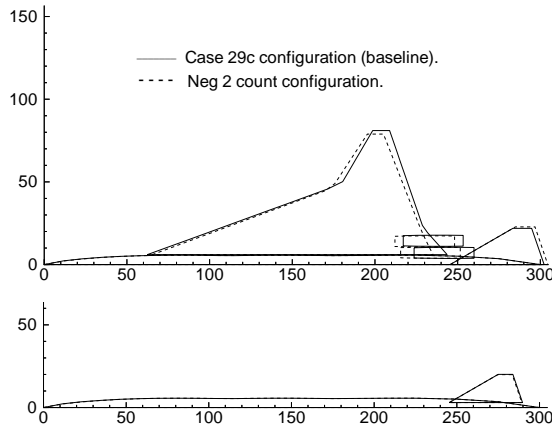


Figure 45: Baseline and negative 2 drag count planforms

decreased the optimizer takes advantage of the improved performance and chooses a wing planform with less sweep to reduce wing weight. The configuration for +1 count is offset of this trend line and has less sweep compared to the baseline even though the drag is increased. This may only be explained by the numerous local minima in the extremely non-convex design space, which makes it very difficult if not impossible for the optimizer to find the global optimum design. TOGW differences are clearly found for the changed drag designs, with about 18,000 *lbs* saving for -2 counts case and about 57,000 *lbs* gain for +2 counts case. The weight to drag sensitivity curve (Figure 49) can be approximated by an almost straight line if the baseline design is moved up. Imperfections of the plot, partly explained earlier, can also be attributed to the high level of noise in the code while performing detailed evaluations of aerodynamic parameters.

Some major parameters of the configurations for different drag changes are compared in Table 17. Plots in Figures 50 to 52 show how some of the variables and parameters change with the drag change. Note, that the lines do not represent any continuous functions of drag and are drawn only to help in visualizing the trends. The only actual data are in the nodes of the plots.

From the analysis of the plots it can be seen that most of the TOGW increase is due to the extra fuel weight necessary to compensate for the range deficiency because

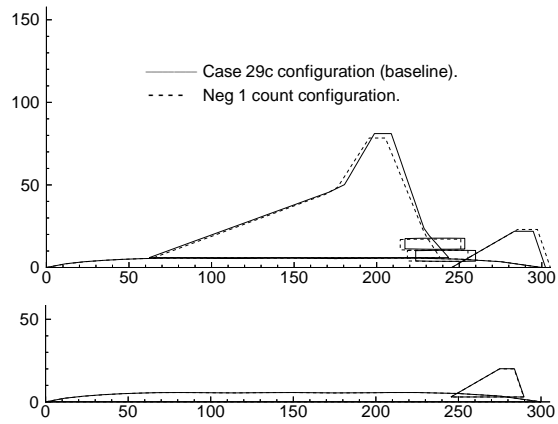


Figure 46: Baseline and negative 1 drag count planforms

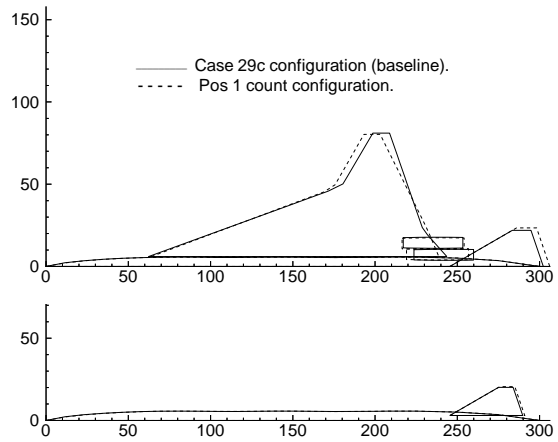


Figure 47: Baseline and positive 1 drag count planforms

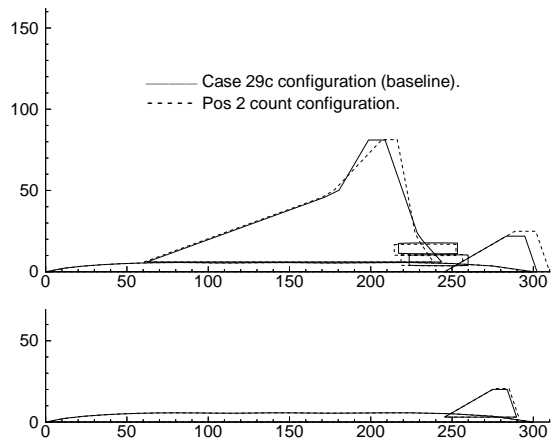


Figure 48: Baseline and positive 2 drag count planforms

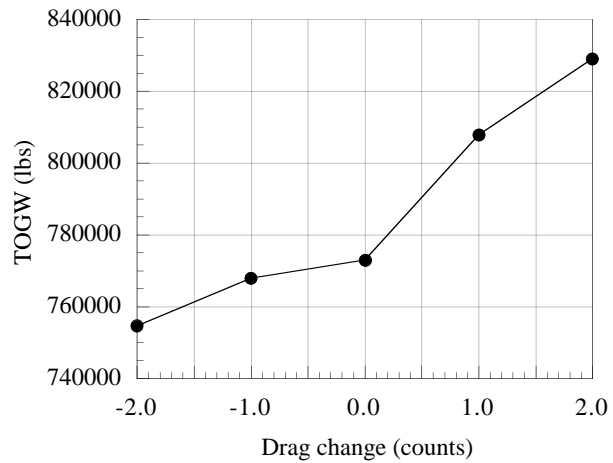


Figure 49: TOGW variation with drag change

Table 17: Comparison of the baseline design (Case 29c) to the changed drag designs

	-2 counts	-1 count	baseline	+1 count	+2 counts
Gross Weight ( <i>lbs</i> )	754,560	767,907	772,981	807,774	829,099
Fuel Weight ( <i>lbs</i> )	391,817	401,316	403,346	426,628	440,564
Fuel Wt / Gross Wt	51.93%	52.3%	52.1%	52.82%	53.14%
Wing Area ( <i>ft</i> <sup>2</sup> )	12,476	12,597	13,191	13,153	13,387
Wing Weight ( <i>lbs</i> )	107,071	107,364	113,086	115,077	119,053
Aspect Ratio	2.00	1.95	1.99	1.96	1.975
Vertical Tail Area ( <i>ft</i> <sup>2</sup> )	444.5	449.2	454.1	479.3	481.9
Vertical Tail Weight ( <i>lbs</i> )	1,851	1,877	1,898	2,014	2,039
Nacelle 1 position, <i>y</i> ( <i>ft</i> )	7.17	7.10	7.08	7.43	7.21
Nacelle 2 position, <i>y</i> ( <i>ft</i> )	14.1	13.8	14.41	13.91	13.46
Horz. Tail Area ( <i>ft</i> <sup>2</sup> )	808.4	825.4	747.2	853.4	966.4
Horz. Tail Weight ( <i>lbs</i> )	8,986	9,208	8,346	9,617	10,946
Engine thrust ( <i>lbs</i> )	48,835	50,554	49,258	53,309	54,155
Prop. system weight ( <i>lbs</i> )	81,992	84,989	82,791	89,873	91,416
Range ( <i>n.mi.</i> )	5,503.9	5,499.4	5,502.9	5,498.2	5,493.1
Landing angle of attack	10.93°	11.17°	10.58°	11.14°	11.09°
Balanced Field Length ( <i>ft</i> )	10,947	10,988	10,922	10,979	10,963
$(L/D)_{max}$	9.165	9.055	9.155	8.940	8.892

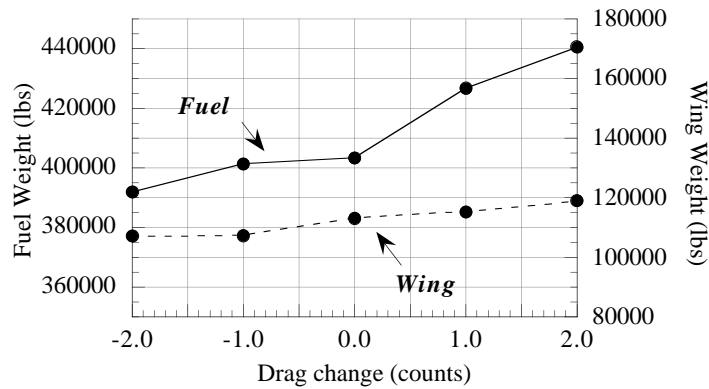


Figure 50: Fuel and wing weight variation with drag change

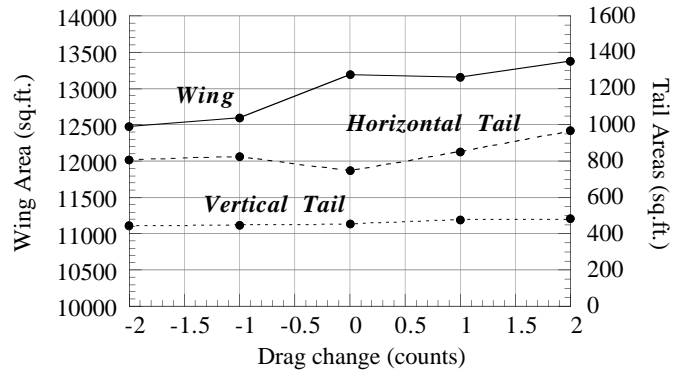


Figure 51: Wing, horizontal and vertical tail areas variation with drag change

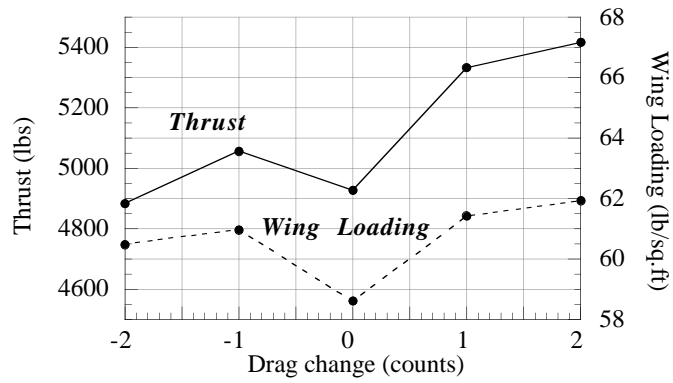


Figure 52: Engine thrust and wing loading variation with drag change



of the extra drag. Structural weight of the HSCT changes very little, as can be seen on the wing weight plot, Figure 50, even though the size of the aircraft is slightly bigger for greater drag (wing area  $13,387 \text{ ft}^2$  for +2 drag count configuration versus  $12,476 \text{ ft}^2$  for -2 drag count). The components' area increase thus is very small and is practically not seen for tail surfaces (Figure 51). Engine thrust, however, does increase with the drag, as can be expected, to compensate for poorer take-off performance and increased cruise drag (Figure 52). Out of the  $74,539 \text{ lbs}$  weight increase from -2 to +2 count designs, the contribution of the fuel weight is  $48,747 \text{ lbs}$  (65.4%), the contribution of the propulsion system weight -  $9,424 \text{ lbs}$  (12.6%), and the wing weight contributes  $11,982 \text{ lbs}$  (16.1%), with the rest  $4,386 \text{ lbs}$  (5.9%) contribution made by all the other components (tails, fuselage, etc.).

Plots of the areas (Figure 51) and thrust/wing loading (Figure 52) for different designs indicate that for the baseline configuration the optimizer found an increased wing design, which might have helped to save some weight of the aircraft by reducing the wing loading and consequently the required thrust for take-off (see Figure 52), saving some weight of the propulsion system and fuel. This may also somewhat explain the offset of the baseline point on the TOGW vs drag change plot, where the baseline is out of the straight line approximated through the rest of the points.

### **6.6.3 TOGW Sensitivity to Rotation Time (Case 29d)**

The rotation time in all previous cases was restricted to 5 seconds. The choice of this value, although reasonable, is somewhat arbitrary. That's why it was decided to investigate the effect of changing the rotation time constraint on the TOGW and other parameters of the HSCT. Two optimization runs were conducted for this purpose, with the rotation time set to 6 seconds (Case 29d-6) and with the rotation time set to 20 seconds (Case 29d-20). All the rest of the constraints and requirements were the same as for Case 29c (relaxed BFL case).

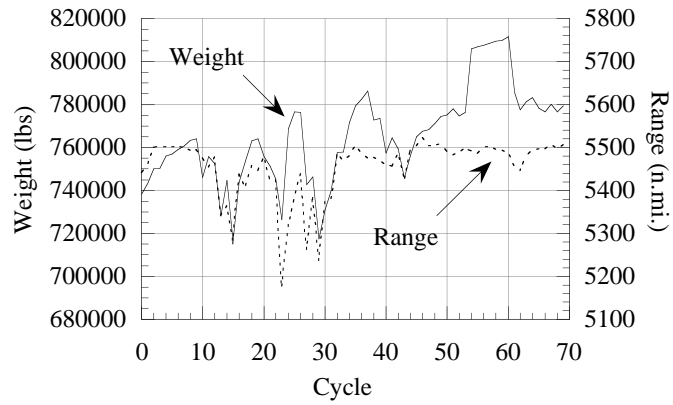


Figure 53: Take-off Gross Weight and Range convergence, Case 29d-6

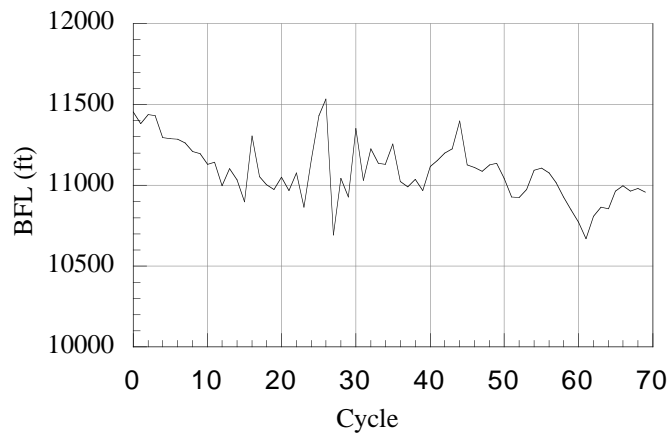


Figure 54: Balanced Field Length convergence, Case 29d-6

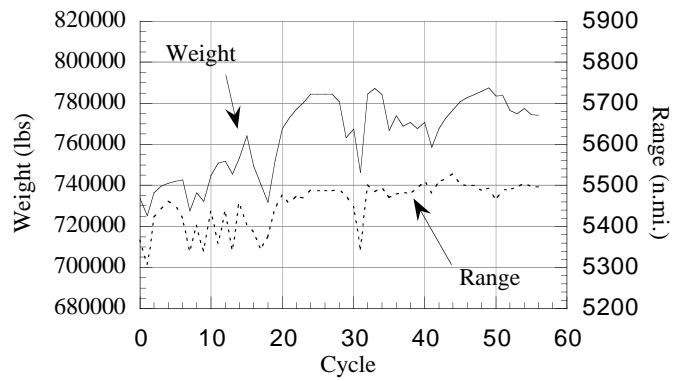


Figure 55: Take-off Gross Weight and Range convergence, Case 29d-20

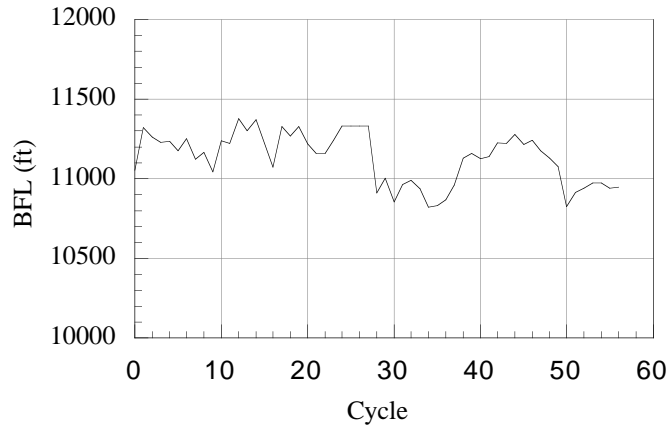


Figure 56: Balanced Field Length convergence, Case 29d-20

The two optimizations were started from the same initial point as the baseline design (Case 29c). Convergence plots of TOGW, range and BFL for both cases are shown on Figures 53 to 56 and the final configurations are compared with the baseline on Figures 57 and 58. Some major parameters of the designs are compared in Table 18.

As one can see, the TOGW of both new designs (6 sec and 20 sec) is heavier than that of the baseline configuration (779,358 and 774,134 *lbs*), even though it was expected to reduce due to relaxing one of the constraints. This indicates that the rotation time constraint is not critical for forming the optimum design of HSCT in the given conditions. Same conclusion may be drawn from observing the actual rotation time of the new designs: 5.81 sec for the 6 sec design, and 5.63 sec for the 20 sec design. Obviously, the rotation time constraint was not active for both of them and had no effect on the final configurations of HSCT in these cases. The fact that the new designs have heavier weights may again be explained by the complex design space, which along with the noise in the system can easily make the optimizer drift from the optimum design and settle in one of the local minima.

Table 18: Comparison of Final Designs for Case 29d and 29c

	Case 29d-6	Case 29d-20	Case 29c
Gross Weight ( <i>lbs</i> )	779,358	774,134	772,981
Fuel Weight ( <i>lbs</i> )	407,523	403,910	403,346
Fuel Wt / Gross Wt	52.3%	52.18%	52.1%
Wing Area ( <i>ft</i> <sup>2</sup> )	12,956	12,916	13,191
Wing Weight ( <i>lbs</i> )	112,254	110,290	113,086
Aspect Ratio	2.03	1.98	1.99
Vertical Tail Area ( <i>ft</i> <sup>2</sup> )	456.8	450.7	454.1
Vertical Tail Weight ( <i>lbs</i> )	1,913	1,887	1,898
Nacelle 1 position, <i>y</i> ( <i>ft</i> )	7.09	7.39	7.08
Nacelle 2 position, <i>y</i> ( <i>ft</i> )	14.0	13.4	14.41
Horz. Tail Area ( <i>ft</i> <sup>2</sup> )	675.4	650.6	747.2
Horz. Tail Weight ( <i>lbs</i> )	7,557	7,269	8,346
Time to rotate ( <i>sec</i> )	5.81	5.63	5.27
Engine thrust ( <i>lbs</i> )	51,391	51,856	49,258
Propulsion system weight ( <i>lbs</i> )	86,463	87,233	82,791
Range ( <i>n.mi.</i> )	5,503.5	5,495.2	5,502.9
Landing angle of attack	10.80°	10.92°	10.58°
Balanced Field Length ( <i>ft</i> )	11,035	10,913	10,922
$(L/D)_{max}$	9.079	9.064	9.155

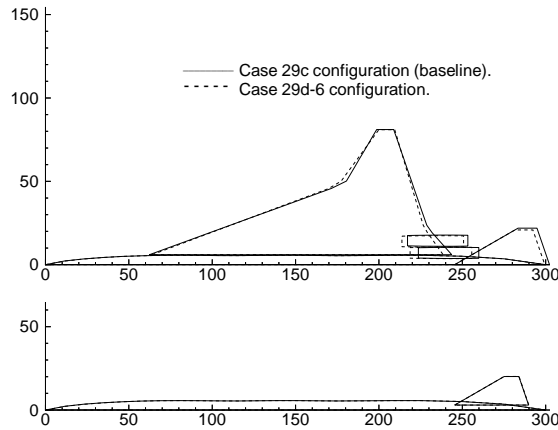


Figure 57: Configurations for Cases 29c and 29d-6

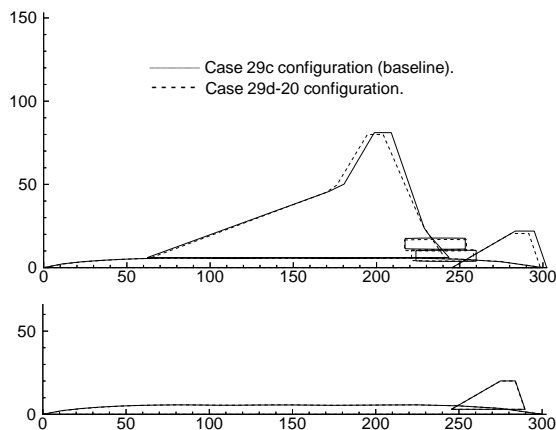


Figure 58: Configurations for Cases 29c and 29d-20

## 6.7 Minimum Time to Climb Calculation

We tried to optimize a design including a minimum time climb segment in the mission. Although the analysis for the minimum time climb segment works, it was not robust enough to use in an optimization. The optimizer repeatedly caused the routine to crash. Work is underway to improve the analysis so it can be used in an optimization.

There are two main problems. First, the routine sometimes has trouble finding the maximum specific excess power for a given energy height. This is due to the multimodal nature of the specific excess power curve for a constant energy height. There are usually two local maximums, one subsonic and the other supersonic. Most of the time the supersonic maximum is above the dynamic pressure limit, but it is necessary for the search routine to find both maximums to determine if the dynamic pressure limit is active. We have broken the search into two regions, which generally allows us to find both maximums, but because of noise in the analysis, the routine has trouble switching from the subsonic maximum to the supersonic maximum.

The other problem is the possible large differences between the flight path calculated using the detailed analysis and the approximate analysis. This difference can cause range discrepancies of over 1,000 *n.mi.* if the detailed and approximate analysis transition from subsonic to supersonic at significantly different places.

Another consideration is computing time. Including the minimum time to climb segment in the mission can double or triple the time required to calculate the range. This calculation is sometimes performed more than one thousand times during an optimization cycle. This causes a very large increase in the time required to optimize a design.

# Chapter 7

## Conclusions

Multidisciplinary design optimization using variable complexity modeling can produce feasible, optimized designs. We have extended and refined our code to explore design issues which are not often considered at this level of aircraft design. We were not successful in every case, but this may be due to unrealistic design requirements. A summary of our optimization cases is shown in Table 19

We have added essential trim and control effects to our HSCT design methodology. The variable complexity technique of interlacing the approximate stability derivative predictions with the more accurate VLM predictions worked satisfactorily. Although the derivatives were only updated with the VLM predictions once every 5 optimization cycles, there was good agreement between the approximate predictions and the more accurate predictions.

Adding the engine-out consideration forces the vertical tail to be sized based on the engine location. We found that the spanwise engine location is constrained by the aerodynamic control requirements. The engines are placed as far inboard as the nacelle lateral spacing constraints allow, and the vertical tail size is minimized. But, as was shown in Case 27b, there is another local minimum which has a larger vertical tail and one nacelle located on the outboard wing section. This takes advantage of the greater bending moment relief effect, which lowers the wing weight by about 2,000 *lbs*.

The inboard nacelle strike constraints were active in every case. In the first five

Table 19: Summary of optimizations

Case	Additional Requirement	Final Weight ( <i>lbs</i> )
26a	None (baseline case)	545,800
27a	Vertical tail sizing	547,300
27b	Vertical tail sizing	543,700
28a	Horizontal tail sizing	630,000
28b	Reduced engine technology	755,400
29a	Balanced field length	865,000
29b	Subsonic leg	966,400
29c	Relaxed BFL	772,981
	Changed drag:	
	-2 counts	754,560
	-1 count	767,907
	+1 count	807,774
	+2 counts	829,099
29d	Changed rotation time:	
	6 seconds	779,358
	20 seconds	774,134



cases, it is not clear what these constraints affected. It is possible that these constraints limit the amount of trailing edge sweep in those cases. In the last two cases, 29a and 29b, these constraints limit the allowable landing angle of attack.

The horizontal tail size is based on the requirement that the aircraft must rotate to the take-off position in under 5 *sec*, except for Cases 29d. The tail size required to do this is highly dependent on the positioning of the landing gear. The horizontal tail size is also very sensitive to flap effects, which have only been crudely modeled in this work. The tail deflection for approach trim was not critical for any of our designs. Another parameter strongly affecting the horizontal tail size is the TOGW of the HSCT. For all of the sensitivity studies' designs, where relaxed BFL led to reduced take-off weight, the size of the horizontal tail is considerably smaller than for previous cases. Relaxed rotation time constraint in Cases 29d didn't have much effect neither on tail size, nor on the TOGW.

The increased vertical tail size and the addition of a horizontal tail add less than 2.5% directly to the gross take-off weight, but they result in drag penalties, which translate to large increases in weight. This increased weight is mostly fuel. The rest of the weight increase is due to the greater amount of fuel being carried, not to structural problems, which would be indicated by changes in the wing planform. Although we found that trim and control increased the weight, adding these considerations provides a more realistic model and better designs.

Reducing the technology level of the engines ( $\Delta T/W|_{eng} = -1$ ) caused a large increase in engine weight and size. This caused a large decrease in range and a large weight penalty was incurred to satisfy all the constraints. Engine sizing was added along with a balanced field length requirement.

Adding a 500 *n.mi.* subsonic leg to our mission caused a large decrease in total range. Overcoming this range deficit while maintaining the balanced field length requirement was difficult. The final design was much heavier than the starting design. Our subsonic leg could be too long. A study of routes and regulations might indicate that the required subsonic leg is shorter than the 500 *n.mi.* that we required. Although this design is extremely heavy, it demonstrates that our MDO technique is capable of producing successful designs, even when faced with requirements that are very demanding.

Performed sensitivity studies showed the dependences of the TOGW and other parameters on the balanced field length, drag coefficient and rotation time restriction. Relaxing the BFL constraint from 10,000 *ft* to 11,000 *ft* reduced the TOGW by over 90,000 *lbs*. The drag parametric study showed a large weight decrease with decrease in drag coefficient. The difference in TOGW between the -2 count and +2 count designs was 74,539 *lbs*, with most of the weight increase being contributed by the fuel weight change (48,747 *lbs* or 65.4%). Finally, the relaxed rotation time constraint did not have any impact on the HSCT configuration and TOGW, and the differences in the TOGW can be attributed to the optimizer drift because of the system noise and the complex non-convex design space.

There are many opportunities for future work. An investigation into the effects of varying the subsonic leg length is necessary. This would indicate the quality of our models for these requirements. A start of the estimation of flap effects using response surfaces has been carried out by Crisafulli *et al*<sup>55</sup>. This improves both the horizontal tail sizing, and the balanced field length models. Also, integrating the minimum time to climb routine with the optimization is necessary.

# References

- [1] Sobieszczanski-Sobieski, J., “Multidisciplinary Optimization of Engineering Systems: Achievements and Potential,” in *Proceedings of an International Seminar, Optimization: Methods and Applications, Possibilities and Limitations* (Bergmann, H. W., ed.), vol. 47 of *Lecture Notes in Engineering*, pp. 42–62, Berlin, Germany: Springer-Verlag, 1989.
- [2] Sobieszczanski-Sobieski, J., “Multidisciplinary Design Optimization: An Emerging New Engineering Discipline,” in *presented at The World Congress on Optimal Design of Structural Systems*, (Rio de Janeiro, Brazil), Aug. 1993.
- [3] Sobieszczanski-Sobieski, J. and Haftka, R. T., “Multidisciplinary Aerospace Design Optimization: Survey of Recent Developments,” AIAA Paper 96-0711, Jan. 1996.
- [4] McGeer, T., “Wing Design for Minimum Drag and Practical Constraints,” *Journal of Aircraft*, vol. 21, pp. 879–886, Nov. 1984.
- [5] Grossman, B., Strauch, G., Eppard, W. M., Gürdal, Z., and Haftka, R. T., “Integrated Aerodynamic/Structural Design of a Sailplane Wing,” *Journal of Aircraft*, vol. 25, no. 9, pp. 855–860, 1988.
- [6] Wakayama, S. and Kroo, I., “A Method for Lifting Surface Design using Nonlinear Optimization,” AIAA Paper 90–3290, Sept. 1990.
- [7] Gallman, J. W., Smith, S. C., and Kroo, I. M., “Optimization of Joined-Wing Aircraft,” *Journal of Aircraft*, vol. 30, pp. 897–905, November-December 1993.

- [8] Chang, I. C., Torres, F. J., Driscoll, F. P., and Van Dam, C. P., “Optimization of Wing-Body Configurations by the Euler Equations,” AIAA Paper 94-1899, June 1994.
- [9] Tzong, G., Baker, M., Yalamanchili, K., and Giesing, J., “Aeroelastic Loads and Structural Optimization of a High Speed Civil Transport Model,” AIAA Paper 94-4378, Sept. 1994.
- [10] Borland, C. J., Benton, J. R., Frank, P. D., Kao, T. J., Mastro, R. A., and Barthelemy, J.-F. M., “Multidisciplinary Design Optimization of a Commercial Aircraft Wing—an Exploratory Study,” AIAA Paper 94-4305, Sept. 1994.
- [11] McCullers, L. A., “Aircraft Configuration Optimization Including Optimized Flight Profiles,” in *Proceedings of Symposium on Recent Experiences in Multidisciplinary Analysis and Optimization* (Sobieski, J., ed.), NASA CP-2327, pp. 396–412, Apr. 1984.
- [12] Scott, P. W., “Developing Highly Accurate Empirical Weight Estimating Relationships: Obstacles and Techniques,” SAWE Paper No. 2091, May 1992.
- [13] Udin, S. V. and Anderson, W. J., “Wing Mass Formula for Subsonic Aircraft,” *Journal of Aircraft*, vol. 29, no. 4, pp. 725–727, 1992.
- [14] Torenbeek, E., “Development and Application of a Comprehensive Design-Sensitive Weight Prediction Method for Wing Structures of Transport-Category Aircraft,” Delft University Department of Aerospace Engineering Report LR-693, Sept. 1992.
- [15] Huang, X., Dudley, J., Haftka, R. T., Grossman, B., and Mason, W. H., “Structural Weight Estimation for Multidisciplinary Optimization of a High-Speed Civil Transport,” to appear *Journal of Aircraft*, vol. 33, May-June 1996.
- [16] Hutchison, M. G., Unger, E., Mason, W. H., Grossman, B., and Haftka, R. T., “Variable-Complexity Aerodynamic Optimization of a High Speed Civil Transport Wing,” *Journal of Aircraft*, vol. 31, pp. 110–116, January-February 1994.

- [17] Hutchison, M. G., Huang, X., Mason, W. H., Haftka, R. T., and Grossman, B., “Variable-Complexity Aerodynamic-Structural Design of a High-Speed Civil Transport Wing,” AIAA Paper 92-4695, Sept. 1992.
- [18] Hutchison, M. G., Mason, W. H., Grossman, B., and Haftka, R. T., “Aerodynamic Optimization of an HSCT Configuration Using Variable-Complexity Modeling,” AIAA Paper 93-0101, Jan. 1993.
- [19] Dudley, J., Huang, X., Haftka, R. T., Grossman, B., and Mason, W. H., “Variable-Complexity Interlacing of Weight Equation and Structural Optimization for the Design of the High-Speed Civil Transport,” AIAA Paper 94-4377, Sept. 1994.
- [20] Sliwa, S. M., “Impact of Longitudinal Flying Qualities Upon the Design of a Transport With Active Controls,” AIAA Paper 80-1570, 1980.
- [21] Sliwa, S. M., “Sensitivity of Optimal Preliminary Design of a Transport to Operational Constraints and Performance Index,” AIAA Paper 80-1895, Aug. 1980.
- [22] Kay, J., Mason, W. H., Durham, W., and Lutze, F., “Control Authority Assessment in Aircraft Conceptual Design,” AIAA Paper 93-3968, Aug. 1993.
- [23] McCarty, C. A., Feather, J. B., Dykman, J. R., Page, M. A., and Hodgkinson, J., “Design and Analysis Issues of Integrated Control Systems for High-Speed Civil Transports,” NASA Contractor Report 186022, May 1992.
- [24] Torenbeek, E., *Synthesis of Subsonic Airplane Design*. Delft University Press, 1982.
- [25] FAA, Washington, DC, *FAR Part 25*.
- [26] Ogburn, M. E., Foster, J. v., Pahle, J. W., Wilson, R. J., and Lackey, J. B., “Status of the Validation of High-Angle-of-Attack Nose-Down Pitch Control Margin Design guidelines,” AIAA Paper 93-3623, 1993.

- [27] Craidon, C. B., “Description of a Digital Computer Program for Airplane Configuration Plots,” NASA TM X-2074, 1970.
- [28] Barnwell, R., “Approximate Method for Calculating Transonic Flow About Lifting Wing-Body Configurations,” NASA TR R-452, pp. 58–61, Apr. 1976.
- [29] Hutchison, M., Unger, E., Mason, W. H., Grossman, B., and Haftka, R., “Variable-Complexity Aerodynamic Optimization of an HSCT Wing Using Structural Wing-Weight Equations,” AIAA Paper 92-0212, Jan. 1992.
- [30] Eminton, E., “On the Minimisation and Numerical Evaluation of Wave Drag,” Royal Aircraft Establishment Report AERO.2564, Nov. 1955.
- [31] MacMillin, P. E., Dudley, J., Mason, W. H., Grossman, B., and Haftka, R. T., “Trim, Control and Landing Gear Effects in Variable-Complexity HSCT Design,” AIAA Paper 94-4381, Sept. 1994.
- [32] Harris, Jr., R. V., “An Analysis and Correlation of Aircraft Wave Drag,” NASA TM X-947, 1964.
- [33] Hutchison, M. G., *Multidisciplinary Optimization of High-Speed Civil Transport Configurations Using Variable-Complexity Modeling*. PhD thesis, Virginia Polytechnic Institute and State University, Blacksburg, Virginia, Mar. 1993.
- [34] Hollenback, O. M. and Bloom, G. A., “Applications of a Parabolized Navier-Stokes Code to an HSCT Configuration and Comparison to Wind Tunnel Test Data,” AIAA Paper 93-3537, Aug. 1993.
- [35] Carlson, H. W. and Miller, D. S., “Numerical Methods for the Design and Analysis of Wings at Supersonic Speeds,” NASA TN D-7713, 1974.
- [36] Carlson, H. W. and Mack, R. J., “Estimation of Leading-Edge Thrust for Supersonic Wings of Arbitrary Planforms,” NASA TP-1270, 1978.
- [37] Cohen, D. and Friedman, M. D., “Theoretical Investigation of the Supersonic Lift and Drag of Thin, Sweptback Wings with Increased Sweep near the Root,” NACA TN-2959, June 1953.

- [38] Hopkins, E. J. and Inouye, M., “An Evaluation of Theories for Predicting Turbulent Skin Friction and Heat Transfer on Flat Plates at Supersonic and Hypersonic Mach Numbers,” *AIAA Journal*, vol. 9, pp. 993–1003, June 1971.
- [39] Diederich, F. W., “A Planform Parameter for Correlating Certain Aerodynamic Characteristics of Swept Wings,” NACA TN-2335, 1951.
- [40] Polhamus, E. C., “Prediction of Vortex-Lift Characteristics by a Leading-Edge-Suction Analogy,” *Journal of Aircraft*, vol. 8, pp. 193–199, 1971.
- [41] Küchemann, D., *The Aerodynamic Design of Aircraft*. Pergamon Press, 1978.
- [42] Whetstone, W. D., *Engineering Analysis Language Reference Manual*. Engineering Information System, Incorporated, July 1983.
- [43] Barthelemy, J.-F. M., Wrenn, G. A., Dove, A. R., Coen, P. G., and Hall, L. E., “Supersonic Transport Wing Minimum Weight Design Integrating Aerodynamics and Structures,” *Journal of Aircraft*, vol. 31, March-April 1994.
- [44] Roskam, J., *Airplane Design Part V: Component Weight Estimation*. Kansas: Roskam Aviation and Engineering Corporation, 1985.
- [45] Hoak, D. E. *et al.*, *USAF Stability and Control DATCOM*. Flight Control Division, Air Force Flight Dynamics Laboratory, WPAFB, Ohio, 45433-0000, 1978. Revised.
- [46] Roskam, J., *Methods for Estimating Stability and Control Derivatives of Conventional Subsonic Airplanes*. Kansas: Roskam Aviation and Engineering Corporation, 1971.
- [47] Heffley, R. K. and Jewell, W. F., “Aircraft Handling Qualities Data,” NASA Contractor Report 2144, 1972.
- [48] Razgonyaev, V. and Mason, W. H., “An Evaluation of Aerodynamic Prediction Methods Applied to the XB-70 for Use in High Speed Aircraft Stability and Control System Design,” AIAA Paper 95-0759, Jan. 1995.

- [49] Powers, S. A., “Critical Field Length Calculations for Preliminary Design,” *Journal of Aircraft*, vol. 18, pp. 103–107, February 1981.
- [50] Loftin, Laurence K., J., *Subsonic Aircraft: Evolution and the Matching of Size to Performance*. NASA Reference Publication 1060, Aug. 1980.
- [51] Nicolai, L. M., *Fundamentals of Aircraft Design*. San Jose, CA: METS Inc, 1975.
- [52] Antani, D. L. and Morgenstern, J. M., “HSCT High-Lift Aerodynamic Technology Requirements,” AIAA Paper 92-4228, Aug. 1992.
- [53] Benoiel, A. M. and Mason, W. H., “Pitch-Up Characteristics for HSCT Class Planforms: Survey and Estimation,” AIAA Paper 94-1819, June 1994.
- [54] Baber, Jr., H. T., “Characteristics of the Advanced Supersonic Technology AST-105-1 Configured for Transpacific Range with Pratt and Whitney Aircraft Variable Stream Control Engines,” NASA TM-78818, Mar. 1979.
- [55] Crisafulli, P., Kaufman, M., Giunta, A., Mason, W., Grossman, B., Watson, L., and Haftka, R., “Response Surface Approximations for Pitching Moment, Including Pitch-Up, in the MDO Design of an HSCT,” to appear AIAA Paper 96-4136, Sept. 1996.
- [56] Etkin, B., *Dynamics of Flight—Stability and Control*. New York: John Wiley & Sons, Inc., 1982.
- [57] Rutowski, E. S., “Energy Approach to the General Aircraft Performance Problem,” *Journal of Aeronautical Science*, vol. 21, pp. 187–195, Mar. 1954.
- [58] Bryson, Jr., A. E., Desai, M. N., and Hoffman, W. C., “Energy-State Approximation in Performance Optimization of Supersonic Aircraft,” *Journal of Aircraft*, vol. 6, pp. 481–488, November-December 1969.
- [59] Grandhi, R. V., Thareja, R., and Haftka, R. T., “NEWSUMT-A: A General Purpose Program for Constrained Optimization using Constraint Approximations,” *ASME Journal of Mechanisms, Transmissions, and Automation in Design*, no. 107, pp. 94–99, 1985.



- [60] Douglas Aircraft Company, "Study of High-Speed Civil Transports," NASA Contractor Report 4235, p. 105, 1989.
- [61] Martin, G. L., Beissner Jr., F. L., Domack, C. S., and Shields, E. W., "The Influence of Subsonic Mission Segments on the Use of Variable-Sweep Wings for High Speed Civil Transport Configurations," AIAA Paper 88-4470, Sept. 1988.

# Appendix A

## Using the HSCT code

The HSCT code requires a number of input files to work correctly. These files control the code and input data. In this chapter, we describe what these files are and how they are set up.

### A.1 Input files

This is brief description of the various files needed by the HSCT code.

`hsct.command` - Controls the program and allows many of the constant parameters to be set.

`design.variables` - Contains a list of the design variables used to modify the basic Craidon geometry.

`wavin` - Contains the initial Craidon geometry file. This file is read as soon as the code is run and sets design details that are not included in design variables, for example the vertical and horizontal tail shapes.

`design.initial` - Contains a list of design variables. Used to create “alpha” plots.

`design.final` - Contains a list of design variables. Used to create “alpha” plots.

`design.hist` - Optimization history. Contains design variables, performance and geometric information from each cycle of optimization. Input to perform TRACE command.

`engdeck` - Defines engine performance. Used to calculate available thrust during mission.

## A.2 Output files

This is a brief description of the files the HSCT code outputs.

`bomb` - A list of design variables. This file is output when the code crashes in certain ways.

`check_rot.out` - Output from the rotation integration constraint calculation. Output only if print parameter in `hsct.command` is positive.

`design.hist` - Optimization history. Contains design variables, performance and geometric information from each cycle of optimization. Output after every optimization cycle.

`design.output` - A list of design variables. Output after every optimization cycle.

`flops.wt` - Output from FLOPS weight calculation. Output only if print parameter in `hsct.command` is positive.

`fuel-flow` - Output from mission calculation. Output only if print parameter in `hsct.command` is positive.

`hsct-lat` - Lateral model of the aircraft for J. Kay's code.

`hsct-long` - Longitudinal model of the aircraft for J. Kay's code.

`hsct-parm` - Parameter file for J. Kay's code.

`hsct.out` - Main output file for HSCT code.

`hsct.planform` - Plot of main components of aircraft. Output in TecPlot format.

`hst.plan` - Plot of wing planform.

`look` - Craidon geometry file, output after the end of the optimization.

`nom.wing` - Craidon geometry file, output after MODIFY GEOM command.

`takeoff.output` - Output from takeoff integration, including balanced field length.  
Output only if print parameter in `hsct.command` is positive.

`vlm.dat` - Output from internal vlm analysis.

`wt.statement` - Output from Matt Hutchison's weight routine.

### **A.3 Other files**

The HSCT code uses Jacob Kay's control authority assessment code to calculate the stability derivatives for the aircraft. There are a few files associated with this program.

`input` - A file of input responses for Kay's code.

`jkvlm` - The output from Kay's code.

`hsct.deriv` - Lateral and longitudinal stability derivatives output from Kay's code,  
formatted for the `hsct.command` file.

`vlmmod4` - Kay's VLM based control authority assessment code.

`kay.out` - Redirected standard output from Kay's code.

`RESULTS` - TecPlot output from Kay's code.

## A.4 The `hsct.command` file

The `hsct.command` file controls the HSCT code and is primary file for parameter input. The file consists of a number of optional parameter sections followed by the commands for the code. First, we'll describe each section and the parameters that are involved. Then, we'll explain the various commands that the HSCT accepts.

### A.4.1 Parameter sections

There are nine optional sections which must come before the commands and must be in the order listed if they are included. Although certain sections may be excluded, it is often best to leave all of the sections in. The sections which are not necessary will be ignored. If a section is included, all the parameters in that section must be set. The sections are:

**FLIGHT CHARACTERISTICS** - Sets up various flight parameters, should always be included.

**Altitude at start of cruise** - *feet*, altitude at the beginning of the supersonic cruise-climb. Overwritten by design variable 25.

**Climb rate in cruise** - *ft/min*, climb rate for the supersonic cruise-climb. Overwritten by design variable 26.

**Mach number** - supersonic cruise mach number.

**Design lift coefficient** - used for estimating drag polar.

**Fraction of leading edge suction** - overwritten by internal calculation.

**Mission fuel weight** - *lbs*, overwritten by design variable 24.

**Optim Control** - Enters optimizer settings. Must be included when optimizing or calculating constraints.

**Starting cycle** - number of initial cycle. If set to 1, code will analyze design in `design.variables` and output results to `design.hist` as cycle 0.

**Ending cycle** - number of final optimization cycle.

**Move limits** - limits the amount a design variable may change.  $0.1 = 10\%$  maximum change for design variables.

**Number of constraints** - sets the number of constraints expected.

**Use RS for wing bending material weight** - Flag to indicate whether or not to use the response surface for the wing bending material weight. Possible values are:

**2** : Use 15 term response surface based on the intervening variables if no response surface constraints are violated. If constraints are violated, use the FLOPS estimate.

**1** : Use 61 term response surface based on the design variables if no response surface constraints are violated. If constraints are violated, use the FLOPS estimate.

**0** : Use the FLOPS estimate.

**-1** : Use 61 term response surface based on the design variables regardless of the constraint values.

**-2** : Use 15 term response surface based on the intervening variables regardless of the constraint values.

**STAB DERV** - Sets up the lateral/directional stability and control derivatives for the initial design. Requires the derivatives:  $C_{y\beta}$ ,  $C_{l\beta}$ ,  $C_{n\beta}$ ,  $C_{y\delta_r}$ ,  $C_{l\delta_r}$ ,  $C_{n\delta_r}$ ,  $C_{y\delta_a}$ ,  $C_{l\delta_a}$ , and  $C_{n\delta_a}$ . This section must be included for all optimizations which include vertical tail optimization.

**Long. Derivatives** - Sets up the longitudinal stability and control derivatives for the initial design. Requires the derivatives:  $C_{L\delta_e}$  and  $C_{M\delta_e}$ . This section must be included for all optimizations which include horizontal tail optimization.

**Landing Gear** - Sets constant landing gear parameters. Must always be included.

**Main gear length** - Length of main gear in *feet*.

**Nose gear length** - Length of nose gear in *feet*.

**Tipback angle** - Tipback angle is defined in Figure 3. Usually set to 15°.

**Overturn angle** - Overturn angle is defined in Figure 4. Usually set to 63°.

**Take Off** - Sets parameters used to calculate take off length, including rotation and balanced field length (BFL). Also used to set constraint on BFL. Should be included if horizontal tail size is optimized.

**CLmax** - Maximum lift coefficient attainable in take off configuration. This parameter is calculated internally as the lift coefficient at maximum landing angle of attack.

**Altitude** - Altitude of airfield in *feet*. Higher altitudes cause longer take off distances.

**ground friction** - Coefficient of friction for runway surface.

**braking friction** - Coefficient of friction for brake system.

**stall\_k** - Used to calculate rotation velocity,  $V_r$ . The stall speed,  $V_s$ , is multiplied by the parameter *stall\_k*,  $k$ , to get the  $V_r$  ( $V_r = kV_s$ ). *stall\_k* is generally between 1.10 and 1.25.

**Braking reaction time** - Time between failure of an engine and application of the brakes, in *seconds*.

**Height of obstacle** - The takeoff is complete when the aircraft clears the obstacle height. This height is specified in *feet* and is usually either 35 *ft* or 50 *ft*.

**Maximum BFL** - Sets constraint on the maximum allowable balanced field length (BFL). This is only used in optimizations which include engine sizing and is specified in *feet*.

**Maximum distance** - Not currently used.

**Landing** - This section includes parameters for the landing angle of attack calculation, crosswind landing trim calculation, and landing constraints. Must always be included.

**Speed** - Landing speed in *knots*.

**Maximum landing angle of attack** - Sets constraint on landing angle of attack. Specified in *degrees*.

**CLmax** - Maximum attainable lift coefficient in landing configuration.

**Clmax** - Maximum section lift coefficient.

**Fuel ratio at landing** - Fraction of fuel remaining at landing.

**Cross wind speed** - The crosswind speed in *knots*, used for crosswind landing trim constraint.

**Miscellaneous** - Contains parameters that did not fit in other sections. Must always be included.

**Fuel fraction of weights** - Fraction of fuel remaining for FLOPS weight and center of gravity calculation.

**Fuel density** - Fuel density in *lbs/ft<sup>3</sup>*.

**Percent wing volume available for fuel** - Fraction of wing volume that can be used for fuel storage.

**Minimum range** - Range constraint in *n.mi.*.

**Minimum chord length** - Minimum wing chord length in *feet*.

**Minimum engine nacelle spacing** - Minimum distance between the engine nacelles, in *feet*.

**Print** - This flag controls the amount of output. A 0 indicates minimum output, with no output during an optimization cycle.

**Structural interlacing factor** - This factor is the ratio of the structural optimization bending material weight to FLOPS bending material weight. Generally not used, set to 1.0.

**Engines** - Contains parameters which determine the size, thrust, weight and the number of engines. This section must always be included.



**Thrust per engine** - The thrust each engine can produce in *lbs*. This parameter is ignored when thrust is a design variable.

**Reference thrust for calculating engine weight** - Thrust of reference engine, in *lbs*. The ratio of thrust to reference thrust is used to calculate the engine weight and size.

**Reference weight** - The weight of the reference engine, in *lbs*.

**Reference diameter of nacelle** - Diameter of the reference engine nacelle, in *feet*.

**Reference length of nacelle** - Length of reference engine nacelle, in *feet*.

**Number of engines** - Number of engines, used for calculating total thrust. Will not change the number of pods in craidon geometry file.

## A.4.2 Commands

There are many different commands that may be entered. The commands are performed in the order they are found in the `hsct.command` file. Often, the order of the commands is not important. The biggest exception to this is the `MODIFY GEOM` command, which should be the first command if design variables are to be used to modify the craidon geometry.

**MODIFY GEOM** - Modifies the current craidon geometry with the design variables in the file `design.variables`. Outputs craidon geometry to `nom.wing`.

**WEIGHT** - Calculates the weight of the current craidon geometry. Outputs the files `wt.statement` and `flops.wt`. The file `wt.statement` is the weight statement produced by Matt Hutchison's version of the FLOPS weight equations. The file `flops.wt` is the output from the actual FLOPS weight routine, which includes the center of gravity and inertia calculations.

**OPTIM** - Optimizes the design. Starts with the design in `design.variables`. Starting and ending cycle and move limits are set in section `Optim Control`,

see Section A.4.1. At the end of each cycle, outputs design variables and performance data to file `design.hist`. Plots wing planform to `hst.plan`. Also writes out data for the different components of the aircraft, in TecPlot format, to file `hsct.planform`. Writes final craidon geometry to file `look`, and final design variables to `design.output`.

**PLOT** - Plots the wing planform of current craidon geometry. Outputs wing to `hst.plan`. Also writes out data for the different components of the aircraft, in TecPlot format, to file `hsct.planform`.

**ALPHA $x$**  - Creates an alpha plot. Starts with design in `design.initial` and moves to `design.final`. Has five options, choice is determined by number after ALPHA command:

**ALPHA1** : GTOW, Range, Landing alpha

**ALPHA2** : Wave Drag

**ALHPA3** : Drag due to lift

**ALPHA4** :  $C_{L\alpha}$ ,  $C_{M\alpha}$

**ALPHA5** : Constraints

Output is written to `hsct.out`.

**TRACE** - Inputs design history from `design.hist`, calculates performance and geometric parameters for each design in file. Outputs to `hsct.out`.

**TEST** - Does a performance analysis of current craidon geometry. Writes output to `hsct.out`.

**MODEL** - Creates model of current craidon geometry for use in Jacob Kay's stability derivative estimation program. Outputs `hsct-lat`, `hsct-long`, and `hsct-parm`. These are the lateral model, longitudinal model, and the parameter file. Then Kay's code is run (`v1mmod4`) and it outputs the derivatives to a file `hsct.deriv`.

**ATMOS** - Interactively runs the standard atmosphere routine. User chooses english or metric units and then inputs the altitude and mach number desired. Note: a velocity may be entered in place of the mach number by entering it as a negative number. The program then outputs mach number, altitude, density, temperature, pressure, Reynold's number, dynamic pressure ( $q$ ), and the velocity ( $V$ ).

**CONSTR** - Evaluates the constraints using the current craidon geometry and outputs the results to `hsct.out`.

## A.5 Experiences optimizing with the HSCT code

The procedure for optimizing a design with the HSCT code is actually simple. Getting it to work takes practice and patience. Setting move limits and getting the optimizer away from bad designs can be challenging tasks. If the move limits are too large, the optimizer will often enter design space where the approximations differ greatly from the detailed analysis. In this section, we will explain what needs to be done to start an optimization and give suggestions for getting a successful design.

To start an optimization, the initial set of design variables should be placed in the file `design.variables`. The optimization parameters must be set in the `hsct.command` file. The most important ones are beginning and ending cycle and the move limits. Generally, the optimizations are done in sets of five cycles. So, to start an optimization, the beginning cycle is set to 1 and the ending cycle is set to 5. Starting move limits are usually in the range of 10% to 20%.

If the vertical or horizontal tails are being optimized, the stability and control derivatives for the initial design must be set. This is done by running the HSCT code with the initial design in `design.variables` and the commands:

```
MODIFY GEOM
MODEL
END
```

These commands input the design variables, model the design and run Kay's code. This produces the file `hsct.deriv` which can be cut and pasted directly into the `hsct.command` file. The other sections should be set as is appropriate for the design and the command `OPTIM` should be inserted after the `MODIFY GEOM` command. This will cause the code to optimize for the specified number of cycles and then calculate new stability derivatives for final design.

After the code has finished running, the final design is stored in `design.output` and the new stability derivatives are in `hsct.deriv`. To continue this optimization, the beginning and ending cycles should be changed (to 6 and 10) and the move limits adjusted. If there were large differences between the exact and approximate ranges, then a large reduction in the move limits is needed. If the approximate range is not too far off, then a small reduction will suffice. Picking move limits takes experience, but there is no absolutely right answer. If, after optimizing, the design is poor, it might be necessary to reduce the move limits and restart that set of cycles. Sometimes, the final design is worse than the initial design, if the approximations have failed badly. After adjusting the move limits, the new stability derivatives should be pasted into the command file.

Sometimes, the optimizer will reach a local minimum which does not satisfy the constraints. The optimizer will get stuck at this design point and make no changes to the design. Restarting with different move limits will sometimes help this. If the range on the final design is less than the required range, adding fuel weight will improve the range and give the optimizer a better design to start with. If the second or third cycle out of a set of five produced a better design than the final design, simply place these design variables in the `design.variables` file and run the `MODEL` command. Then continue the optimization from this cycle.

## A.6 Sample `hsct.command` file

```
FLIGHT CHARACTERISTICS
50000.0  Altitude at start of cruise (ft.)
100.0   Climb rate in cruise (ft / min)
2.4     Mach number
0.10    Design lift coefficient
```

0.8	Fraction of leading edge suction ( $0 < x < 1$ )
290905.0	Mission fuel weight (lbs.)
Optim Control	
1	Starting cycle
5	Ending cycle
0.32	Move limits
67	Number of constraints
1	Use RS for wing bending material weight
STAB DERV	
-0.06119	-0.00541 0.02833 C(y, 1, n)beta
0.04608	0.00368 -0.03074 C(y, 1, n)dr
0.0	-0.01776 -0.00011 C(y, 1, n)da
Long. Derivatives	
0.19597	-0.20396 C(L, M)de
Landing Gear	
19.75	Main gear length
18.75	Nose gear length
15.00	Tipback angle (deg)
63.00	Maximum overturn angle (deg)
Take Off	
0.90	CLmax
0.00	Altitude (ft)
0.03	ground friction
0.30	braking friction
1.165	stall_k
3.0	Braking reaction time (sec)
35.00	Height of obstacle (ft)
10000.00	Maximum BFL (ft)
9000.00	Maximum distance (ft)
Landing	
145.0	Speed (knots)
12.0	Maximum landing angle of attack (deg)
1.0	CLmax
2.0	Clmax
0.5	Fuel ratio at landing
20.0	Cross wind speed (knots)
Miscellaneous	
1.0	Fuel fraction of weights
48.75	Fuel density (lbs/ft <sup>3</sup> )
0.50	Percent wing volume available for fuel
5500.00	Minimum range (nm)
7.0	Minimum chord length (ft)
7.0	Minimum engine nacelle spacing (ft)
2	Print? (0 = no intermediate files output)
1.0	Structural interlacing factor
Engines	
39000.0	Thrust per engine
65482.0	Reference thrust for calculating engine weight
17424.0	Reference weight
4.782	Reference diameter of nacelle
27.186	Reference length of nacelle
4	Number of engines
MODIFY GEOM	

TEST  
OPTIM  
MODEL  
END

## A.7 Sample design variable file

Design variables after cycle 24, Jane's converged 'case 3'  
28

	Number of design variables
1.75951	1) x100, wing root chord (ft.)
1.49119	2) x100, L.E. break, x (ft.)
4.22614	3) x10, L.E. break, y (ft.)
1.80419	4) x100, T.E. break, x (ft.)
6.88180	5) x10, T.E. break, y (ft.)
1.72304	6) x100, L.E. wing tip, x (ft.)
0.71245	7) x10, wing tip chord (ft.)
7.42557	8) x10, wing semi-span (ft.)
4.01262	9) x0.1, location of max. t/c on airfoil (x/c)
3.64571	10) x1, L.E. radius parameter
2.56129	11) x0.01, t/c at wing root
2.26982	12) x0.01, t/c at L.E. break 1
2.55090	13) x0.01, t/c at wing tip
0.04174	14) x100, fuselage restraint 1, x (ft.)
0.17574	15) x10, fuselage restraint 1, r (ft.)
0.15033	16) x100, fuselage restraint 2, x (ft.)
0.38024	17) x10, fuselage restraint 2, r (ft.)
1.33271	18) x100, fuselage restraint 3, x (ft.)
0.53779	19) x10, fuselage restraint 3, r (ft.)
2.50427	20) x100, fuselage restraint 4, x (ft.)
0.46870	21) x10, fuselage restraint 4, r (ft.)
3.00118	22) x10, nacelle 1 y location (ft.)
3.63456	23) x10, nacelle 2 y location (ft.)
2.80319	24) x1e05, flight fuel (lbs.)
6.31896	25) x1e04, starting cruise altitude (ft.)
0.38069	26) x100, cruise climb rate (ft./min.)
4.50015	27) x100, vertical tail area
7.50000	28) x100, horizontal tail area

# Appendix B

## HSCT Code Structure

This appendix contains all of the routine headers from each source code module. First the C source modules are described, then the FORTRAN modules. The modules are in alphabetical order. The routines are in the order found in the source file.

### B.1 Overview of code structure

```
main()
  Read_Craid_Geom()           /* Input 'wavin' file */
  Alloc_wet()
  choice = Read_Command_File() /* Input parameters and commands */
  init_eng_()                 /* Set up FLOPS engine deck */
  enint_()
  do {
    switch(choice) {         /* Execute appropriate command */
      : WEIGHT                /* Calculate weights */
        Aircraft_Weight()    /* Hutchison's weight routine */
        Write_Weight()
        Detailed_weight()    /* FLOPS weight routine */
        Write_Weight()
        mk_geometric_constraints()
        break
      : MODIFY GEOM          /* Modify craidon with DV's */
        Read_Des_Var()       /* Input 'design.variables' */
        Modify_with_DV()
        Write_Craid_Geom()   /* Output 'nom.wing' */
        break
      : OPTIM                 /* Optimize */
```

```

Read_Des_Var()                /* Input 'design.variables' */
for(i = opt->iter_start; i <= opt->iter_end; i++)
  Modify_with_DV()            /* Loop over number of cycles */
  setupAeroAnalysis()
  if (opt->num_dv >=27)        /* If more than 27 DV's */
    Detailed_weight()         /* Set up stability and */
    cl_land()                 /* control derivatives */
    attack()
    Landing_Perform()
    if (i == opt->iter_start)
      Setup_deriv()
      Setup_LongDeriv()
    Wet_area()
    if (opt->num_dv >= 29)     /* If more than 29 DV's */
      setupT0()               /* set up take off calc */
    if (i == 1) writeDesHistory() /* First cycle, write analysis */
    optcntrl_()               /* Call NEWSUMT */
    lagrange()
    Modify_with_DV()          /* Update craidon with new DV's */
    writeDesHistory()         /* Output analysis */
    Plot_Wing()               /* Plot design */
    plotConfig()
    if (opt->num_dv >= 27 && aircraft.misc.print)
      approx()
  Write_Craid_Geom()          /* Output 'look', final craidon */
  Write_Des_Var()             /* Output 'design.output' */
  Plot_Wing()                 /* Plot final design */
  plotConfig()
  break

: ALPHAx
  Read_Des_Var()              /* Read 'design.initial' */
  Read_Des_Var()              /* Read 'design.final' */
  Modify_with_DV()
  setupAeroAnalysis()         /* Set up aerodynamics */
  if (opt->num_dv >=27)        /* Set up S&C derivatives */
    Detailed_weight()
    cl_land()
    attack()
    Landing_Perform()
    Setup_deriv()
    Setup_LongDeriv()
  if (opt->num_dv >= 29)       /* Set up take off approximation */
    Wet_area()
    setupT0()
  doAlpha()                   /* Perform alpha analysis */
  break

: TRACE
  if (opt->num_dv >= 28)

```



```

        Setup_LongDeriv()
designTrace()                                /* Perform design trace */
break

: TEST
  if (opt->num_dv >= 28)                      /* Set up derivatives and aero */
    Setup_LongDeriv()
  if (opt->num_dv >= 29)
    setupAeroAnalysis()
doAnalysis()                                /* Perform analysis of design */
break

: MODEL
  Detailed_weight()
  MakeModel()                                /* Create models for VLM code */
  system("vlmmod4 < input > kay.out\n"); /* Call Kay's code */
  break

: ATMOS
  k = Std_Atmos()                            /* Interactively input data */
  break                                       /* Call atmosphere routine */

: CONSTR
  if (opt->num_dv >=27)                       /* Set up S&C derivatives */
    Detailed_weight()
    cl_land()
    attack()
    Landing_Perform()
    Setup_deriv()
    Setup_LongDeriv()
  if (opt->num_dv >= 29)                      /* Set up take off approximation */
    Wet_area()
    setupTO()
constraints()                                /* Call constraint routine */
break

while(choice = Read_Command_File(&aircraft)); /* Read next command */
Free_wet()
exit(0);

```

## B.2 aero.c

```

/*\
| The functions in this source code direct the execution of the
| different aerodynamic methods. Specifically, I have simple
| and complex models for supersonic drag due to lift, supersonic
| wave drag and subsonic (i.e. landing, M = 0) lift-curve
| slope
|
| mgh, 8/11/92
\*/

```

```

/*****\
| "setupAeroAnalysis()" allocates storage and sets up the specific
| approximation desired for the different aerodynamic analyses.
| Currently, there are models for supersonic drag due to lift,
| supersonic wave drag and subsonic (landing, M = 0) lift-curve slope.
| The approximations are selected using the 'model' flags in the
| optimization control structure.
|
| mgh, 8/11/92
\*****/
void setupAeroAnalysis(struct OptimControl *opt, struct Control cntrl,
    struct Wing *wing, struct Fuse *fuse, struct Pod *pod,
    struct Surface *fin, struct Surface *canard,
    struct Flight_Char *flight, Engine *eng)

/*****\
| "Lift_Drag()" directs the calculation of the drag due to lift and
| returns the parameters CLa (lift-curve slope) and CToCT2 (the
| leading edge suction parameter (CT / CL^2)).
\*****/
void Lift_Drag(double *CLa, double *CToCL2, double *CMA, double *CM0,
    double M, struct OptimControl *opt, struct Control cntrl,
    struct Wing *wing, struct Flight_Char *flight, struct Surface *canard,
    double htdef)

/*****\
| "Wave_Drag()" directs the calculation of the wave drag and
| returns the parameter Cd_wave.
\*****/
double Wave_Drag(struct OptimControl *opt, struct Control cntrl,
    struct Wing *wing, struct Fuse *fuse, struct Pod *pod,
    struct Surface *fin, struct Surface *canard,
    struct Flight_Char *flight)

/*****\
| "lowSpeedCLa()" directs the calculation of the low speed lift-curve
| slope, using either the VLM or an approximate model.
\*****/
void lowSpeedCLa(struct OptimControl *opt, struct Control cntrl,
    struct Wing *wing, struct Surface *canard, double htdef,
    double *CLa, double *CMA, double *CM0) {

/*****\
* "subCLaCMA()" calculates the subsonic low speed lift-curve slope,
* and pitching moment slope using the VLM model.
\*****/
void subCLaCMA(struct OptimControl *opt, struct Control cntrl,
    struct Wing *wing, struct Surface *canard, double xref,
    double htdef, double *CLa, double *CLaHT, double *CMA,
    double *CM0) {

```



```

static void ReadFuse(FILE *infile, struct Control cntrl,
    struct Fuse *fuse)

/*\
| Read in pod description.
\*/
static void ReadPod(FILE *infile, struct Control cntrl, struct Pod *pod)

/*\
| Read in fin description.
\*/
static void ReadFin(FILE *infile, struct Control cntrl,
    struct Surface *fin)

/*\
| Read in canard description.
\*/
static void ReadCanard(FILE *infile, struct Control cntrl,
    struct Surface *canard)

/*****\
| Function to write Craidon geometry data to a file (formatted).
\*****/
void Write_Craid_Geom(char *filename, struct Control cntrl,
    struct Wing *wing, struct Fuse *fuse, struct Pod *pod,
    struct Surface *fin, struct Surface *canard)

/*\
| Write elements of a double vector to a string in formatted form. Vector
| is assumed to begin at element 1. The format for writing is %7.3f and
| is repeated "num_flds" per line.
\*/
static void vec2str(char **strfile, int *line, int num_flds, double *vec,
    int num_elem)

/*****\
/*\
| Read in elements of an integer vector from a data file.
\*/
static void str2ivec(FILE *infile, int fld_ln, int num_flds, int *vec,
    int num_elem)

/*****\
/*\
| Read in elements of a double vector from a data file.
\*/
static void str2vec(FILE *infile, int fld_ln, int num_flds, double *vec,
    int num_elem)

```

```

/*****\
| Function to write Craidon geometry data to a file (formatted).
| for Alex's pitchup code.
\*****/
void Write_Alex_Geom(char *filename, double LEradpar,
    struct Control cntrl, struct Wing *wing, struct Fuse *fuse,
    struct Pod *pod, struct Surface *fin, struct Surface *canard)

```

## B.4 dataio.c

```

/*\
| The routines in this file are used for input and output of 'data'.
| Specifically, this refers to anything that controls the execution
| of the program and the 'normal' output from it.
|
| mgh, 3/4/92
\*/

/*****\
| This function opens a data file, allocates storage for the design
| variable vector based on information in the file, then loads in the
| actual members of the vector.
\*****/
void Read_Des_Var(double **des_var, int *num_dv, char *file_name)

/*****\
| This routine writes out the design variables to a file.
\*****/
void Write_Des_Var(double *des_var, int num_dv, char *file_name)

/*****\
| This routine writes out the design variables to a design history
| file.
\*****/
void writeDesHistory(Aircraft *aircraft, int cycle) {

/*****\
| This routine reads the command file.
|
| The basic idea is to follow a strict set of allowable commands in the
| command file (and, if necessary, read in further data) and return
| a value to the main program that directs the action.
\*****/
int Read_Command_File(Aircraft *aircraft) {

/*****\
| Write out weight information to output file.
\*****/
void Write_Weight(FILE *out, double wt )

```

```

/*****\
| Write out drag information.
\*****/
void Write_Drag(FILE *out, double Cl, double Cd_wave, double Cd_fric,
    double Cd_lift, struct Flight_Char flight, struct Atmosphere atm)

/*****\
| Write out drag polar data.
\*****/
void Write_Drag_Polar(FILE *out, double Cl, double Cd_wave,
    double Cd_fric, double Cd_lift, struct Atmosphere atm,
    struct Flight_Char flight, int title)

/*****\
| Write range results.
\*****/
void Write_Range(FILE *out, double range, struct Flight_Char flight)

/*****\
| "Plot_Wing()" writes out the wing planform coordinates to a file
| for plotting.
\*****/
void Plot_Wing(struct Control cntrl, struct Wing wing)

/*****\
| "plotConfig()" writes out the data for the different components of
| the aircraft for plotting. I use the 'TecPlot' format. The data is
| simply the planform--that is, the projection in the z = 0 plane.
| Rewritten on 7/25/94, pem
\*****/
void plotConfig(struct Control cntrl, struct Wing *wing, struct Fuse *fuse,
    struct Pod *pod, struct Surface *fin, struct Surface *canard) {

```

## B.5 f77iface.c

```

/*\
| The functions in this source code act as interfaces between
| C code and FORTRAN code.
|
| mgh, 3/4/92
\*/

/*****\
|
| This routine takes the aircraft information structures and converts
| them into the information needed for the Craidon geometry description.
| This routine is called from the wavedrag code. Note that the geometry
| structures are passed as pointers because FORTRAN does not have a
| 'structure' data type it does pass the address of these variables.
|

```

```

| ERU, 3/31/91
\*****
void get_variables_(j0,j1,j2,j3,j4,j5,j6,nwaf,nwafor,nfus,nradx,nforx,np,npodor,
                  nf,nfinor,ncan,ncanor,ncase,mach,nx,ntheta,nrest,ncon,icyc,
                  kkode,jrst,ialph,iou2,iou3,refa,xaf,waforg,tzord,waford,sfus,
                  podorg,xpod,podord,finorg,xfin,finord,canorg,xcan,canord,
                  xrest,xfus,abc,opt,cntrl,wing,fuse,pod,fin,canard,flight)

```

## B.6 fminbr.c

```

*****
*          C math library
* function FMINBR - one-dimensional search for a function minimum
*   over the given range
*
* Input
* double fminbr(a,b,f,tol)
* double a;   Minimum will be seeked for over
* double b;   a range [a,b], a being < b.
* double (*f)(double x); Name of the function whose minimum
* will be seeked for
* double tol; Acceptable tolerance for the minimum
* location. It have to be positive
* (e.g. may be specified as EPSILON)
*
* Output
* Fminbr returns an estimate for the minimum location with accuracy
* 3*SQRT_EPSILON*abs(x) + tol.
* The function always obtains a local minimum which coincides with
* the global one only if a function under investigation being
* unimodular.
* If a function being examined possesses no local minimum within
* the given range, Fminbr returns 'a' (if f(a) < f(b)), otherwise
* it returns the right range boundary value b.
*
* Algorithm
* G.Forsythe, M.Malcolm, C.Moler, Computer methods for mathematical
* computations. M., Mir, 1980, p.202 of the Russian edition
*
* The function makes use of the "gold section" procedure combined with
* the parabolic interpolation.
* At every step program operates three abscissae - x,v, and w.
* x - the last and the best approximation to the minimum location,
*   i.e. f(x) <= f(a) or/and f(x) <= f(b)
*   (if the function f has a local minimum in (a,b), then the both
*   conditions are fulfilled after one or two steps).
* v,w are previous approximations to the minimum location. They may
* coincide with a, b, or x (although the algorithm tries to make all
* u, v, and w distinct). Points x, v, and w are used to construct
* interpolating parabola whose minimum will be treated as a new
* approximation to the minimum location if the former falls within
* [a,b] and reduces the range enveloping minimum more efficient than
* the gold section procedure.
* When f(x) has a second derivative positive at the minimum location
* (not coinciding with a or b) the procedure converges superlinearly
* at a rate order about 1.324

```

```
*
*****
```

## B.7 main.c

```
/*\
| This code is the driver for the drag analysis and design changes
| on the HSCT design. It acts as a sort of "switchyard" to control
| all the aspects of the computation.

main()

/*****\
| "analys()" is the function called by NEWSUMT for the optimization function
| evaluations. All the arguments passed are from (and for) NEWSUMT. The
| "info" switch simply directs the evaluation of either the objective
| function or the constraints.
|
| Switch on "info". 1: evaluate objective function; 2: evaluate
| constraints; 3: evaluate objective function derivatives (used
| only if analytic information is available -- not used in this
| problem); 4: constraint derivatives (again, used only if analytic
| expressions are available); and, 5: linear constraint derivatives
| (not used). For this problem, all derivatives are determined from
| finite differences driven from "sumt1s()".
\*****/
void analys_(int *info, double *x, double *obj, double *dobj, double *ddobj,
double *g, double *dg, double *fdcv, int *n1, int *n2, int *n3, int *n4,
double *ran, int *nrandm, int *ian, int *niondm)

/*****\
| "constraints()" evaluates the constraints and puts the results in
| vector form for "analys()" (and, hence, NEWSUMT).
|
\*****/
void constraints(Aircraft *aircraft, double *g) {

/*****\
| MK Geometric constraints for wsearch program
| Note that this routine only accounts for design constraints dealing
| with the aircraft geometry! This allows us to skip all stability and
| aerodynamic analysis and thus saves computational time...
\*****/
int mk_geometric_constraints(Aircraft *aircraft, int geo_std, int geo_phase1,
int geo_phase2, int range, int aero, int save_to_file)
```

## B.8 modify.c

```
/*\
```



```

| This source code contains the functions necessary to modify
| the aircraft geometry, given a set of design variables.
|

/*****\
| This function converts the design variables into the standard
| geometry and flight parameters. My purpose in doing this is to
| isolate as much as possible the design variables from the rest of
| the code. Hopefully, this will help make the program
| easier to revise and also make design variable selection more
| versatile.
|
| In keeping with this philosophy, this routine is the ONLY place in
| the entire program where any (and all) modifications using the design
| variables takes place.
\*****/
void Modify_with_DV(double *des_var_orig, int ndv, struct Control cntrl,
    struct Wing *wing, struct Fuse *fuse, struct Pod *pod,
    struct Surface *fin, struct Surface *canard,
    struct Flight_Char *flight, Engine *eng)

/*****\
| Modify wing geometry using parameter description.
\*****/
static void Modify_Wing(struct Control cntrl, struct Wing *wing,
    struct Wing_param *wing_param)

/*****\
| "adjustWing()" shifts the wing location to fit the fuselage properly
| and also to maintain the c/4 location of the MAC. You have to be
| careful here, in that the only things I can change is actual wing
| position, not wing shape. Consequently, I look first at the wing
| root location, reference a change from the position and then specify
| the changes in location.
\*****/
static void adjustWing(struct Control cntrl, struct Wing *wing,
    struct Fuse *fuse)

/*****\
| "adjustPod()" sets the pod locations with respect to the wing.
| You have to be careful here, because there are some assumptions
| made on the grouping of the pods.
\*****/
static void adjustPod(struct Control cntrl, struct Wing *wing,
    struct Pod *pod)

/*****\
| "blend_line()" implements the exponentially blended linear description
| of the wing leading and trailing edges.
|

```

```

|     nseg : number of linear segments
|     xrt  : x-coordinate of root
|     yrt  : y-coordinate of root
|     swp  : vector of sweep angles
|     ybrk : vector of projected bread y-locations
|     blnd : vector of absolute values of blending parameters
|     y    : y-value of interest
|
| Returns x location corresponding to y-value of interest.
\*****/
static double blend_line(int nseg, double xrt, double yrt, double *swp,
    double *ybrk, double *blnd, double y)

/*****\
| The purpose of this function is to return the half-thickness of
| the airfoil given the x-location (in terms of x/c) "x", the location
| of max. t/c (in terms of x/c) "m", the thickness-to-chord ratio "t",
| the leading edge radius/half-angle (see below) "I", and the
| trailing edge half-angle, "tau".
\*****/
static double foil_thk(double x, double m, double t, double I, double tau)

/*****\
| "Modify_Fuse()" uses the Eminton approach to define an optimal
| wave drag body with given volume.
\*****/
static void Modify_Fuse(int nrest, double *xfuse, double *rfuse,
    struct Control cntrl, struct Fuse *fuse, double V)

/*****\
| "qFunc()" implements the q function to define the fuselage shape.
\*****/
static double qFunc(double x, double y)

/*****\
| SetLg is a function that sets that y and z location of the landing gear.
\*****/
void SetLg(Aircraft *aircraft) {

```

## B.9 numerics.c

```

/*\
| This file contains functions used for numerical purposes (e.g. LU
| decomposition, root finding, etc.).
|
/*****\
| The following are the array allocation/de-allocation functions
| taken from "Numerical Recipes in C". They have been modified only
| in that they call 'bomb()' on problems, and not 'nrerror()'.

```

```

\*****/
double *vector(int nl, int nh)
/*****/
double *dvector(int nl, int nh)
/*****/
int *ivector(int nl, int nh)
/*****/
double **matrix(int nrl, int nrh, int ncl, int nch)
/*****/
int **imatrix(int nrl, int nrh, int ncl, int nch)
/*****/
void free_vector(double *v, int nl, int nh)
/*****/
void free_dvector(double *v, int nl, int nh)
/*****/
void free_ivector(int *v, int nl, int nh)
/*****/
void free_matrix(double **m, int nrl, int nrh, int ncl, int nch)
/*****/
void free_imatrix(int **m, int nrl, int nrh, int ncl, int nch)

/*****\
| "ludcmp()" decomposes a matrix into L-U form. The routine and its
| parameters are defined on p. 43 of Numerical Recipes.
\*****/
void ludcmp(double **a, int n, int *indx, double *d)

/*****\
| "lubksb()" performs back-substitution using an L-U decomposed
| matrix to solve linear systems. The routine and its parameters
| are defined on p. 44 of Numerical Recipes.
\*****/
void lubksb(double **a, int n, int *indx, double *b)

/*****\
| "svbksb()" solves  $A x = b$  for  $x$  where  $A$  is specified by  $u$ ,  $w$ , and  $v$ 
| as returned by "svdcmp()". The routine and its parameters are
| defined on p. 65 of Numerical Recipes.
\*****/
void svbksb(double **u, double *w, double **v, int m, int n,
            double *b, double *x)

/*****\
| "svdcmp()" computes the singular value decomposition of a matrix  $A$ .
| The routine and its parameters are defined on p. 68 of Numerical
| Recipes.
\*****/
void svdcmp(double **a, int m, int n, double *w, double **v)

/*****\
| "spline()" returns a vector of weights that define a cubic spline.
| The routine and its parameters are defined on p. 96 of Numerical

```

```

| Recipes.
\*****/
void spline(double *x, double *y, int n, double yp1, double ypn, double *y2)

/*****\
| "splint()" performs the spline interpolation given the weights from
| the "spline()" routine. The routine and its parameters are defined
| on p. 97 of Numerical Recipes.
\*****/
void splint(double *xa, double *ya, double *y2a, int n, double x, double *y)

/*****\
| "el2()" returns the general elliptic integral of the second kind.
| The routine and its parameters are defined on p. 200 of Numerical
| Recipes.
\*****/
double el2(double x, double qqc, double aa, double bb)

/*****\
| "cel()" returns the general complete elliptic integral. The routine
| and its parameters are defined on p. 201 of Numerical Recipes.
\*****/
double cel(double qqc, double pp, double aa, double bb)

/*****\
| Fifth-order Runge-Kutta with monitoring of local truncation error to
| ensure accuracy and adjust stepsize. p.719 of Numerical Recipes.
\*****/
void rkqs(double y[], double dydx[], int n, double *x, double htry, double eps,
          double yscal[], double *hdid, double *hnext, Aircraft *aircraft,
          void (*derivs)(double, double [], double [], Aircraft*))

/*****\
| Use the fifth-order Cash-Karp Runge-Kutta method, also return an
| estimate of local truncation error using the embedded fourth-order
| method. From p.719 of Numerical Recipes
\*****/
void rkck(double y[], double dydx[], int n, double x, double h, double yout[],
          double yerr[], void (*derivs)(double, double[], double[], Aircraft*),
          Aircraft *aircraft)

```

## B.10 options.c

```

/*\
| The functions in this file actually execute the commands
| selected in 'main()'. The goal here is to keep the 'main()'
| function from becoming too cumbersome with a lot of stuff
| that is germane only to a small piece of the code.
|

```

```

/*****\
| 'doAnalysis()' directs the analysis of a given design and writes
| the results to a file.
\*****/
void doAnalysis(FILE *out, Aircraft *aircraft) {

/*****\
| 'doAlpha()' performs the 'alpha' calculation to estimate the
| performance of the approximate models between two points in the
| design space. All the results are written to a file (pointer is
| 'out').
\*****/
void doAlpha(FILE *out, Aircraft *aircraft, int choice) {

/*****\
| 'designTrace()' reads in the design variables from the design
| history file, and calculates performance or geometric parameters
| for the results from each design cycle from the history file.
\*****/
void designTrace(FILE *out, Aircraft *aircraft) {

```

## B.11 perform.c

```

/*\
| The routines in this file are used for performance analysis (i.e. the
| range calculation, landing, etc.)
|

/*****\
| Range calculation. Times in seconds, distances are feet or meters.
\*****/
double Range(Aircraft *aircraft)

/*****\
| Climb_calc() directs the integration for a climb segment
\*****/
void Climb_calc(Aircraft *aircraft, Mission_segment *segment, int seg,
FILE *output)

/*****\
| Climb_eq() calculates the time derivatives of h, W, R, and V
| for different types of climbs.
\*****/
void Climb_eq(double t, double *y, double *dydt, Aircraft *aircraft) {

/*****\

```

```

| MinTimeV() calculates the negative of the specific excess power
\*****/
double MinTimeV(double V2, Aircraft *aircraft)

/*****\
| Cruise_calc() directs the integration for a cruise segment
\*****/
void Cruise_calc(Aircraft *aircraft, Mission_segment *segment, int seg,
FILE *output)

/*****\
| Cruise_eq() calculates the time derivatives of W, R, and V
\*****/
void Cruise_eq(double t, double *y, double *dydt, Aircraft *aircraft) {

/*\
| Determine engine sfc data.
\*/
static double Find_SFC(double thrust, double h, double M)

/*****\
| "attack()" calculates and returns the landing angle of attack in
| radians.
\*****/
double attack(double CL, double *CLa, struct OptimControl *opt,
struct Control cntrl, struct Wing *wing, struct Surface *canard,
int grEffect)

/*****\
| The following routine calculates the landing CL (3-D) of the
| aircraft given the entire geomery description and the landing speed.
\*****/
double cl_land(double aircraft_weight, double Sw, double landing_speed,
double altitude, double fuel_ratio, double temp, double fuel_wt)

/*****\
| Calculate fuel flow, given lift and drag parameters and
| atmospheric info.
| rparm[1] = Cd0
| 2 = CLa
| 3 = CToCL2
| 4 = flight->crs.start_alt
| 5 = hdot
| 6 = flight->Cl_design
| 7 = flight->LES
| 8 = h (calculated unless hdot=0)
| 9 = Mach number
| 10 = wing area (S)
| 11 = CL (returned)
| 12 = CD (returned)

```

```

| 13 = thrust (returned)
\*****/
void FuelFlow(double t, double *W, double *fuel_flow, double *rparm)

/*****\
| 'Landing_Perform' simply calls the vlm routine and returns
| a variable of type struct Landing, with the CL, xpc, and ypc
\*****/
void Landing_Perform(struct OptimControl opt, struct Control cntrl,
    struct Wing wing, struct Surface *canard, struct Landing *landing) {

/*****\
'VRotate()' calculates the required speed for the nosewheel to
leave the ground.
\*****/
double VRotate(Aircraft *aircraft, double htdef)

/*****\
'Rotate()' simulates the take off rotation by intergrating
    Mcg = Iyy * theta''
\*****/
void Rotate(Aircraft *aircraft, double htdef, double Vrotate,
    double Vtakeoff, double *Vfinal)

/*****\
'ApproachTrim()' calculates the horizontal tail deflection
required to trim during approach.
\*****/
double ApproachTrim(Aircraft *aircraft) {

```

## B.12 servmath.c

```

*****
* Service C functions
*     concerning the mathematical computations

double fmin(x1,x2) /* Minimum of two doubles */
double fmax(x1,x2) /* Maximum of two doubles */
int iabs(x) /* Absolute value of a integer */
int imin(x1,x2) /* Minimum of two integers */
int imax(x1,x2) /* Maximum of two integers */
double powi(x,e) /* x up integer power */
double nrandom() /* Random number NORMAL distributed as N(0,1) */

```

## B.13 simpaero.c

```

/*\

```

```

| The functions in this file are used for the approximate (or
| "simple") aerodynamic analysis.
|
|
|/*****\
| "crankWing()" calculates and returns the lift curve slope and the
| thrust coefficient for cranked wings of the type shown in NACA
| 2959 (Cohen and Friedman). The geometric parameters use the
| notation given in the paper.
|
| Input:
|   M - Mach number
|   c0 - Root chord
|   c1 - distance from wing apex to LE break
|   c2 - distance from wing apex to LE of tip
|   s1 - spanwise location of LE break
|   s - wing semi-span
|
| Output:
|   CLa - supersonic lift-curve slope
|   CToCL2 - ratio of leading-edge thrust coefficient to CL^2
|/*****\
void crankWing(double M, double c0, double c1, double c2, double s1,
               double s, double *CLa, double *CToCL2)

|/*****\
| "crWingParam()" directs the calculation of the determination of
| the cranked wing (i.e. Cohen and Friedman stuff). The leading
| edge of the wing is used to minimize the chi-squared error of the
| fit with the actual wing. The root chord is chosen so as to
| preserve the actual wing area.
|/*****\
void crWingParam(struct Control cntrl, struct Wing *wing, double *c0_ptr,
                double *c1_ptr, double *c2_ptr, double *s1_ptr, double *s_ptr)

|/*****\
| "leChiSq()" determines the chi-squared error in the LE wing fit for
| the cranked (i.e. Cohen and Friedman) wing planform. It does so
| by fitting two line segments defined by c1, c0, s1 and s in a
| least squares sense. c0 is known from the data, and s1 and s are
| determined for minimum chi-squared error for a GIVEN c1. The
| value of c1 is determined iteratively (external to this routine)
| and is supplied here only as a parameter. See notes.
|
| mgh, 11/3/92
|/*****\
static double leChiSq(double *x, double *y, int imax, double c1, double c2,
                    double *s1, double *s)

|/*****\
| This function finds the characteristics of an equivalent arrow wing

```



```

| using the given wing geometry.
\*****/
void Equiv_Arrow_Wing(struct Control cntrl, struct Wing *wing,
    double *swp_le, double *swp_te, double *AR)

/*****\
| "Exact_Arrow()" calculates and returns the exact values of Cla and Ct / CL^2
| for arrow wings with subsonic leading edges. From that Grumman report.
\*****/
void Exact_Arrow(double *CLa, double *CT, double beta, double m, double ksi)

/*****\
| "gauss_integrate()" integrates the given function using Gaussian
| quadrature. The function to be integrated is passed by pointer.
\*****/
static double gauss_integrate(double (*func)(double, double), double a,
    double b, double k)

/*****\
| "ell_int2()" evaluates the elliptic integrand of the second kind,
| for use in evaluation of the integral.
\*****/
static double ell_int2(double phi, double k)

/*****\
| "awave()" calculates the approximate wave drag.
\*****/
void awave(double *x, struct Control cntrl, struct Wing *wing,
    struct Fuse *fuse, struct Pod *pod, struct Surface *fin,
    struct Surface *canard, struct Flight_Char *flight, double *cd0)

/*****\
| "getarew()" forms an equivalent trapezoidal wing from the wing for
| the approximate wave drag calculation. I'm not sure because Eric
| wrote this part...
\*****/
static double getarew(double ar, double toc, double kp)

/*****\
| "far()" does something for the approximate wave drag calculation. i
| I'm not sure what because Eric wrote this part...
\*****/
static double far(double arew, double toc, double kp, double ar)

/*****\
| "conv_struct()" converts stuff for the approximate wave drag
| calculation. I'm not sure what because Eric wrote this part...
\*****/
static void conv_struct(double *x, struct Control cntrl,

```

```

    struct Wing *wing, struct Fuse *fuse, struct Pod *pod,
    struct Surface *fin, struct Surface *canard,
    struct Flight_Char *flight, double *m, double *r0ot, double *xtoc,
    double *ar, double *beta, double *toc, double *hot, double *lle,
    double *lte, double *taper, double *area)

/*****\
| This is Eric's version of the equivalent arrow wing for landing consider-
| ations.
\*****/
void Equiv_Arrow_Wing_2(struct Control cntrl, struct Wing *wing,
    double *swp_le, double *swp_te, double *AR)

/*****\
| "cla()" calculates and returns the lift-curve slope for use in the
| landing angle of attack estimation.
\*****/
static double cla(struct Control cntrl, struct Wing wing, double cl)

/*****\
| The following routine calculates the local cl distribution on a wing
| given the wing and control structures and the distribution of
| circulation out the span.
\*****/
void local_cl(struct Control cntrl, struct Wing wing, double U,
    double *Gam, double *c_l)

/*****\
| "ozwald()" estimates the Oswald efficiency factor, I guess. Eric
| wrote it.
\*****/
static double ozwald(double cl, double ar, struct Control cntrl,
    struct Wing wing)

/*****\
| "lodmax()" estimates the subsonic, maximum L/D ratio.
\*****/
double lodmax(struct Control cntrl, struct Wing wing, struct Fuse *fuse,
    struct Pod *pod, struct Surface *fin, struct Surface *canard,
    struct Flight_Char flight, double wt)

/*****\
| "cl_func()" generates a circulation distribution, I think. Eric
| wrote it.
\*****/
static double cl_func(double cl, double ar, double wt, struct Control cntrl,
    struct Wing wing, struct Fuse *fuse, struct Pod *pod,
    struct Surface *fin, struct Surface *canard,
    struct Flight_Char flight, double *cd_0, double *e)

```

```

/*****\
| "approxLowSpeedCLa()" estimates the low speed lift-curve slope for
| use in estimating the landing angle of attack performance. Given
| the wing geometry, it returns the estimate for CLa. Three different
| models are implemented, and are selected with the 'choice' variable
| (hardwired in the routine). See notes for explanations of the three
| models.
\*****/
double approxLowSpeedCLa(struct Control cntrl, struct Wing *wing)

/*****\
' dEdalpha()' calculates the downwash derivative d-Epsilon/d-alpha
\*****/
double dEdalpha(struct Control cntrl, struct Wing wing, struct
    Surface *canard) {

/*****\
'approxCMa' calculates an approximate pitching moment curve slope
This is subsonic. Takes moment about wing aero. center
\*****/
void approxCMa(struct OptimControl *opt, struct Control cntrl,
    struct Wing wing, struct Surface *canard, double htdef, double CLa,
    double *CMa, double *CM0) {

/*****\
'approxCLde' calculates the approximate, subsonic change in CL wrt
a change in the horizontal tail incidence or deflection. Assumes
the horizontal tail CLalpha has been defined.
\*****/
double approxCLde(struct OptimControl *opt, struct Control cntrl,
    struct Wing wing, struct Surface *canard)

/*****\
'approxCMde' calculates the approximate, subsonic change in CM wrt
a change in the horizontal tail incidence or deflection. Assumes
the horizontal tail CLalpha has been defined.
\*****/
double approxCMde(struct OptimControl *opt, struct Control cntrl,
    struct Wing wing, struct Surface *canard)

```

## B.14 stability.c

```

/*****\
| This file includes routines that calculate and use the stability
| derivatives.
|
\*****/

```

```

double Y_engine(double Cy_beta, double Cl_beta, double Cn_beta, double Cy_dr,
               double Cl_dr, double Cn_dr, double b, double S, double q, double dr,
               double thrust, double CL, double beta, struct deriv *deriv) {

/* This function inputs stability derivatives and geometric data needed */
/* to update the derivatives for the current tail size. It returns the */
/* farthest distance from the x axis that an engine can be placed. */
/* */
/* Note: Inputting a thrust of 1 will return the greatest yawing moment */
/* that the current tail can handle. */

/* Inputs: */
/* Most inputs are described in the subroutine approx */
/* deriv : An array that holds the current stability derivatives and */
/* the previous approximations. */
/* thrust : The thrust difference causing the yawing moment, i.e. the */
/* thrust of the engine that is out. */

void approx(double cf_c, double Sv, double alpha, double M, double *Cy_beta,
           double *Cl_beta, double *Cn_beta, double *Cy_dr, double *Cl_dr,
           double *Cn_dr, double xcg, double zcg, double bf, double num_fin,
           struct Wing *wing, struct Control cntrl, struct Fuse *fuse,
           struct Surface *fin) {

/* This subroutine calculates the approximate stability derivatives: */
/* Cy-beta (vertical tail contribution) */
/* Cl-beta (vertical tail contribution) */
/* Cn-beta (vertical tail contribution) */
/* Cy-delta r */
/* Cl-delta r */
/* Cn-delta r */
/* */
/* by Peter MacMillin, 6/8/93 */

/* Variables: */
/* Inputs */
/* cf_c : ratio of rudder chord to mean vertical tail chord */
/* Sv : area of the vertical tail */
/* alpha : angle of attack of plane */
/* M : Mach number */
/* xcg, zcg: x and z distances to the plane's cg */
/* d1 : fuselage diameter at quarter chord point of vert. tail */
/* zw : z distance from the wing root quarter chord point to */
/* body centerline */
/* d : maximum fuselage diameter at wing-body intersection */
/* bf : rudder span */
/* num_fin: number of vertical tails on configuration */

/* Local */
/* bv : span of the vertical tail */
/* LAM_c2 : sweep of the half chord, vertical tail */
/* Cr, Ct : root and tip chords of the vertical tail */
/* lv : x distance from plane cg to vertical tail aero. center */
/* zv : z distance from plane cg to vertical tail aero. center */

```

```

/*  a,b      : parameters for curve fits */

/*  Output */
/*  Cy_beta, Cl_beta, Cn_beta, Cy_dr, Cl_dr, Cn_dr : see intro */

/*****\
| 'engine_out()' calculates how far out the outboard engine can
| be placed, given a thrust and tail size. Uses the engine out
| criteria.
\*****/

double engine_out(struct OptimControl opt, struct Control cntrl,
                 struct Wing *wing, struct Fuse *fuse, struct Pod *pod, struct Surface *fin,
                 struct Surface *canard, struct Flight_Char flight,
                 struct deriv *derv, double alpha, double CL, double xcg) {

/*****\
| 'Crosswind()' calculates the bank, rudder and aileron deflections
| required to trim at a given sideslip angle. Used to check crosswind
| landing constraint
\*****/
void Crosswind(struct Control cntrl, struct Wing wing, struct Fuse *fuse,
              struct Surface *fin, struct deriv *derv, double alpha, double CL,
              double xcg, double beta, double *da, double *dr, double *phi) {

/*****\
| Setup_deriv() adjusts the stability derivatives for angle of attack |
| at landing, and calculates the approximate derivative for the ratio |
| pem 1/5/95
\*****/
void Setup_deriv(Aircraft *aircraft) {

/*****\
| 'Setup_LongDeriv()' calculates the ratios of the input CLde and
| CMde with the approximate values calculated internally.
\*****/
void Setup_LongDeriv(struct OptimControl *opt, struct Control cntrl,
                   struct Wing wing, struct Surface *canard, Long_deriv *long_deriv)

```

## B.15 takeoff.c

```

/*****\
| This file contains routines necessary to calculate take off
| and balanced field lengths.
|

/*****\
| setupTO() assumes that much of the setup has already been done.
| It assumes the Wet_area and Detailed_weight have been calculated

```

```

| and that the longitudinal stability derivatives have been setup.
\*****/
void setupT0(Aircraft *aircraft)

/*****\
| takeoffBFL() directs the calculation of the balanced field
| length. Using aircraft->opt.takeoff.model it either uses a
| 'exact' integration or an 'approximate' equation.
\*****/
double takeoffBFL(Aircraft *aircraft)

/*****\
| LoftinBFL() calculates the balanced field length (BFL) using
| an equation from L. Loftin's book. Key factors are W/S and
| T/W, and CLmax
\*****/
double LoftinBFL(double W, double S, double T, double CLmax,
    double h, int units)

/*****\
| Take_off() currently calculates both the all engines operating (AEO)
| takeoff distance and the one engine inoperative (OEI) balanced field
| length (BFL).
\*****/
void Take_off(Aircraft *aircraft)

/*****\
| Use Powers' analytic integration to calculate time and distance
| required to go from v0 to vf. Note: v0 does not need to be less than
| vf.
\*****/
void Ground_Run(double t0, double x0, double v0, double *tf, double *xf,
    double *vf, Aircraft *aircraft, int print, FILE *out) {

/*****\
| 'Ground_time()' directs the numerical integration of the ground run
| equations to calculate distance and velocity changes in going from
| t0 to tf.
\*****/
void Ground_time(double t0, double x0, double v0, double *tf, double *xf,
    double *vf, Aircraft *aircraft, int print, FILE *out) {

/*****\
| 'Climb_Out()' directs the numerical integration of the climb out
| segment of the takeoff integration. Integrates from intial conditions
| to y = yf.
\*****/
void Climb_Out(double t0, double x0, double u0, double y0, double v0,
    double *tf, double *xf, double *uf, double *yf, double *vf,
    Aircraft *aircraft, int print, FILE* out) {

```

```

/*****\
| 'Qinterp()' fits a quadratic function to thrust data
\*****/
void Qinterp(double *V, double *T, double *a, double *b, double *c) {

/*****\
| 'Ground()' calculates derivatives for the ground run segment
\*****/
void Ground(double t, double *y, double *dydx, Aircraft *aircraft) {

/*****\
| 'Air()' calculates derivatives for the climb out segment
\*****/
void Air(double t, double *y, double *dydx, Aircraft *aircraft) {

/*****\
| 'C_Lift()' calculates the lift coefficient for the aircraft given
| current aircraft attitude and elevator deflections. Uses the Polhamus
| LE suction analogy to calculate base CL. Includes ground effect and
| flap effects, when at an altitude less the five span lengths.
\*****/
double C_Lift(Aircraft *aircraft, struct Atmosphere *atm, double CLa,
double alpha, double CLde, double de)

/*****\
| 'Sub_Drag()' calculates the subsonic drag on the aircraft given the
| current aircraft altitude and lift coefficient. Can include drag on
| undercarriage, windmilling engine, and ground effects.
\*****/
double Sub_Drag(Aircraft *aircraft, struct Atmosphere *atm, double CDO,
double CL, int LGout, int ENGout)

/*****\
| 'C_Moment()' calculates the pitching moment for the aircraft.
| Includes elevator and flap effects.
\*****/
double C_Moment(Aircraft *aircraft, struct Atmosphere *atm, double CMa,
double alpha, double CMde, double de, double CMO, double CMdf, double df)

/*****\
| 'Rotate_new()' directs the rotation integration
\*****/
void Rotate_new(double t0, double x0, double u0, double y0, double v0,
double *tf, double *xf, double *uf, double *yf, double *vf,
double *alpha_f, Aircraft *aircraft, int print, FILE *out)

/*****\

```

```

| 'Rotate_eq()' calculates the dervatives for the rotation segment
\*****/
void Rotate_eq(double t, double *y, double *dydx, Aircraft *aircraft)

/*****\
| Check_rotate() performs the rotation integration and returns the v
| component of velocity (upward) to make sure we are able to rotate into
| takeoff position.
\*****/
double Check_rotate(Aircraft *aircraft)

```

## B.16 util.c

```

/*\
| This source file contains "utility" type routines that may be used
| in multiple places throughout the code. While written at various
| times, they were assembled here at the date shown.
|

/*****\
| Check control structure to make sure I can handle options selected.
| Shut down if there are any problems.
\*****/
void Check(struct Control cntrl)

/*****\
| Function to shut down the program and display a message.
\*****/
void bomb(char *error_text)

/*****\
| Calculate wing planform area.
\*****/
void Wing_Area(struct Control cntrl, struct Wing *wing)

/*****\
| "fuseEqRad()" calculates and returns the area and radius for an
| equivalent circle given the data for a fuselage section.
\*****/
void fuseEqRad(int npts, struct Section sec, double *area, double *rad)

/*****\
| This routine calculates and returns the area of a quadrilateral
| in 3 dimensions. The data is passed as 3 four-element vectors,
| x, y, and z -- whose elements are ordered around the perimeter
| of the quadrilateral. The area is determined from the magnitudes
| of the cross products of two sides of each of the component
| triangles.

```



```

\*****/
double Area(double *x, double *y, double *z)

/*****\
| "linear_approx()" returns a linear approximation (i.e. first order Taylor
| series) to a given function given the initial value, a pointer to the
| gradient vector (assumed to start at index of one), the number of elements
| in the vectors, and the initial and current independent variable vectors.
\*****/
double linear_approx(double f0, int num, double *dfdx, double *x0, double *x)

/*****\
| "Max()" returns the largest member of the vector "vec", looking from
| element "istart" to "istop".
\*****/
double Max(double *vec, int istart, int istop)

/*****\
| Standard atmosphere routine. Uses struct of type Atmosphere.
| Expects altitude in question and Mach number in the data structure.
| Viscosity calculated using Sutherland model. All calculations are
| performed in SI units, then converted to English units, if desired.
| Function modifies structure, and returns 0 if all is well, and 1
| if there's a problem. For units, use metric = 1 for SI and 0 for
| English.
\*****/
int Std_Atmos(struct Atmosphere *atm, int metric)

/*****\
| The purpose of this function is to check the wing geometry for
| any physically impossible situations. The routine returns 0 if
| everything is OK, and 1 if problems are found.
\*****/
int check_wing(struct Control cntrl, struct Wing *wing)

/*****\
| The following routine calculates the volume of the aircraft wing
| given the wing and control structures. This is an exact volume
| calculation of the approximate wing surface description.
|
| ERU 2/13/91
\*****/
double wing_vol(struct Control cntrl, struct Wing wing)

/*****\
| "Set_Des_Var()" sets the design variables to a new value defined
| by a scalar 'distance' between 2 designs. (For use with alpha/ksi
| plots.)
\*****/
void Set_Des_Var(int num_dv, double alpha, double *des_initial,

```

```

    double *des_final, double *des_var)

/*****\
| "Set_Beta()" does something, I just know it. Eric wrote it.
\*****/
void Set_Beta(int num_dv, double *des_initial, double *des_var,
    double *beta_prime, double *beta)

/*****\
| Design variable scaling function.
\*****/
double scale_DV(int i)

/*****\
| The following routine determines the lagrange multipliers for an
| optimization minima given the derivatives of the objective and
| constraint functions with respect to the design variables. An
| epsilon limit is used on the value of the constraints as a criteria
| to determine if a constraint is active for the analysis.
|
|                                     - ERU   7/91
\*****/
void lagrange(int num_dv, int num_con, double *dobj, double *g, double *dg,
    int *num_active, double *lagr_mult)

/*****\
| 'locate()' locates one's position in an array. This is a Numerical
| Recipes routine, so take a look at page 98 to get the parameters.
\*****/
void locate(double *xx, int n, int x, int *j)

/*****\
| 'chord()' given a y distance from the root chord, this calculates
| the chord length for that position, i.e. enter zero, and the
| returns the root chord length. NOTE: chord length will be scaled
\*****/
double chord(double y, struct OptimControl opt) {

/*****\
| 'plan()' given a y distance from the root chord, this calculates
| the leading edge x, y, z and the chord length for that position
\*****/
struct Plan plan(double y, struct Wing *wing, struct Control cntrl) {

/*****\
| This routine creates a model of the airplane for Jacob Kay's vlm code
| It is extremely hard wired, don't play with it...
\*****/
void MakeModel(struct Control cntrl, struct Wing wing, struct Fuse *fuse,

```

```

        struct Pod *pod, struct Surface *fin, struct Surface *canard,
        struct Flight_Char flight, struct OptimControl opt,
        double gtow) {

/*****\
  "Htmac()" calculates the horizontal tail mean aero. chord
\*****/
void Htmac(struct Surface *canard, double *mac, double *x) {

/*****\
  'Wmac()' calculates the wing mean aero. chord and location
\*****/
struct Plan Wmac(struct Control cntrl, struct Wing wing) {

/*****\
  'CosLam()' Calculates the area weighted average of cosine of
  the sweep angle at f percent of the chord
\*****/
double CosLam(struct Control cntrl, struct Wing *wing, double f) {

/*****\
  'Alloc_wet()' Allocates memory for the wetted areas
\*****/
void Alloc_wet(struct Control cntrl, wet *wet_area) {

/*****\
  'Free_wet()' frees memory used in wetted area calculation
\*****/
void Free_wet(struct Control cntrl, wet *wet_area) {

/*****/
/* Calculates y(x_in) given (x1,y1) and (x2,y2) using linear interpolation */
double Lin_interp(double x_in, double x1, double x2, double y1, double y2) {

```

## B.17 weight.c

```

/*\
| Weight calculation routines.
|
| The functions in this source code calculate the group weights for
| a transport aircraft. All the equations used were taken directly
| from Arnie McCullers FLOPS code.
|

/*****/
| 'Aircraft_Weight()' calculates and returns the gross weight of the
| given aircraft. For the moment, there's a bunch of hard-wired stuff

```

```

| in here.
| The gross weight must be calculated by iteration, and I use secant
| method (1/10/95 pem) with a 'seed' value of twice the fuel weight.
\*****/
double Aircraft_Weight(struct Control cntrl, struct Wing *wing,
    struct Fuse *fuse, struct Pod *pod, struct Surface *fin,
    struct Surface *canard, struct Flight_Char *flight, double struc_inter,
    Engine *eng)

/*****\
| 'linint()' interpolates the given array and returns the value of
| interest.
|
|     y : eta station of interest
|     eta : array of eta stations
|     f : corresponding array of value of interest
|     n : number of y and f
|
\*****/
static double linint(double y, double *eta, double *f, int n)

/*\
| "bndmat()" calculates the normalized value of the amount of wing spar
| box material required to support the given load. I translated this
| directly from the FLOPS FORTRAN coding.
\*/
static void bndmat(double *w_ptr, double *ew_ptr, double *eta, double *c,
    double *t, double *sw, double *eeta, int n, int nsd, int n2)

/*\
| Generate array of wing integration stations. Once again, this is translated
| directly from the FORTRAN -- my apologies.
\*/
static void deta(int nsd, int *ns_ptr, double *y, int n, double *eta)

/*****\
/* 'Detailed_weight()' calculates the parameters required to run the */
/* FLOPS 5.4.2 version of the weight routine. */
/*****/
void Detailed_weight(Aircraft *aircraft) {

```

## B.18 flops\_inter.f

c Routines in this module are used to interface the HSCT code with the  
c FLOPS routines that we use.

c Init\_eng sets up units and control variables and calls the engine  
c initialization routine.

```

subroutine Init_eng

c FLOPS weight routines. Slightly modified to return inertias and to
c calculate center of gravities every time.
c
c pem, 3/30/94

SUBROUTINE wsetup(NEW1,XL1,WF1,DF1,SHT1,TRHT1,SVT1,TRVT1,ETA1,
+ DNAC1,XNAC1,D4,D6,TOC1,CHD1, ETAW1, SWL1, VMAX1, D2,
+ FWMAX1,D5,DIH1,YEF1,YEA1,NETAW1,W23,W24,W17,W21,W35,W36,W32,
+ W27,W28,W20,W10,W13,W22,W38,W6,W39,W2,W19,W18,W7,W8,W30,W34,
+ W15,W16,W31,W9,W25,W11,W29,W3,W1,cgw1,cght1,zht1,cgvt1,zvt1,
+ cgf1, nglen, mglen, cgef1, zef1, cgea1, zeal, cgfwf1, zbw1,
+ zrvt1,ymlg1,zmlg, swpvt1, arvt1, tcvt1, swpht1, arht1, tcht1,
+ cgtotx, cgtotz, xix, xiy, xiz, xip, tipbck, intfac, thr1,
+ refthr, refweng, iprint, irsuse)

```

## B.19 harris.f

```

subroutine harris(cdwave,opt_, cntrl_,wing_,fuse_,pod_,fin_,
. canard_,flight_)
c
c zero lift wave drag - entire configuration
c
c aware is an extremely fast version of program d2500 with no
c loss of accuracy - l. a. mccullers and p. g. coen, july 1990
c
c .....
c subroutine adist
c
c computes area distribution for any of 5 components
c
c
c
c subroutine emlord (ell,sn,sb,nn,xx,ss,drag,r,k)
c
c k=1, normal mode for matrix le 33
c k=2, precalculated matrix elements le 99
c
c
c subroutine fusfit
c
c computes curve fit coefficients for input body segments
c
c
c
c subroutine iuni(nmax,n,x,ntab,y,iorder,x0,y0,ipt,ierr)
c*****
c*
c* purpose
c*
c* subroutine iuni uses first or second order
c*
c* lagrangian interpolation to estimate the values
c*

```

```

C*           of a set of a set of functions at a point x0. iuni *
C*           uses one independent variable table and a dependent *
C*           variable table for each function to be evaluated. *
C*           the routine accepts the independent variables spaced *
C*           at equal or unequal intervals. each dependent *
C*           variable table must contain function values corres- *
C*           ponding to each x(i) in the independent variable *
C*           table. the estimated values are returned in the y0 *
C*           array with the n-th value of the array holding the *
C*           value of the n-th function value evaluated at x0. *
C*
C*           use
C*           call iuni(nmax,n,x,ntab,y,iorder,x0,y0,ipt,ierr) *
C*
C* parameters
C*
C*           nmax  the maximum number of points in the independent *
C*                 variable array. *
C*
C*           n     the actual number of points in the independent *
C*                 array,where n .le. nmax. *
C*
C*           x     a one-dimensional array, dimensioned (nmax) in the *
C*                 calling program, which contains the independent *
C*                 variables. these values must be strictly monotonic. *
C*
C*           ntab  the number of dependent variable tables *
C*
C*           y     a two-dimensional array dimensioned (nmax,ntab) in *
C*                 the calling program. each column of the array *
C*                 contains a dependent variable table *
C*
C*           iorder interpolation parameter supplied by the user. *
C*
C*           =0    zero order interpolation the first function *
C*                 value in each dependent variable table is *
C*                 assigned to the corresponding member of the y0 *
C*                 array. the functional value is estimated to *
C*                 remain constant and equal to the nearest known *
C*                 function value. *
C*
C*           x0    the input point at which interpolation will be *
C*                 performed. *
C*
C*           y0    a one-dimensional array dimensioned (ntab) in the *
C*                 calling program. upon return the array contains the *
C*                 estimated value of each function at x0. *
C*
C*           ipt   on the first call ipt must be initialized to -1 so *
C*                 that monotonicity will be checked. upon leaving the *
C*                 routine ipt equals the value of the index of the x *
C*                 value preceding x0 unless extrapolation was *
C*                 performed. in that case the value of ipt is *
C*                 returned as *
C*           =0    denotes x0 .lt. x(1) if the x array is in *
C*                 increasing order and x(1) .gt. x0 if the x array *
C*                 is in decreasing order. *
C*           =n    denotes x0 .gt. x(n) if the x array is in *

```

```

C*           increasing order and x0 .lt. x(n) if the x array *
C*           is in decreasing order. *
C* *
C*           on subsequent calls, ipt is used as a pointer to *
C*           begin the search for x0. *
C* *
C*           ierr    error parameter generated by the routine *
C*           =0      normal return *
C*           =j      the j-th element of the x array is out of order *
C*           =-1     zero order interpolation performed because *
C*                   iorder =0. *
C*           =-2     zero order interpolation performed because only *
C*                   one point was in x array. *
C*           =-3     no interpolation was performed because *
C*                   insufficient points were supplied for second *
C*                   order interpolation. *
C*           =-4     extrapolation was performed *
C* *
C*           upon return the parameter ierr should be tested in *
C*           the calling program. *
C* *
C*           required routines          none *
C* *
C*           source                     cmpb routine mtlup modified *
C*                                       by computer sciences corporation*
C* *
C*           language                   fortran *
C* *
C*           date released               august 1,1973 *
C* *
C*           latest revision             august 1,1973 *
C* *
C*****

```

```

subroutine matinv ( max, n, a )

```

```

C*****
C
C   purpose - matinv inverts a real square matrix a.  determinant
C             calculations and simultaneous equation solutions have
C             been stripped from this version.
C
C             max - the maximum order of a as stated in the
C                   dimension statement of the calling program.
C
C             n   - the order of a, 1.le.n.le.max.
C
C             a   - a two-dimensional array of the coefficients.
C                   on return to the calling program, a inverse
C                   is stored in a.
C                   a must be dimensioned in the calling program
C                   with first dimension max and second dimension
C                   at least n.
C
C*****

```

```

subroutine out
c
c     prints and plots
c

subroutine slope
c
c     checks body slopes against mach angle
c

function sngon(n,p)
c
c     finds the area of the smallest convex polygon containing
c     an entirely arbitrary set of n points, each specified by
c     two cartesian coordinates.

subroutine spod ( n, m, nn, beta, xcut, theta, x, r, xzero,
* yzero, zzero, s, bcos, bsin )
c
c     projected area for circular body

subroutine spod2 ( nx, b, c, xcut, n, nang, xi, zi, ri, xafus,
* arno, xbfus, arba, xzero, yzero, zzero, s )
c
c     projected area for warped circular body

subroutine spod3 ( nx, b, c, xcut, nang, n, xi, surf, xafus, arno,
* xbfus, arba, xzero, yzero, zzero, s )
c
c     projected area for arbitrary body

subroutine start
c
c     inputs and initializes configuration description
c

subroutine swing ( nn, xcut, s, bcos, bsin, p )
c compute projected area of a lifting surface solid element

subroutine xmat
c
c     computes,inverts,and stores (nx-1)x(nx-1) matrix
c

```



## B.20 optimizer.f

This module contains the source for NEWSUMT-A and an interface routine. For information on the NEWSUMT-A routines see Reference [59].

```
c NEWSUMTA optimizer source code. THIS IS NOT QUITE A STANDARD
c VERSION OF NEWSUMTA!! I've included the 'optcntrl' routine which
c is my interface with the rest of the world (i.e. the C coding)
c
c*****
c The following is a front end driver for NEWSUMTA.
c The purpose of this routine is to link the main program which
c is in C to the optimizer which is in FORTRAN. Note that the
c external routine analys() is in C and that any extra information
c about the design this routine needs will be read in from a file
c in that routine. Also note that the number of design variables
c must also be set in the parameter statement of this routine in
c addition to being set in the main input program (this is not very
c convenient but no other option is available in FORTRAN).
c*****
c      subroutine optcntrl(xlimit,x0,dobj,g,dg,numdv,numcon)
c
c      n1 : number of design variables (JUST BELOW)
c      n2 : number of constraints (JUST BELOW)
c
c      x : vector of design variables
c      x0 : initial design variable vector
c
c      The remaining vectors in the following dimension
c      statement are described in the NEWSUMT User's Guide
c
```

## B.21 rs\_weight.f

This module contains the various wing bending material weight response surfaces used.

```
C*****C
C Response surface function for wing bending material weight C MK
C*****C
C Response Surface Function
  FUNCTION RS3B (SX01)
C
C Response Surface Function
  FUNCTION RS3 (SX01)
C
C Response Surface Function
  FUNCTION RS61B (SX01, SX02, SX03, SX04, SX05, SX06, SX07, SX08,
C      SX09, SX10, SX11, SX12, SX13, SX14, SX15, SX16,
C      SX17, SX18, SX19, SX20, SX21, SX22, SX23, SX24,
C      SX25)
```

```

C Response Surface Function
  FUNCTION RS66(SX01, SX02, SX03, SX04, SX05, SX06, SX07, SX08,
C           SX09, SX10, SX11, SX12, SX13, SX14, SX15, SX16,
C           SX17, SX18, SX19, SX20, SX21, SX22, SX23, SX24,
C           SX25)

      FUNCTION RS15(SX01, SX02, SX03, SX04, SX05, SX06, SX07, SX08,
C           SX09, SX10)

C Response Surface Function
  FUNCTION RS15B (SX01, SX02, SX03, SX04, SX05, SX06, SX07, SX08,
C           SX09, SX10)

C Response Surface Function
  FUNCTION RS61 (SX01, SX02, SX03, SX04, SX05, SX06, SX07, SX08,
C           SX09, SX10, SX11, SX12, SX13, SX14, SX15, SX16,
C           SX17, SX18, SX19, SX20, SX21, SX22, SX23, SX24,
C           SX25)

```

## B.22 sfeng.f

This module contains engine deck interpolation routines and is taken directly and without modification from FLOPS<sup>11</sup>.

## B.23 sfwate.f

This module contains weight calculate routines and is taken from FLOPS<sup>11</sup>, but contains an interface routine which we will list here. It is otherwise unchanged.

```

C*****C
C Function to load design variables into memory for RS      C MK
C*****C
      FUNCTION RSSETUP( RSDVA )

```